DESIGN OF A ROTARY UNION FOR COOLANT TRANSFER TO RADAR SYSTEM

RADAR SİSTEMİNE SOĞUTMA SIVISI TRANSFERİ İÇİN DÖNER EKLEM TASARIMI

YİĞİT VURAL

PROF.DR. BORA YILDIRIM

Supervisor

Submitted to

Graduate School of Science and Engineering of Hacettepe University

as a Partial Fulfillment of the Requirements

for the Award of the Degree of Master of Science

in Mechanical Engineering

2023

to Bomonti

ABSTRACT

DESIGN OF A ROTARY UNION FOR COOLANT TRANSFER TO RADAR SYSTEM

Yiğit Vural

Master of Science, Department of Mechanical Engineering
Supervisor: Prof.Dr. Bora Yıldırım
June 2023, 118 pages

In this thesis, a rotary joint for cooling fluid transfer to the radar system is developed. The design and analysis to meet the specified technical requirements were verified by tests. In dynamic sealing tests, the sealing, friction, and life performances of PTFE-based seals with ENP and HVOF coatings under different temperature and pressure conditions were investigated. It has been shown that the coating on the AISI4140QT steel rotor using WC/Co/Cr 86/10/4 powder by HVOF method can provide sealing without abrasion in long-term use.

Keywords: rotary union, dynamic sealing, high-velocity oxygen fuel, electroless nickel plating

ÖZET

RADAR SİSTEMİNE SOĞUTMA SIVISI TRANSFERİ IÇIN DÖNER EKLEM TASARIMI

Yiğit Vural

Yüksek Lisans, Makine Mühendisliği Bölümü
Tez Danışmanı: Prof.Dr. Bora Yıldırım
Haziran 2023, 118 Sayfa

Bu tezde radar sistemine soğutma sıvısı transferi için döner eklem geliştirilmiştir. Belirlenen teknik isterlerleri sağlayacak şekilde yapılan tasarım ve analizler, testlerle doğrulanmıştır. Dinamik sızdırmazlık testlerinde PTFE bazlı keçelerin ENP ve HVOF kaplama ile farklı sıcaklık ve basınç şartları altında sızdırmazlık, sürtünme ve ömür performansları incelenmiştir. HVOF yöntemiyle WC/Co/Cr 86/10/4 toz kullanılarak AISI 4140+QT ıslah çeliği rotor üzerine yapılan kaplamanın uzun süreli kullanımda aşınmadan sızdırmazlık sağlayabildiği gösterilmiştir.

Anahtar Kelimeler: döner eklem, dinamik sızdırmazlık, yüksek hızlı oksi-yakıt püskürtme, akımsız nikel kaplama

ACKNOWLEDGEMENTS

TABLE OF CONTENTS

LIST OF FIGURES

LIST OF TABLES

NOMENCLATURE

Symbols

°C	Degree Celsius
K	Resistance coefficient
L	Typical length
Ø	Diameter
P	Power
Pa	Pascal
Q	Volumetric flow rate
η	Shear viscosity (Dynamic viscosity)
ρ	Density
ω	Rotational speed
ΔP	Pressure loss, pressure difference
σ	Von-mises stress
τ	Shear stress
f	Friction factor
v	Fluid velocity

Abbreviations

A	Area
AC	Alternative Current
AISI	American Iron and Steel Institute
BSPP	British Standard Pipe Parallel
C	Carbon or Carbide
CAD	Computer Aided Design
CFD	Computational Fluid Dynamics
CMC	Ceramic-Metal Composite
Co	Cobalt
COG	Center of Gravity
COTS	Commercial off-the-shelf
Cr	Chrome
CS	Cross-section
Cv	Valve flow coefficient

CVD	Chemical Vapor Deposition
D	Diameter
DC	Direct Current
DSTI	Dynamic Sealing Technologies, Inc
DUT	Device Under Test
ENP	Electroless Nickel Plating
FEA	Finite Element Analysis
FEM	Finite Element Method
FRJ	Fluid Rotary Joint
FRU	Fluid Rotary Union
FVM	Finite Volume Method
g	grams, gravitational acceleration
h	hours
HB	Brinell Hardness Scale
HRB	Rockwell B Hardness Scale
HRC	Rockwell C Hardness Scale
HVOF	High Velocity Oxygen Fuel
Hz	Hertz
ICD	Interface Control Document
kW	kilowatt
lpm	liters per minute
ml	milliliters
MMC	Metal-Matrix Composite
Mo	Molybdenum
ms	milliseconds
MTBR	Mean Time Between Replacements
N	Newton
N/A	Not Applicable
NBR	Nitrile Butadiene Rubber
Nm	Newton-meters
PMC	Polymer-Matrix Composite
PSC	Plasma Spray Coating
PTFE	Polytetrafluoroethylene

PVD	Physical Vapor Deposition
QT	Quenched & Tempered
Re	Reynold's number
RJ	Rotary Joint
rpm	rotation per minute
RU	Rotary Union
S	Sulphur
SST	Shear Stress Transport
T	Torque
V	Velocity
VAC	Velocity at Axial Channel
VCR	Velocity at Circulation Ring
VRC	Velocity at Radial Channel
W	Tungsten

Subscripts

AC	Axial channel
B	Balseal
CR	Circulation ring
CS	Cross-section
K	Kastaş
RC	Radial channel
T	Trelleborg

1. INTRODUCTION

1.1 Problem Definition

Electrical power and signals are primarily transmitted through cables, while pipes and hoses are used for fluid transmission. The transfer of fluids between stationary structures can be easily facilitated using cables and hoses. However, the transmission of electricity or fluids becomes more complex when it is required between components that undergo relative rotation, such as wind turbines and radars. In such scenarios, the issue of tangling arises, necessitating the incorporation of an additional component to mitigate this problem. Rotary unions and slip rings are specialized equipment that have been developed precisely to address this challenge.

Rotary unions serve the purpose of fluid transfer, while slip rings are specifically designed for the transmission of electrical power or signals. Both these components primarily comprise two essential elements: the stator and the rotor. The transfer of the respective media takes place between the stator and rotor in the case of slip rings and rotary unions. In slip rings, the transfer between the rotor and stator is predominantly facilitated by electrically conductive brushes. Conversely, fluid transfer within fluid rotary unions is achieved through internal channels that allow for efficient passage between the stator and rotor.

Rotary joints represent mobile hydraulic or pneumatic components utilized in installations. Due to their inclusion of moving parts and the necessity for effective sealing between these elements, persistent friction and associated challenges arise. The design of such mechanical components is influenced by fundamental factors encompassing structural integrity, weight, ease of production and assembly, ergonomic considerations, and resilience to environmental conditions like temperature, humidity, and corrosion resistance. Additionally, given its functionality as a revolute joint, both static and dynamic states necessitate thorough examination. Since the unit is a hydraulic element, further scrutiny is warranted concerning factors such as fluid compatibility, material selection for the structure, behavior under hydraulic pressure, and pressure loss within the unit.

1

In addition to the aforementioned considerations, the paramount issue in the design process lies in establishing a structure that can sustain a durable seal, exhibiting minimal friction and consequent wear between continuously rotating parts. The primary challenge herein revolves around the judicious selection of an appropriate seal for the intended application. Moreover, it entails ensuring the desired hardness and roughness attributes of the surface that will come into contact with the seal material. To validate these requisites, especially life, rigorous testing procedures are imperative.

1.2 General Information

Several rotary devices like wind turbines, radars and excavators need transfer of hydraulic power, coolant, or dry air etc. Flexible hoses or rigid pipes are used to transfer fluids. But if this equipment is used in between relatively rotating units, hoses would tangle, and pipes would break. Rotary unions are the equipment which fulfill the transfer in between relatively rotating units.

Rotary unions basically consist of two main subassemblies: stator and rotor. These two parts have one degree of freedom which is axial rotation motion. RU is connected from the stator to the static part of the unit where it is used. On the other hand, rotor of the RU is connected to the rotating part of the unit mentioned (Figure 1-1). Thus, fluid can be transferred under desired conditions.
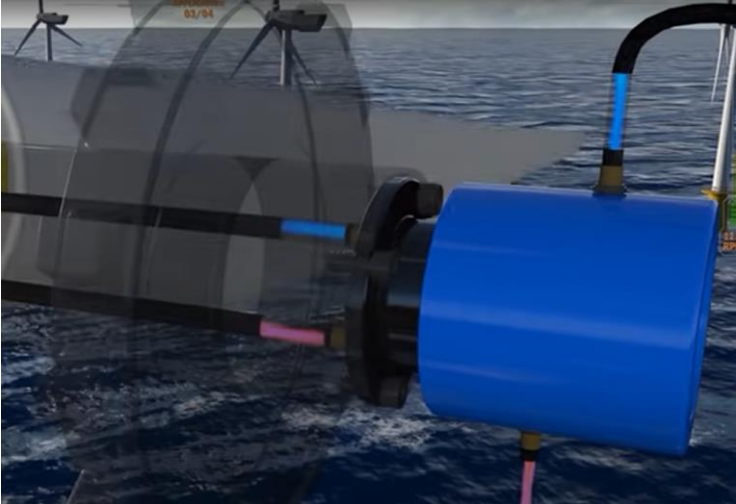
Figure 1-1. RU assembled on a wind turbine [1]

Fluid passes through the channels inside the RU as seen in Figure 1-2. There are radial channels which are mostly on the stator and axial channels on the rotor. These channels are connected to each other, and they are closed to the atmosphere. Rotary seals are used to prevent internal and external leakage.
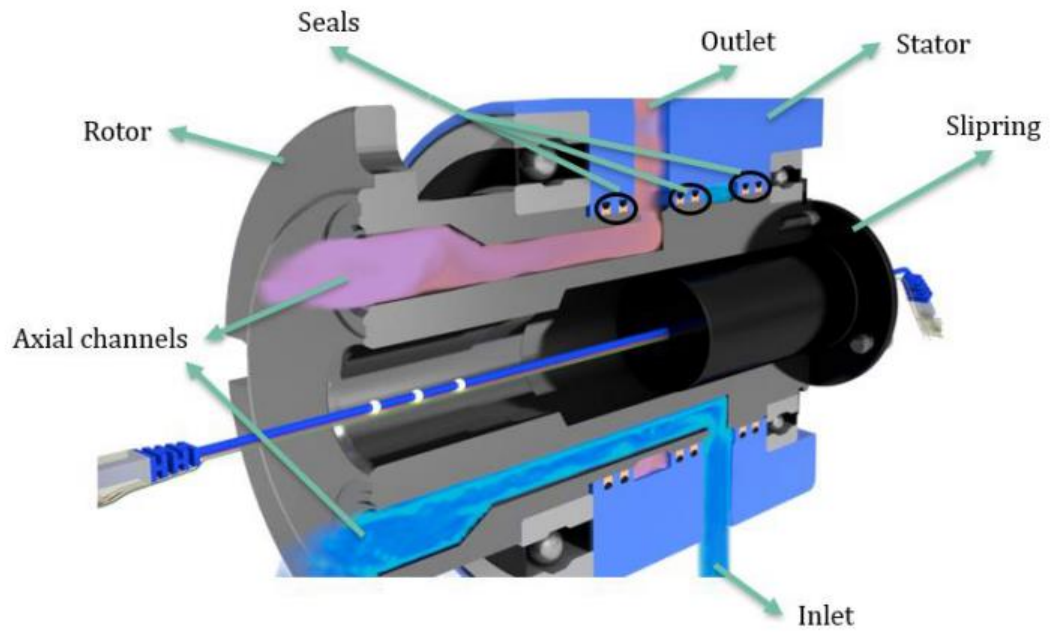
Figure 1-2. Inside view of a 2-channel RU [1]

The fluid follows the path described below:

- Entrance (Blue line on Figure 1-2)
  - Fluid enters from the inlet port of the stator.
  - Fluid passes through the radial channel in between the rotor and stator.
  - Fluid turns to the axial port of the rotor and exits RU.

- Return (Pink line on Figure 1-2)
  - Fluid enters from the axial port of the rotor.
  - Fluid turns to the radial channel in between the rotor and stator.
  - Fluid turns to the outlet port of the stator.

Thus, the continuation of the flow is ensured without internal and external leakage since the channels of stator and rotor coincide and rotary seals are used around the separate flows. As the flow continues, the rotor is allowed to rotate using bearings.

1.3 Literature Survey

1.3.1 Detailed Information and RU Types

The simplest form of an RU is swivel joint (Figure 1-3). Swivel joint is a basically a fitting which allows rotational motion in hydraulic lines. It had three claims when it was invented [2]. Firstly, it enables pipes it is connected to tilt motion. This motion gives one degree of freedom to each to the system and probable contractions would be prevented. Secondly, assembly process becomes much easier and reliable thanks to the allowance of rotations. Another object is that this system permits line a little axial motion.
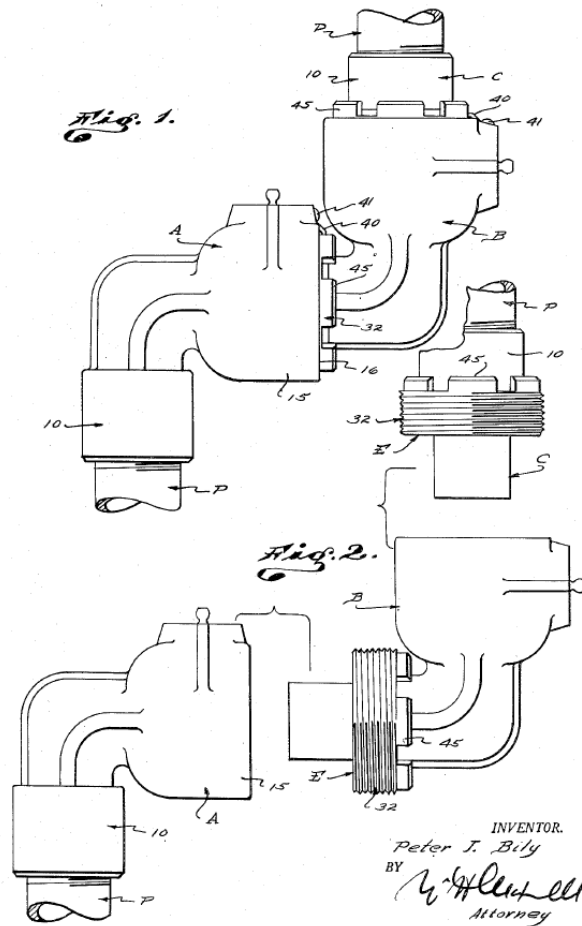
Figure 1-3. Swivel joint construction for handling fluids [2]

Quick couplers are common examples of rotational hydraulic equipment (Figure 1-4). Main objective of these equipment is to facilitate the assembly process. Almost all of them permit rotational motion to the pipeline under pressure without any leakage. Even if the main objective of these products is not to maintain relative rotation, they have considerable amount of life.

Figure 1-4. Physical appearance of a commonly used quick coupler [3]
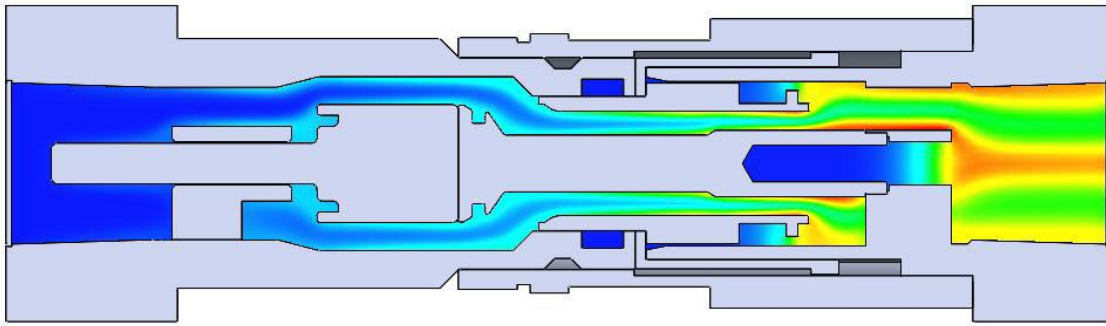
Figure 1-5. Inside view of a quick coupler [4]

On the other hand, the main objective of the rotary union is to maintain relative rotational motion. In other words, they are expected to work continuously under hydraulic pressure without leakage. Even if RU can convey liquid, gas, or vacuum, they are mostly used to transmit coolant, hydraulic oil and dry air. Since the systems RU includes electronic subsystems besides mechanical parts, electrical power or data also should be transferred in the system. So, RU's can be single unit as well as hybrid subsystems which consist of RU and slip ring.

Fluid Rotary Unions are used in various applications like marine, defense, industrial, oil and gas, etc. In the defense industry, coolant fluid, typically glycol/water mixture in radars and hydraulic oils in tanks and other ground vehicles are mostly conveyed. On the other hand, oxygen rich air is transmitted in diver life support systems in marine applications generally. Hydraulic fluids, air, coolant, vacuum is conveyed in industrial applications. Besides, the same RU can be used for both liquid and gas, even two-phase fluid.

The first difference when an RU is observed is the number of channels. If an RU has one inlet and one outlet, it is described as one channel RU (Figure 1-6). For every radial hole on the stator, there must be one axial hole on the rotor. These are the inlet and outlet of one channel. Single channel RU can be used where return line is not needed like diver life support system, air conditioning, etc.

6

Figure 1-6. Single Channel RU, MOOG Model 306 [5]

Where RU is intended to be used for cooling, a return line would be needed besides the supply port. Two channel unions are suitable for this application.
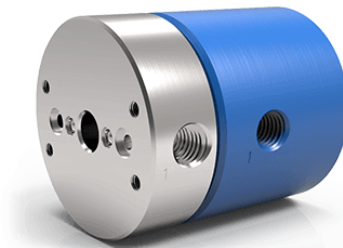
Figure 1-7. Dual channel RU, DSTI LT Series [6]

Also, multi-channel unions can be needed depending on various applications (Figure 1-8).

Figure 1-8. Multi-channel RU's, DSTI LT Series [7]

1.4 Technical Requirements

RU to be designed is intended to be used in a radar on wheeled ground vehicle. Hence, military standards should be taken into account when determining technical

requirements. Other specifications which military standards do not include are determined as initial guesses considering similar products in market.

The RU is intended to transfer coolant which will be mounted on a radar used in military applications. Thus, two channels: supply and return, are necessary and sufficient.

A slip ring is intended to be connected to the RU. So, the cables must pass through the rotor. The inner dimension is selected as 100 mm minimum for an initial guess. The outer dimension and height are determined as 280 mm and 300 mm as well.

Ambient and fluid temperature ranges are selected with respect to the operational, storage and transit conditions regarding "Department of Defense Test Method Standard" MIL-STD-810G Table C-I [8]. According to this table, minimum and maximum temperatures are selected as -30°C and 63°C.

The mixing ratio of glycol and water should be selected regarding low temperature limit. Since the lowest temperature is selected as -30°C, the freezing point of the mixture must be below this point. Freezing point of %50 water - %50 ethylene glycol is measured as -35.4°C [9]. Hence, media is selected as %50 water - %50 ethylene glycol mixture.

Operating pressure, angular velocity, flow rate and pressure loss are determined regarding the radar system where RU will be used.

Operating life, leakage rate and frictional torque are determined as initial guesses by taking consideration of products in market. Operating pressure, angular velocity, rotor diameter and material selection would affect frictional torque. These values became the determining factor in that comparison.

Since this unit will be used in a wheeled ground military vehicle, MIL-STD-810G is taken into account determining structural considerations. MIL-STD-810G Method 514.6, Procedure I, Category 20-a Table 514.6C-IV, Figure 514.6C-2 is selected as

vibration profile and 40g / 11 ms sawtooth MIL STD-810G method 516 is selected as shock profile.

Regarding all the considerations above, the requirements which RU must comply with are listed below.

Table 1-1 Technical requirements

(A: Analysis, D: Demonstration, I: Inspection, T: Test)

Requirement Type	Determined Requirement	Verification			
		A	D	I	T
Number of channels	2 channels, supply and return		•		
Mechanical dimensions	Maximum Outer Diameter: Ø280 mm Minimum Inner Diameter: Ø100 mm Maximum Height: Ø300 mm			•	
Ambient temperature range	-30°C ~ +63°C	•			•
Fluid temperature range	-30°C ~ +63°C	•			•
Working media (Fluid type)	50% water - 50% ethylene glycol mixture		•		
Operating pressure	Nominal: 6 bar Maximum: 10 bar Burst: 15 bar	•			•
Angular velocity	60 rpm				•
Pressure loss	0.5 bar at maximum flow rate	•			•
Flow rate	Maximum: 25 lpm	•			•
Leakage rate	< 0.1 ml/h				•
Operating life	> 1 million Cycle				•
Frictional torque	< 50 Nm				•
Structural considerations	Vibration: MIL-STD-810 G Method 514.6, Procedure I, Category 20-a Table 514.6C-IV, Figure 514.6C-2 Shock: 40g / 11 ms sawtooth MIL STD-810G method 516	•			•

All the requirements listed above must be input into the design and controlled by determined design methods. Table 1-1 shows which input will be provided by which design method.

These considerations will be considered in preliminary and detailed design phases.

2. PRELIMINARY DESIGN

2.1   Design Considerations

All the design inputs will be covered, evaluated, and compared between each other. Some design methods will be used in this thesis. Although geometrical design seems to be the most part of the work, in fact, other methods like FEM and CFD analyses, seal selection, material and surface engineering are essential. In fact, providing dynamic sealing under certain friction and life requirements is the challenge of this design.

Design inputs and design methods are listed in Table 2-1. This table shows the relation between the design input and relevant design method where relation is labeled with black dots intersection cells. Pre-determined design inputs, in other words, technical requirements will be met using the related design method or methods. For example, the number of channels is a design input, and it is determined as two. This requirement will be met by geometrical design. Other design methods have no effect meeting this requirement. On the other hand, all the design methods stated will be used to ensure the mechanical dimensions. CFD analysis will determine the channel dimensions, FEM analysis will determine wall thickness, seal selection will determine the seal and housing dimensions, material and surface engineering will determine also wall thickness. As a result, Table 2-1 will guide us on our way to use the right design method to ensure the technical requirements.

Table 2-1 Design method vs design inputs

		Design Method					
		Geometrical Design	CFD Analysis	FEM Analysis	Seal Selection	Material and Surface Engineering	Analytical Calculation
Design Inputs	Number of Channels	•					
	Mechanical Dimensions	•	•	•	•	•	•
	Fluid Properties		•		•	•	•
	Ambient Temperature Range		•	•		•	•
	Fluid Temperature Range		•	•	•		•
	Operating Pressure	•		•	•		
	Pressure Loss	•	•				•
	Flow Rate		•				•
	Leakage Rate	•			•	•	
	Operating Life				•	•	
	Frictional Torque	•			•	•	
	Structural Considerations	•		•			

Using Table 2-1, it can be seen that technical requirements would be ensured using the right design method. In preliminary design phase, mostly geometrical design will be done.

2.2 Initial Geometrical Design

As mentioned before, union consists of two main subassemblies: rotor and stator. Both assemblies can be made of one or multiple pieces. These conditions depend on machine elements which will be used in the union like bearings, seals, and fasteners. Initial geometry of the rotor can be seen in Figure 2-1. Inner diameter is selected as 100 mm which is design input. This region can be optimized later with respect to wall thickness.

Red and yellow diametral areas represent the bearing housing and blue area represents the mating surface of seal. Since these products have certain dimensions which will be given by the supplier, a dimension range should be determined in order to provide data input to seal and bearing selection. Having these diameter values small will provide the following advantages:

- Low weight
- Low linear speed
- Low friction surface
- Low pressure loss

Channel size is the determining factor for these dimensions. Thus, an analytical approach can be applied for an initial guess for the channel sizes. But stator parts must be modeled as well in order to complete the fluid line.
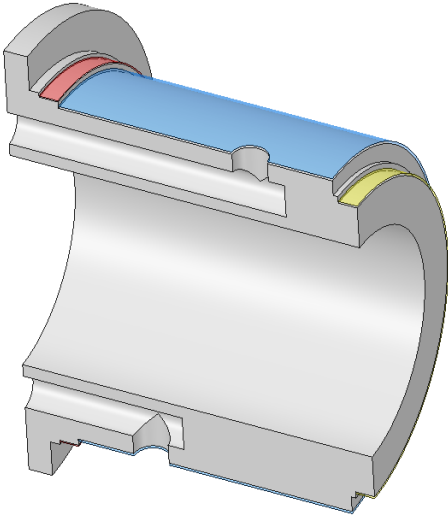
Figure 2-1 initial geometry of the rotor (half)

Mechanical contact between rotor and stator will be provided using bearings. Bearings will connect rotor and stator statically and axially but allow rotational motion. The stator can be a single piece or consist of more than one piece. This selection which depends on the assembly of seals and bearings will be detailed later but stator is modeled as a single part for an initial guess (Figure 2-2). Also, it is assumed that three

seals are used. For that kind of application, two-way seals are needed which means rotary seal prevents leakage from both sides to another. This situation may change due to the seal selection, but it does not affect the flow geometry. Thus, pressure loss can be calculated analytically using that model.
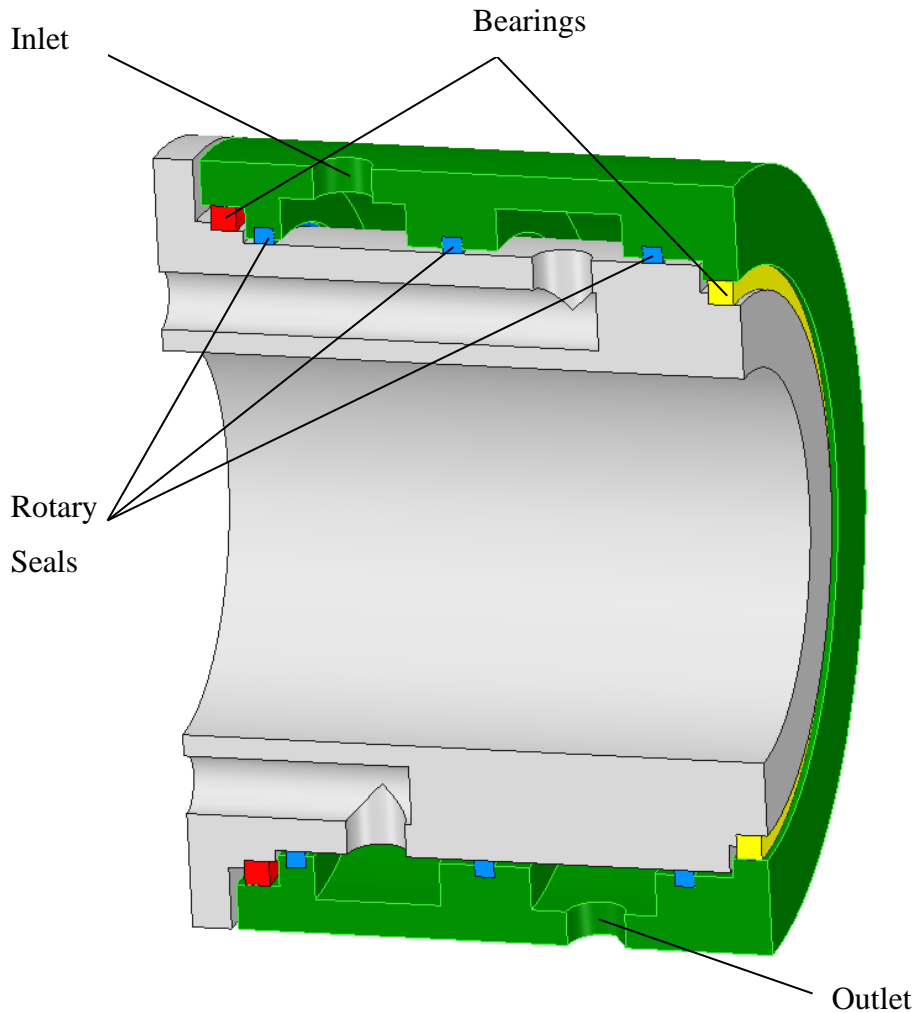
Figure 2-2 Initial geometry of RU (half)

2.3   Analytical Approach for The Pressure Loss

At this point, flow line geometry is obtained using the initial 3D model (Figure 2-3). It seems there are two separate lines which are colored as blue and red. Blue and red lines represents inlet and outlet lines, respectively. Coolant enters the RU in radial port of in a relatively low temperature and exits the RU from the axial outlet. While it cools down the targeted unit, it warms up and comes back to the RU in a relatively high temperature. In order to minimize the heating degree of the coolant, relatively short line

is selected as the inlet line and the reason why the lines are colored that way is the temperature difference between lines.
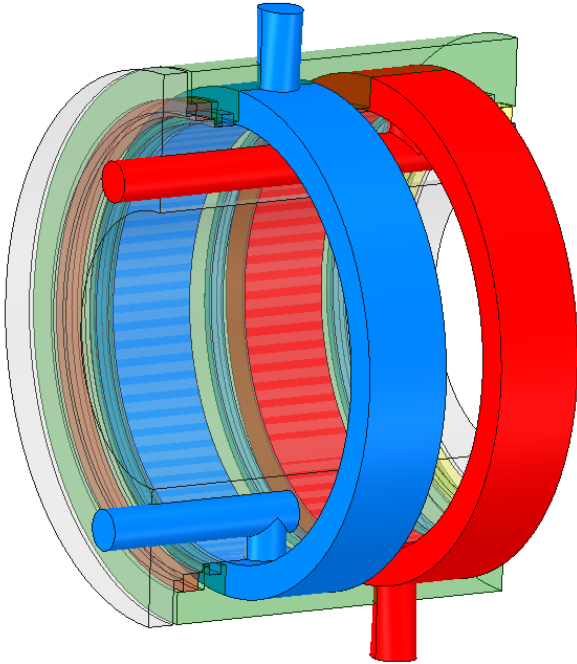
Figure 2-3 Basit flow line geometry

Since the only geometrical difference between those two lines is the length of the axial channel, the pressure difference of the long road is selected to be calculated. Total pressure loss will be assumed to be twice the pressure loss of the red line and that assumption will serve as a safety factor.

The Flow regime plays an important role in calculating the pressure loss values. In order to determine the flow regime, Reynold's number must be investigated. Reynold's number is a unitless value which is used to determine whether a flow is laminar or turbulent. The Reynold's number is the ratio of inertial loads to viscous loads in the flow and is calculated for circular pipes as follows [10].

$$Re = \frac{Inertial\ forces}{Viscous\ forces} = \frac{\rho v D}{\eta}$$

Besides, equivalent hydraulic diameter values can be calculated for rectangular tubes if a transformation is needed. Flow is considered as turbulent over Re=2300 as a rule of

14

thumb and this value is called as the critical Reynold's number. The critical Reynold's number value changes for different geometries and different flow conditions. This value is accepted with empirical methods for circular pipes [10].

In straight pipes, Darcy-Weisbach formula (Henry Darcy & Julius Weisbach) can be used for both laminar and turbulent flow except extreme velocities causing downstream pressure [11].

$$\Delta P = \frac{\rho f L v^2}{2D}$$

Friction factor is a unitless value which is determined experimentally. For laminar flows, friction factor can be calculated by f=64/Re. When the flow is fully turbulent, friction factor also depends on relative roughness, which is the comparison of the roughness and diameter of the pipe. Friction factor values can be obtained using friction factor diagram presented by L. F. Moody [12].

In fittings like elbows and tees, flow pattern is disturbed, and an additional pressure loss takes place. Turns, separations and combinations in flow geometry were treated as equivalent fittings. Pressure loss for fittings can be calculated as follows [13].

$$\Delta P = K \frac{\rho v^2}{2}$$

Resistance coefficient is a dimensionless value gathered from experimental data and it varies according to the fitting type.

The flow geometry is divided into seven segments (Figure 2-4) in order to calculate the pressure loss values separately.
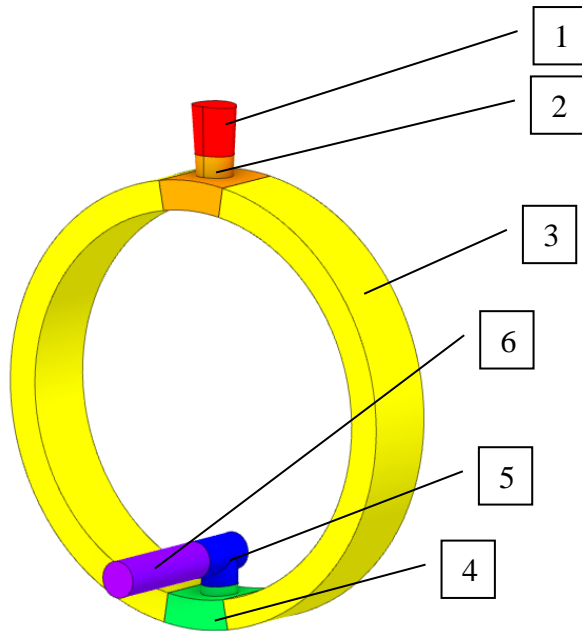
Figure 2-4 Flow geometry segments

Table 2-2 Flow geometry segment descriptions

Segment	Description
1	Straight hole
2	Tee, separation
3	Circular path
4	Tee, combination
5	Elbow
6	Straight hole

Each segment is simplified as pipe elements with a decent error (Table 2-2). In this calculation, following assumptions are made:

- Rectangular cross-section in the second segment, assumed to be a circle with the same area. A similar assumption is made in the fourth segment.
- Circular path in the third segment is treated like a straight path with the same perimeter and cross-section.
- The flow is assumed to be equally divided in two in the second segment.

Fluid properties for %50 water and %50 ethylene glycol mixture at -30°C are listed below (Table 2-3).

Table 2-3 Media properties [14]

Volumetric Ratio	50%-50%	
Temperature	-30	°C
Dynamic Viscosity	0.00372	kg/ms
Density	1075.5	kg/m^3

Initial guesses are made for each dimension, and they are optimized regarding mechanical envelope. Table 2-4 is obtained after certain number of iterations. Since the results obtained belong to a single line, it is assumed that the pressure drop will be twice the calculated value. The pressure drop per unit was calculated as 0.252 bar, and since the technical requirement is 0.5 bar, a safety factor of 1.98 was obtained.

Table 2-4 Pressure losses of flow geometry segments

Segment	Dimension 1 [mm]	Description 1	Dimension 2 [mm]	Description 2	Pressure loss [mbar]
1	15	Diameter	50	Length	2.1
2	15	Inlet diameter	20	Outlet diameter	30.61
3	10x35	CS	250	Length	1.4
4	20	Inlet diameter	20	Outlet diameter	30.61
5	15	Inlet diameter	15	Outlet diameter	53.31
6	15	Diameter	200	Length	8.4
				Σ(ΔP)	**252.86**
				SF	**1.98**

It was aimed to keep the slope of the pressure drop curve constant along the flow direction. Nevertheless, more pressure drop occurred at the separation, combinations, and elbows than in other regions (Figure 2-5). this was optimized as much as possible due to geometrical constraints.
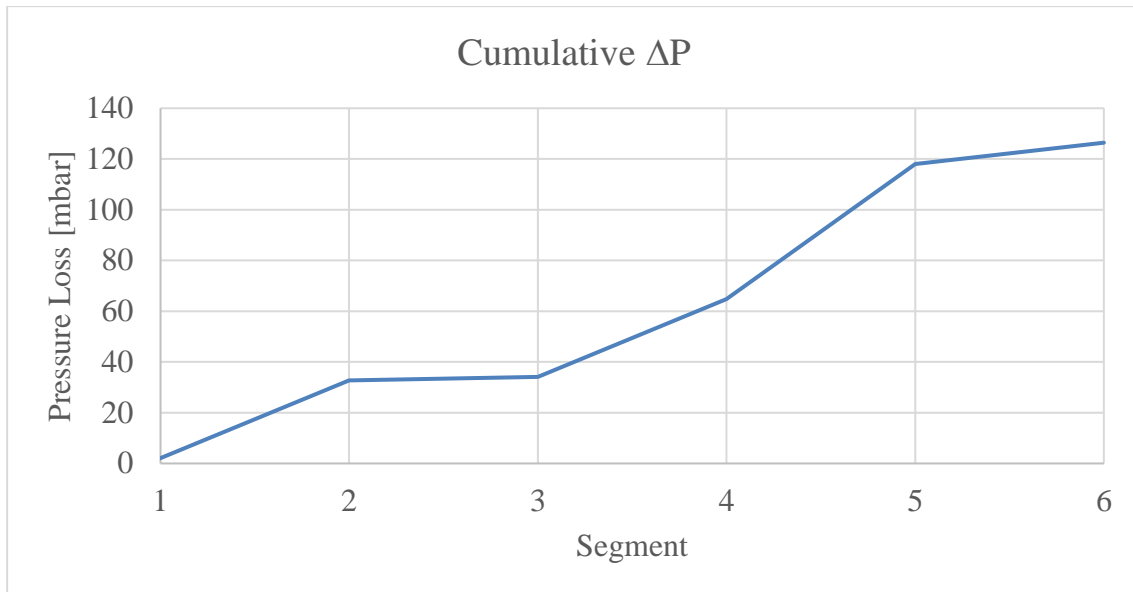
Figure 2-5 Cumulative pressure loss throughout the flow direction

The dimensions obtained as a result of analytical pressure drop calculations using Darcy-Weicbach formula [11] were used as reference dimensions for seal and bearing selection. in this case, a seal with a bore diameter of around 160 mm should be used.

2.4 Rotary Seal Selection

2.4.1 Theory and Selection Process

Rotary seals provide impermeability in between relatively rotating parts. Seal selection must be done with respect to the following criteria: pressure, linear velocity, temperature range, fluid type, lifetime. In special conditions like medical, food, aviation or space, additional specifications may be needed. Seals are generally mounted to the shaft and hole with interference or transition fit so that impermeability can be provided. Thus, they must act like spring. For that reason, either they include elastic materials like elastomer or spring, or they are made of an elastic material. In low pressures, impermeability is provided by the compression force provided by the seal itself. As the hydraulic pressure increases, that compression force becomes insufficient to hold the fluid particles. Of course, impermeability in high pressure can be obtained by increasing the compression force, but then high compression forces would lead to enormous frictional torque which decreases system efficiency and mean time between replacements (MTBR). Instead, geometry of the seal is designed such a way that

18

hydraulic pressure makes lips of the seal push against the mating surface (Figure 2-6) [15].
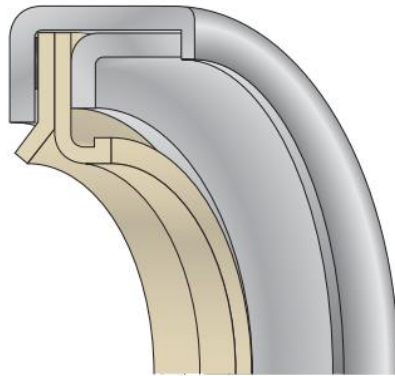
Figure 2-6 Parker Flexilip Rotary Seal [16]

Rotary seals also withstand limited linear velocities due to their material, geometry, additional elements like locking ring, etc. This maximum speed value also can change with respect to pressure limit. So to say, a rotary seal can withstand high velocity under low pressure, vice versa.

Resistance over temperature range mainly depends on seal material. Since temperature resistance range of elastomer materials which are used in seals are critically narrow as against most metals, it becomes the determining factor on that situation. Also, viscosity and density of fluid changes with respect to temperature. These two values also affect the permeability of the fluid.

Fluid type affects seal mainly in two ways: permeability and corrosion. Fluids with smaller molecular volume and wider gaps between molecules have a tendency to leak from smaller gaps. So, gases like small molecules like hydrogen are difficult to seal. On the other hand, viscous fluids like oils are much easier to seal. Besides, seal materials must have corrosion resistance over media used. Corrosion resistance is a specific quality of materials which can be described as propensity to undergo chemical reaction with mating material.

Lifetime is directly related to the wear resistance of both seal and the mating surface. As a rule of thumb, two mating materials apply wear to each other and amount of wear of softer material will be higher. So, the seal must be hard enough not to wear quickly but

it also must be softer than the mating material not to damage it. Because it is easier and cheaper to replace the unit's seals than to replace the rotor when it is worn out enough to allow leakage. So, high frictional torque leads to high wear which shortens the life of seal [17].

As a result of the analytical pressure loss calculations, seal inner diameter is decided to be selected as 160 mm. Since dynamic seals are another specialty, a COTS product will be used. The seal manufacturers whose products are most likely to be suitable are as listed: Aesseal, Balseal, EagleBurgmann, SKF, Trelleborg, Vulcan Seals, Roplan, AS&P, Parker, Kastaş.

The two most important features which are considered for a seal are frictional torque and life. Frictional torque is mostly dependent on the P x v (pressure times linear velocity) [18]. These features mostly cannot be provided by seal manufacturers because of the lack of test values. Since rotary seals are mostly used in heavy industry, rotation motion is provided by hydraulic pressure. Thus, frictional torque estimation is not required by most consumers.

After examining all the catalogs and contacting the manufacturers with technical specifications which seal must have, the options have been reduced to three, which are "Balseal X625753", Trelleborg TG3201600-M15N and Kastaş K702-160. Trelleborg is chosen to be analyzed as a suitable product since frictional power calculation is given in product catalog. Kastaş is a Turkish brand which also manufactures equivalents of various models of Trelleborg in rotary seal category. Kastaş cannot give friction and life estimation but makes equivalent products of Trelleborg. Any product which will be chosen from Trelleborg can be supplied from Kastaş, procured, and tested without any manufacturing cost in DUT and test rig. Also, it is accessible and has relatively low-cost products since it is a company that manufactures in Turkey.

2.4.2   Balseal X625753

Balseal is a seal manufacturer which makes spring energized seals. Spring energized seals provide closely constant frictional torque. This torque is adjusted with the stiffness of the spring inside the seal. The leakage rate increases critically after wear occurs in

traditional seals. But in spring energized seals, spring offers longer service life even wear occurs [19].
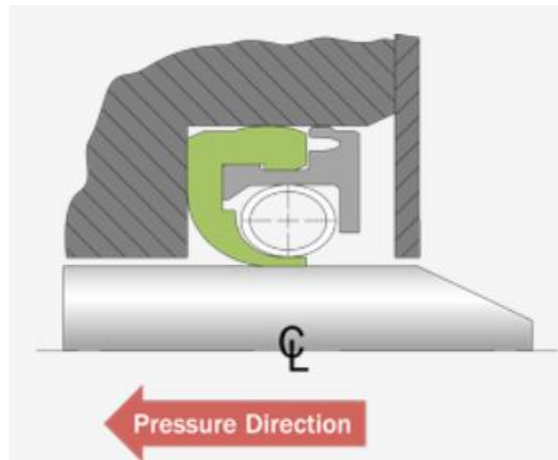
Figure 2-7 Balseal high speed seal [19]

 Balseal spring energized seals mainly consists of two parts: elastomer and spring. But a locking ring is used in high-speed seals. Generally, high speed seals are used above 15 m/s but this model is offered by the manufacturer since it promotes consistent sealing contact in thermal cycling conditions. Green part of the seal shown in Figure 2-7 is the elastomer which plays the main role in impermeability. The ring in the center represents the spring, which is described above. The locking ring is seen in grey which is tightly assembled to the seal. Seals working with high hydraulic pressure may tend to leak at low pressures because their lip structure is designed to seal at high pressure values. Although this seal provides impermeability up to 80 bars, it can also seal at low pressures thanks to the steel spring which applies compressive force continuously.

Estimated Seal Radial Loads
Determining force and torque at various media pressures,
and determining spring force as a percentage of the total radial forces
and determining the seal contact stress, and as a % of the media force.

Seal X #	Seal OD in	Seal ID in	Spring Series	Spring Length in	Spring Rate lbs/in	Spring Load Force lbs	Seal contact forces and pressure from media	
							psi =>	145
								lbs
								psi
X625753	6.693	6.299	105LC	20.100	1.18	23.74	from media =>	291.6
					20%		total load =>	315.3
Media Type=>	Environment				Defl.		% spring =>	8%
Shaft Matrl.	Stainless Steel						Contact pressure (psi) =>	210
Shaft Finish	0.1-0.4 µm Ra						(cntct psi % of media) =>	145%
Speed (ft/min)	99							
Wear Factor (in^3-min/ft-lb-hr)	3.5E-10						Coeff. of Friction @70°F (21°C)	
Min Thickness to Failure (in)	0.005						0.040	
Max Thickness to Failure (in)	0.008						SP36 HT	
Wear Rate (in/hr)	7.26E-06						Running Force Oz.	202
Wear Rate (in/rotation)	2.02E-09						Running Force lbs.	12.6
Min Rotations to Failure	2.48E+06						Running Force Newtons.	56
Max Rotations to Failure	3.97E+06							
Average Rotations to Failure	3.22E+06						Breakout Force Oz.	262
Min Days to Failure	30						Breakout Force lbs.	16.4
Max Days to Failure	49						Breakout Force Newtons.	73
Average Days to Failure	40							
							Running Torque in-Oz.	636
							RunningTorque in-lbs.	39.7
							Running Torque Newton-m	4.5
K = W/(V*P)								
K = Wear Factor	in^3-min/(ft-lb-hr)						Breakout Torque in-Oz.	826
W = Wear Rate	in/hr						Breakout Torque in-lbs.	51.6
V = Speed	ft/min						Breakout Torque Newton-m	5.8
P = Pressure	PSI							

Figure 2-8 X625753 friction and wear estimation [Balseal technical support, personal communication, June 20, 2021]

Balseal X625753 is a one-sided seal which means it only prevents leakage from one side. Hence, four seals will be needed if Balseal X625753 is used. Breakout torque and running torque at 14.5 bar hydraulic pressure is estimated as 5.8 Nm and 4.5 Nm, respectively (Figure 2-8). Thus, breakout and running torque values will be 23.2 Nm and 18 Nm, respectively and these values meet technical requirements.

2.4.3   Trelleborg TG3201600-M15N

Trelleborg offers various number of products which are specialized for specific needs. "Turcon Roto Glyd Ring" model is selected for low pressure and long service life features.

Figure 2-9 Turcon Roto Glyd Ring [20]

Turcon Roto Glyd Ring is a double sided, fully elastomer seal. Since it is double sided, it can ensure impermeability between two sides up to a certain pressure difference (Figure 2-9). This situation allows us to use three seals in total which cannot be applicable with Balseal. Also, it can be assembled by deforming the seal into a kidney shape (Figure 2-10). This application allows stator to be manufactured as one piece with three grooves. This situation would ease the assembly process and increase manufacturing precision.
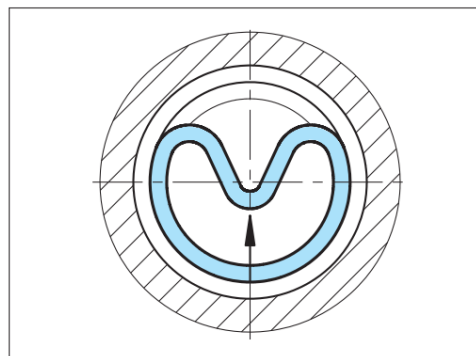
Figure 2-10 Inserting the seal ring into the closed groove [21]

$$P \simeq P_{50} \times \left(\frac{d}{50 \; mm} \right) \; [W]$$
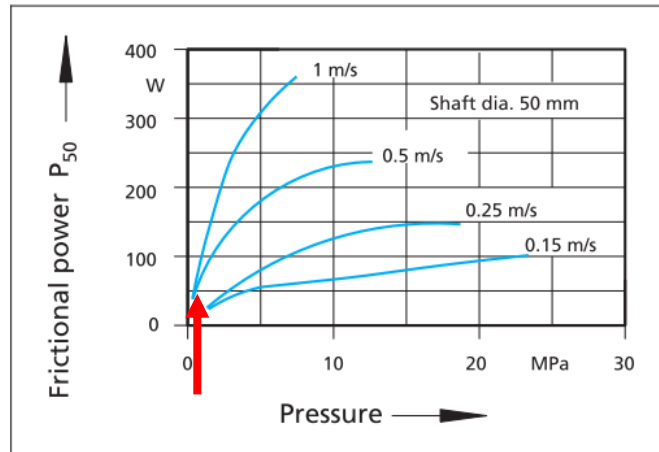
Figure 2-11 Friction power estimation for Turcon Roto Glyd Ring [22]

Friction estimation is calculated using Figure 2-11. Since angular velocity is 60 rpm and shaft diameter is 160 mm, linear velocity is calculated as 0.5 m/s. It can be seen that frictional value at 0.5 m/s, 15 bar (1.5 MPa) is approximately 50 W. Using the formula given by manufacturer above the graph, frictional power for 160 mm diameter is calculated as 160 W.

$$P = P_{50} \times \left(\frac{d}{50 \; mm} \right) = 50W \times \left(\frac{160 \; mm}{50 \; mm} \right) = 160 \; W$$

Hence, estimated frictional torque is found to be 25.5 Nm using 160 W frictional power and 60 rpm angular velocity as follows.

$$T = \frac{P}{\omega} = \frac{160 \; W}{60 \; rpm} = 25.5 \; Nm$$

Since this seal can be used as double-sided seal, three seals would be sufficient as mentioned before and 76.4 Nm torque can be obtained.

50 Nm torque limit is mentioned to the manufacturer and asked whether frictional power can be decreased by decreasing maximum pressure limit of the seal. Upon this, Turcon M15N seal material is offered by the manufacturer. M15 is a special material of Trelleborg which is used for light to medium applications with high sealing effects in

fluids with good lubrication. This material mainly consists of PTFE with additional materials like carbon, MoS_2, glass fiber or bronze (this information is not supplied by the manufacturer) to increase durability. "N" letter at the end of the model code represents o-ring material used in seal. N is used for 70 Shore A NBR o-ring. O-ring and M15 elastomer come assembled and detachable. Certain frictional torque value is not known for TG3201600-M15N, but a critical decrease would take place because of the difference in hardness of mating material.

2.4.4   Kastaş K702-160

Kastaş K702-160 (Figure 2-12) has the same geometry with Trelleborg TG3201600-M15N. It has similar structural and material properties too, except the M15 elastomer. The manufacturer does not supply any information about friction, wear and life but since Trelleborg TG3201600-M15N will be tested and groove dimensions of the two models are same, Kastaş K702-160 is also ordered for the ease of testing.

Figure 2-12 Kastaş K702 [23]

Kastaş K702-160 also consists of two parts as seen in Figure 2-12. O-ring material is NBR, and inner ring material is bronze infused PTFE [23]. Since it is also a double-sided seal, using three seals would be sufficient.

2.4.5   Selection

As mentioned above rotary seal options are narrowed down to three products: Balseal X625753, Trelleborg TG3201600-M15N and Kastaş K702-160.

Although Trelleborg offers ease of assembly and double-sided sealant capability, precise data about frictional torque, wear and life are not given from the manufacturer.

Only reference data given about the frictional data is shown in Figure 2-11 and total torque for three seals is calculated as 76.8 Nm, which is above the maximum desired frictional torque value. A softer elastomer is offered by the manufacturer which lowers the frictional torque, but the certain value is not known. Besides, the required hardness value for the mating material is 55 HRC, which is 30 HRC for Balseal. Meeting this requirement may be challenging.

The frictional torque and life of Kastaş is also uncertain but it is assumed to have similar properties with Trelleborg since it has the exact same geometry. But it does not offer a softer elastomer like M15 like Trelleborg. So, most probably the frictional torque value would be close to 76.8 Nm.

Balseal gives precise data about the frictional torque, wear and life expectation in different cases which suit design criteria. Despite it requiring fragmented stator assembly and one more seal compared to other options, it meets the technical requirements which is the priority. As a result, it has been decided to use four Balseal X625753 in RU.

2.5   Bearing Selection

Bearing is a machine element which the main load is transferred through elements in rolling contact rather than in sliding contact [24]. Bearings are divided into two sub-categories: ball and roller bearings. In ball bearings, balls make point contact with the ring raceways. Since ball contacts to raceways at one point, that small contact area provides low friction. On the other hand, rollers of the roller bearings make line contacts with raceways which increases load capacity and friction [25]. Bearings of RU will not be exposed to heavy loads. Instead, they will only carry rotor weight in vibration and shock conditions. As a trial, the thinnest standard bearing of SKF is selected and implemented into draft CAD model. Since inner dimensions of rotary seals are 160 mm, bore diameters of large and small bearings are selected as 170 mm and 140 mm as an initial guess. Although these two bearings are the thinnest models of selected bore diameters, they are still too large compared to the seals and they make the stator very large and heavy.
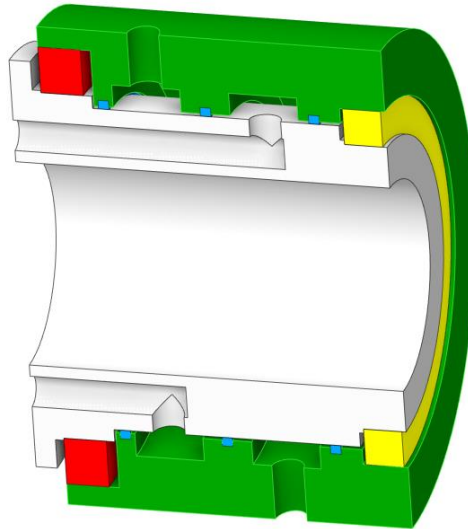
Figure 2-13 RU with SKF Ball Bearings

Standard bearings with bore diameter about 140 mm – 170 mm have dynamic load rating above 100 kN and fatigue load limit above 4 kN. RU will be fixed from stator and bearings will carry the weight of the rotor only. If the rotor is manufactured of steel using valid preliminary design model, its mass will be around 16 kg. Thus, the weight of the rotor would be 157 N and the instantaneous load at shock condition would be 6.3 kN. The loads which bearings undergo are very low compared to their load ratings. The reason behind that is that the RU has large bearing diameters, but the bearings will only carry the weight of the rotor. In this case, bearings have large thicknesses and make the system heavy which is not needed.

Thin section bearings are the solution for parts with large diameters with low loads. They permit rotation motion with low thickness and low weight. Kaydon, Unasis, Saibo are some of the manufacturers who work on this concept.
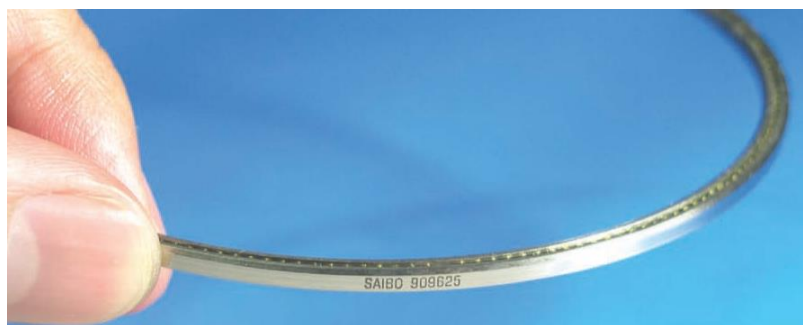
Figure 2-14 Saibo Super Slim Bearing [26]

Kaydon is a sub-brand of SKF, which is focused on making thin section bearings. Kaydon Reali-Slim Bearings with 140 mm bore diameter have approximately 7900 N axial load capacity. Hence, Kaydon Reali-Slim Bearings can be used for this application.

On the other hand, Unasis has split thin section bearings. The inner and outer rings and nylon ball cages of these bearings are split, which allows the bearings elasticity in mounting over features in the mating components [27].

Figure 2-15 Unasis Split Thin Section Bearing [27]

3. DETAILED DESIGN

3.1 Pressure Loss Analysis

3.1.1 Theory

Pressure loss is calculated by analytical methods in preliminary design phase, but flow geometry is simplified, and many assumptions are made during that process. Analytical approach can be used to determine some rough dimensions but in order to get more precise results in fluid dynamics, CFD method shall be used.

Computational fluid dynamics is a science that, with the help of digital computers, produces quantitative predictions of fluid-flow phenomena based on the conservation laws (conservation of mass, momentum, and energy) governing fluid motion [28]. CFD analysis divides the entire fluid volume into a finite number of control volumes and transfers data between their boundaries where the data is obtained as a result of conservation laws.

CFD analysis is conducted to have precise data about the pressure loss inside the RU. Analysis data, boundary conditions, assumptions made, inputs and results are described in detail in the following heading.

3.1.2 CFD Analysis

In order to make a CFD analysis to find the pressure loss, scenario and the boundary conditions of the analysis have to be determined. In this analysis, pressure loss can be thought of as the pressure required to transfer a given flow rate of fluid from inlet to outlet of the unit. In CFD analysis, inlet and outlet boundary conditions must be described. Outlet can be assumed as atmospheric pressure and inlet pressure can be calculated under specified inlet flow rate. If outlet pressure is defined as a value other than zero, the pressure difference would be still the same because pressure loss depends on the flow rate, not the outlet pressure. But in that condition, internal forces would be

higher since the internal pressures increase. Hence, inlet should be described as "mass flow inlet" and outlet should be described as "pressure outlet".

Boundary conditions of the analysis shall be selected for the worst conditions to obtain the maximum pressure loss case. Boundary conditions which affect the pressure loss are flow rate, outlet pressure and the fluid properties. Pressure loss increases exponentially by the increase in the flow rate in pipes [11]. Thus, maximum flow rate must be selected as outlet mass flow rate boundary condition to obtain the maximum pressure loss condition. Outlet pressure can be determined as zero to get the pressure loss from the inlet pressure easily. Fluid has two main properties which constitute inputs for the analysis: density and viscosity. Since viscosity is the resistance offered by a fluid to relative motion, or shearing, between its parts [29], fluids with higher viscosity require higher pressure to be transferred. Likewise, higher density requires more energy, so to say higher pressure to be transferred. Water and ethylene glycol mixture has high viscosity and density in low temperatures. Hence, fluid properties at the lowest temperature can be used as analysis inputs.

Flow geometry is modeled as seen in Figure 3-1. Inlet and outlet are selected as the furthest position to get the maximum pressure loss point. Flow geometry is divided into three parts: radial channel, circulation ring and axial channel. The reason behind that approach is that if pressure loss is higher than expected, at least one of them can be optimized compared with the other design parameters. RU consists of two separate flow volumes which are supply and return lines. Although the geometries of these two lines are similar, pressure loss values of those lines may be different since flow characteristic would change with the direction. Tesla valve, which is a passive-type check valve is a common example which possesses a direction-dependent pressure drop due to its unique structural design [30].

Coolant enters from the radial channel to the unit, circulates around the circulation ring and exits the RU from the axial channel, which is named as supply line in the analysis. Likewise, coolant returns from the device which is cooled down from the other axial channel of the RU. Then follows the reverse path of a similar flow geometry in the RU. Thus, two separate analyses are done to simulate both supply and return lines. The only difference between them other than the flow direction is the length of the axial channel

length in real. In analysis, long channel length is selected to increase the safety factor. The same flow geometry is used in both analyses, but inlet and outlet boundary conditions are interchanged with each other.

Pressure losses occurred close to seals are neglected since they are assumed to be infinitesimal. Figure 3-1 represents the return line, whose axial channel is longer. It can be seen that the flow geometry is symmetrical about XY plane (Figure 3-1). Thus, half of the model can be used with the symmetry boundary condition in order to reduce the computational cost.
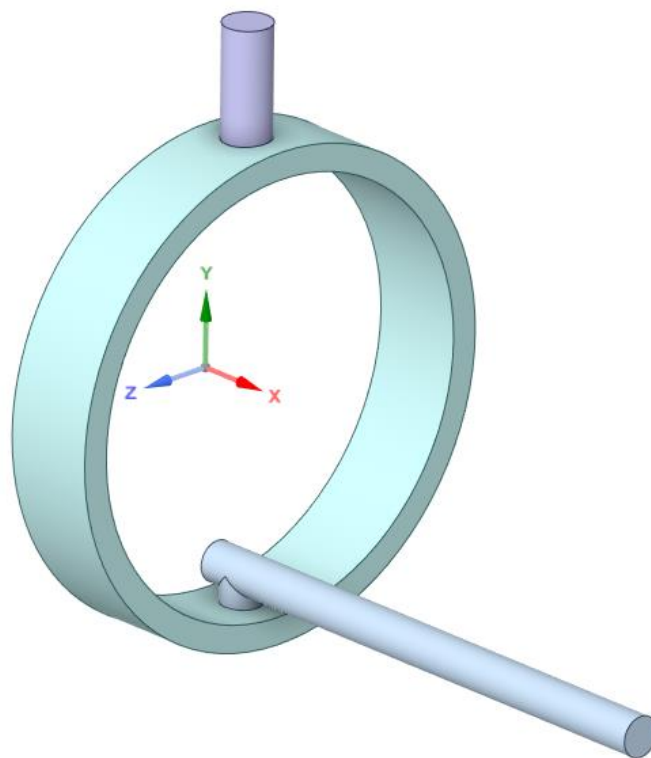
Figure 3-1 Flow geometry

Flow geometry is split into half and Figure 3-2 is obtained. Blue surface represents the symmetry plane. Red and yellow surfaces represent mass flow inlet and pressure outlet, respectively in supply line, and vice versa in return line. All the other surfaces other than specified are determined as wall. Mass flow value at inlet is given as 0.448 kg/s since volumetric flow rate is 25 lpm and density is 1075.5 kg/m^3. Outlet is described as 0 Pa gauge pressure in order to get the pressure loss value directly from the area-weighted average pressure at inlet. This application makes collecting result data easy especially in parametric analyses.
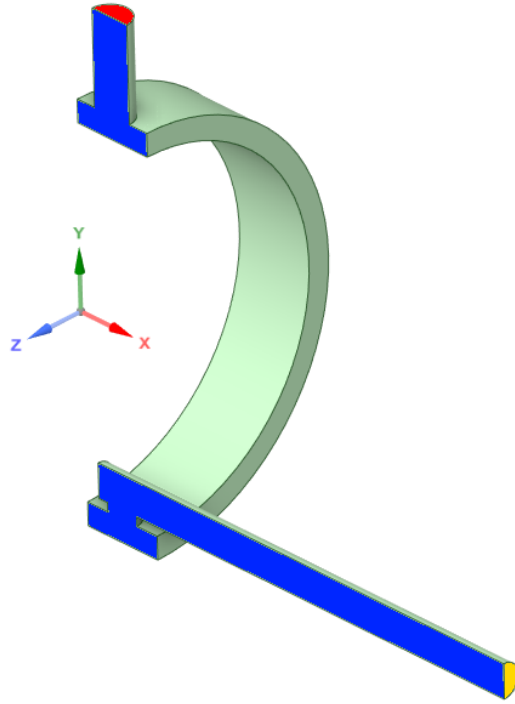
Figure 3-2 CFD analysis model

Analysis results must be independent from the mesh, i.e., changing mesh size should not affect the results. Mesh optimization shall be done to be sure that analysis results are independent from mesh quality. To ensure that, analysis is done with a coarse mesh for an initial guess and element size is reduced gradually until results become stationary. 10 mm element size is used for an initial guess, and it is reduced to 1 mm with 1 mm increment (Figure 3-3). Also, the same cases are repeated with adding inflation with 5 maximum layers, and growth rate of 1.2. Maximum skewness did not exceed 0.86 in the worst conditions among all cases.
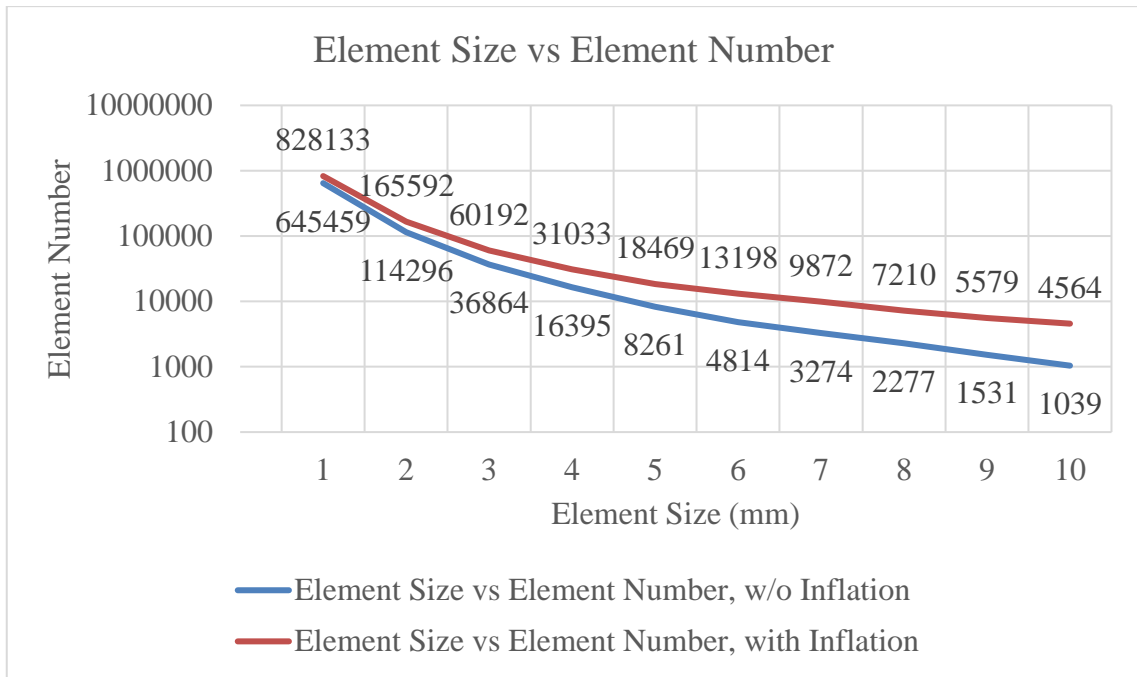
Figure 3-3 Mesh element size vs element number curve

Reynold's number would be higher in narrow sections because velocity of incompressible fluids increases under constant mass flow rate. Inlet and outlet are important since boundary conditions are described on them, and result are collected from them. Entire flow geometry is divided into three separate parts as mentioned above: radial channel, circulation ring and axial channel. Radial channel and axial channel consist of inlet and outlet planes. Also, the axial channel is longer than the other channels, which increases Reynold's number. Cross-sectional areas of three volumes are calculated as follows. Besides, average velocity is calculated using CS areas and volumetric flow rate [31].

$$V = \frac{Q}{A_{CS}}$$

Where Q is volumetric flow rate and A_{CS} is cross-sectional area.

Radial Channel

Diameter: 18 mm

CS area: 254.47 mm^2

V_{RC}:   1.64 m/s

33

<u>Circulation Ring</u>

Outer diameter: 180 mm

Inner diameter: 160 mm

Thickness: 36 mm

CS Area: 3600 mm^2

V_{CR}:   0.12 m/s

<u>Axial Channel</u>

Diameter: 15 mm

CS Area: 176.71 mm^2

V_{AC}:   2.36 m/s

Reynold's number at the radial and axial channel is calculated. Since the circulation ring does not include inlet and outlet boundary condition, it is much wider than other volumes and velocity is smaller, there is no need to calculate the Reynold's number at this region. Reynold's number at radial channel and axial channel are calculated as follows.

<u>Radial Channel</u>

Typical Length: 0.042 m

Re: 19882.48

<u>Axial Channel</u>

Typical Length: 0.2 m

Re: 136337.03

At internal flow, transition to turbulence takes place between Re 2000 and 10^5 [32]. At Reynold's number above 2300 the turbulent slugs link up and the entire pipe is filled with turbulent flow. Thus, a suitable turbulence viscous model must be selected for the CFD analysis since flow is not laminar in both channels.

In CFD analyses, Navier-Stokes equations, which generally describe the conservation of momentum, are used. But in order to predict the behavior of a turbulent flow regime, turbulence models are also needed which use zero, half, one or two equations. Two

equation turbulence models are widely used in industrial applications, and the most common models among two equation models are k–ε and k–ω. The standard k- ε model behaves very well in predicting turbulent shear flows. However, this model is unable to predict accurately flows with adverse pressure gradients, which results in yielding poor results for separated flows. On the other hand, k–ω achieves higher accuracy for boundary layers with adverse pressure gradients. In addition, the recent version of Wilcox (2006) k–ω model is much more accurate for free shear flows and separated flows. A more advanced turbulence model is the Shear Stress Transport (SST) model by Menter. This model combines the advantages of k–ε and k–ω models. In our analysis, pressure loss is to be analyzed in internal flow with a separation. Hence, k–ω turbulence model is more suitable for this application. SST k–ω turbulence model is also used since it gives better results away from the walls. Moreover, a comparison and check are made using two turbulence models. Coupled method is used as pressure-velocity scheme, and second order upwind scheme is used for the space discretization of the momentum and energy equations.

Figure 3-4 and Figure 3-5 represent supply line and return line pressure loss results vs mesh size, respectively. Pressure loss value decreases with the decrease of mesh size. When mesh size decreases, mesh quality increases, and curve becomes steady which means that results remain still independent from the mesh quality. Two different turbulence models are used which are k–ω and SST k–ω. k–ω results are converged to the real results at coarse mesh but with the increase in mesh quality, results become independent from these two turbulence models. Inflation in walls having 5 layers with 1.2 growth rate is used in additional analyses but it has no effect in pressure loss results as seen in figures. As a result, pressure loss is determined as 0.11 bar in supply line and 0.13 bar in return line, which makes 0.24 bar in total. Since pressure loss is under 0.5 bar, design revision is not needed.
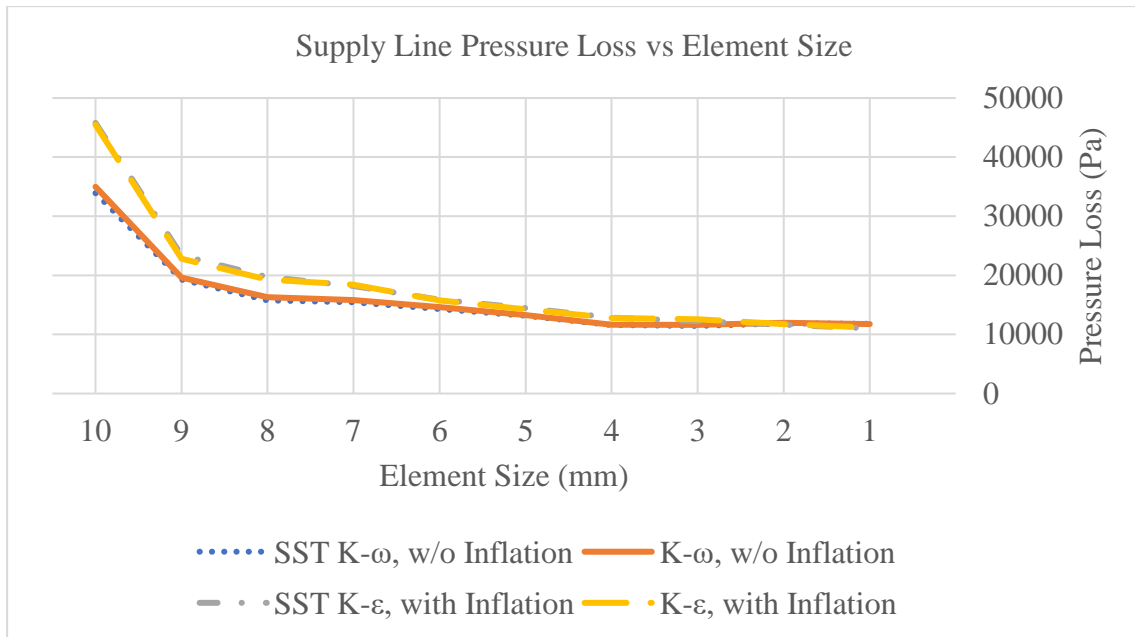
Figure 3-4 Supply line pressure loss vs element size curve
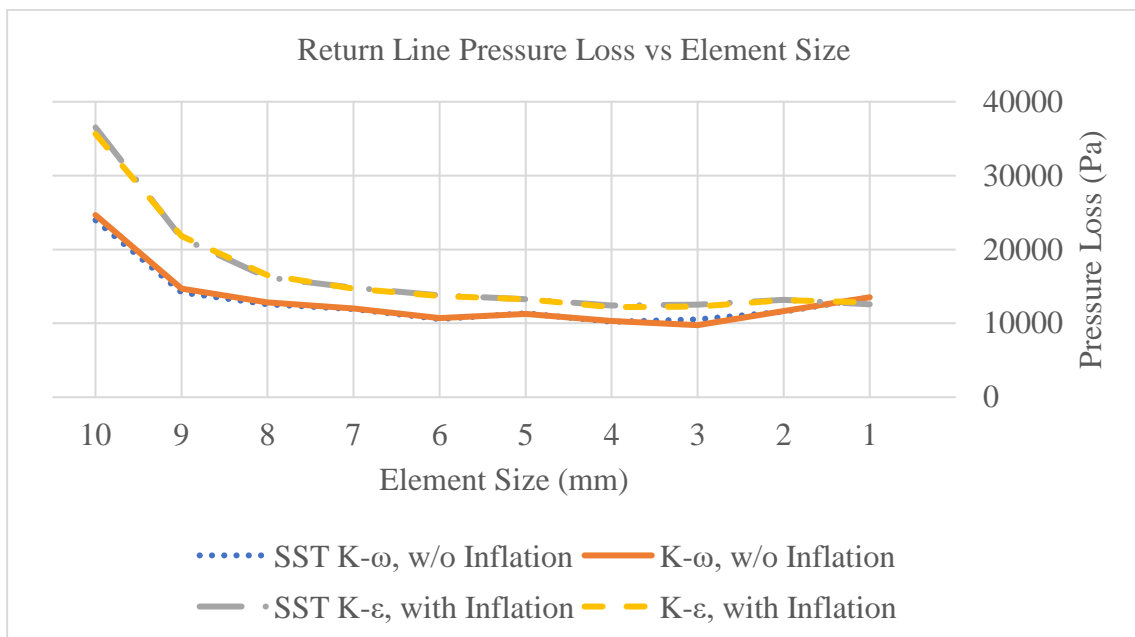
Figure 3-5 Return line pressure loss vs element size curve

Streamlines at the supply line is seen in Figure 3-6. Linear velocity in circulation ring is low compared with the velocity in inlet and outlet regions. Moreover, vortices are seen in inlet region (Figure 3-7) and the tee between the circulation ring and axial channel (Figure 3-8). Besides, static pressure distribution contour is seen in Figure 3-9. Low pressure areas are produced in inlet (Figure 3-10) and joining region (Figure 3-11) due to the turbulent flow regime in those areas.
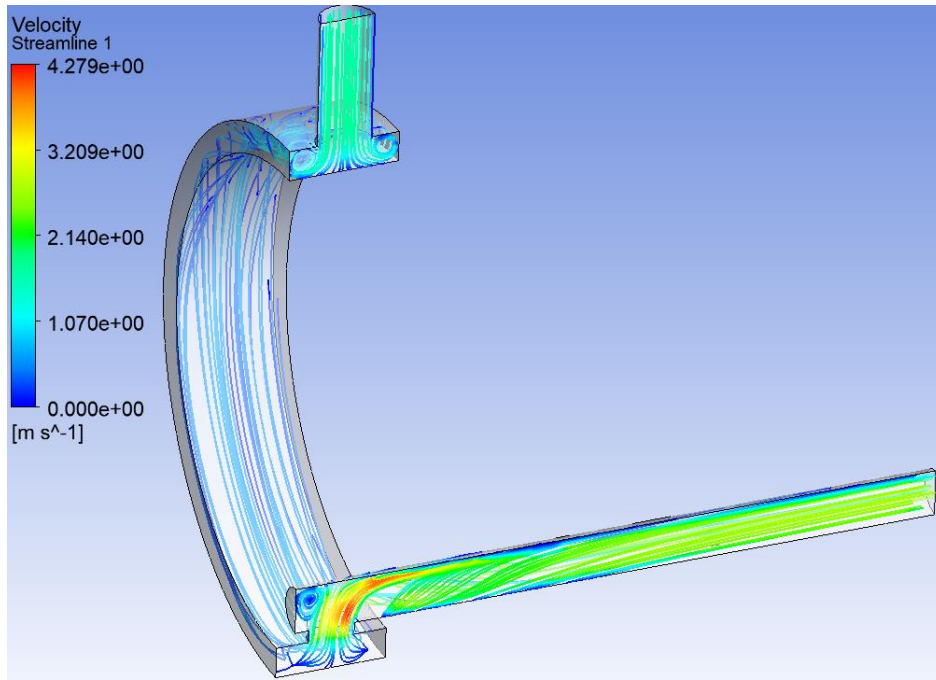
Figure 3-6 Streamlines in supply line
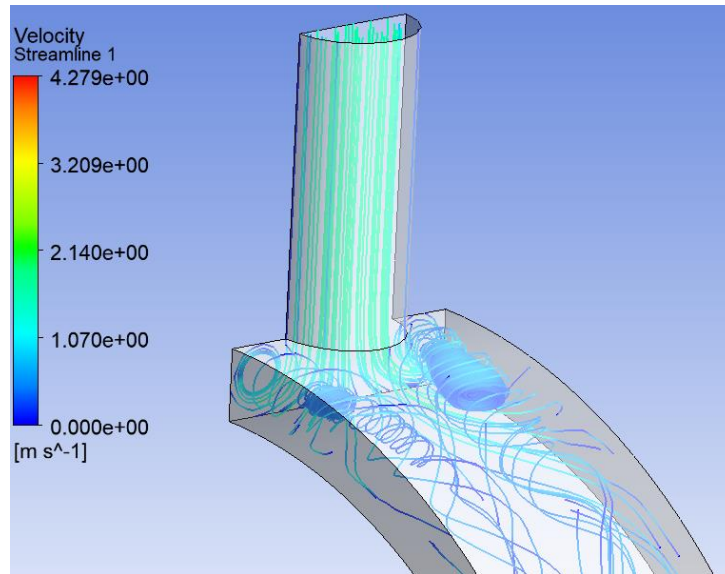
Figure 3-7 Vortex region at separation in supply line
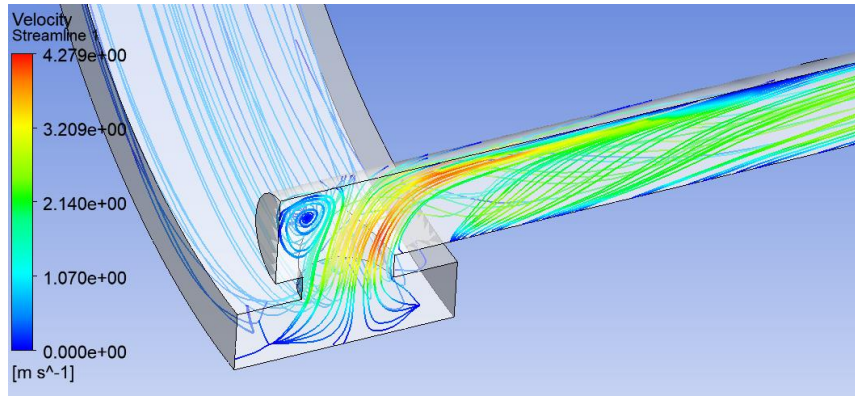
Figure 3-8 Vortex region at joining region in supply line
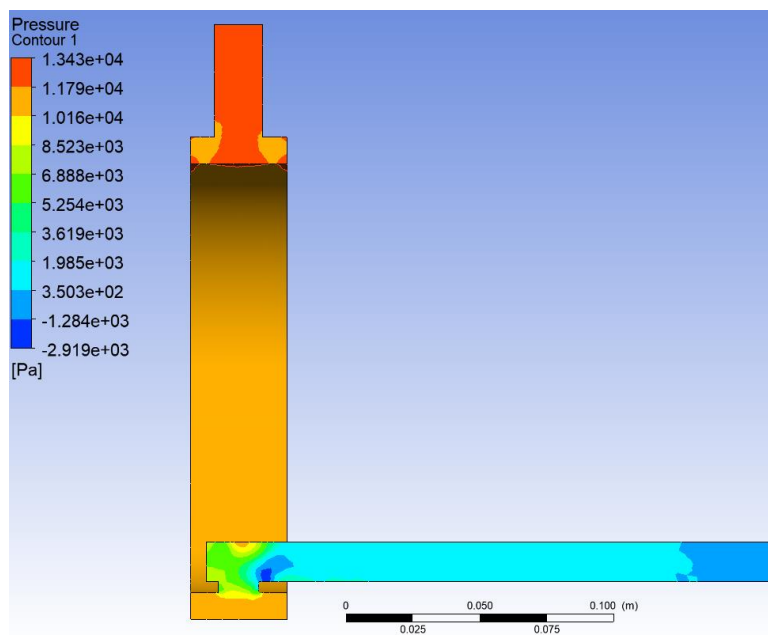
Figure 3-9 Pressure contour in supply line
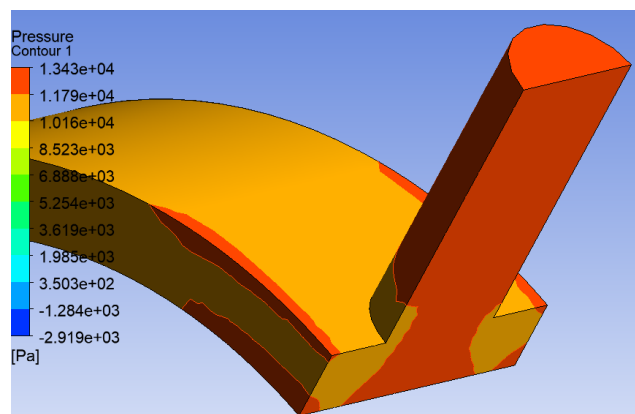
Figure 3-10 Inlet pressure contour in supply line
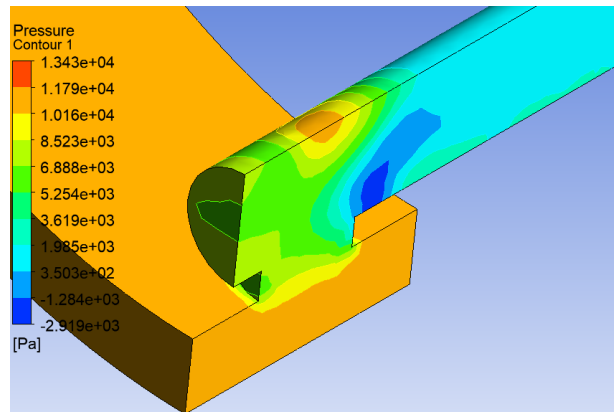
Figure 3-11 Pressure contour at joining region in supply line

Streamlines at the return line is seen in Figure 3-12. Like inlet line, linear velocity in circulation ring is low compared with the velocity in inlet and outlet regions. Most of the turbulent regime is produced in the separation area as seen in Figure 3-13. Pressure contour of the whole flow is seen in Figure 3-15. Most of the pressure loss occurred in the separation region (Figure 3-16) since most of the turbulent flow is produced in this area.

In both lines, most of the pressure loss is produced in the tee between circulation ring and axial channel. This region can be expanded if pressure loss is desired to be lowered in further research.
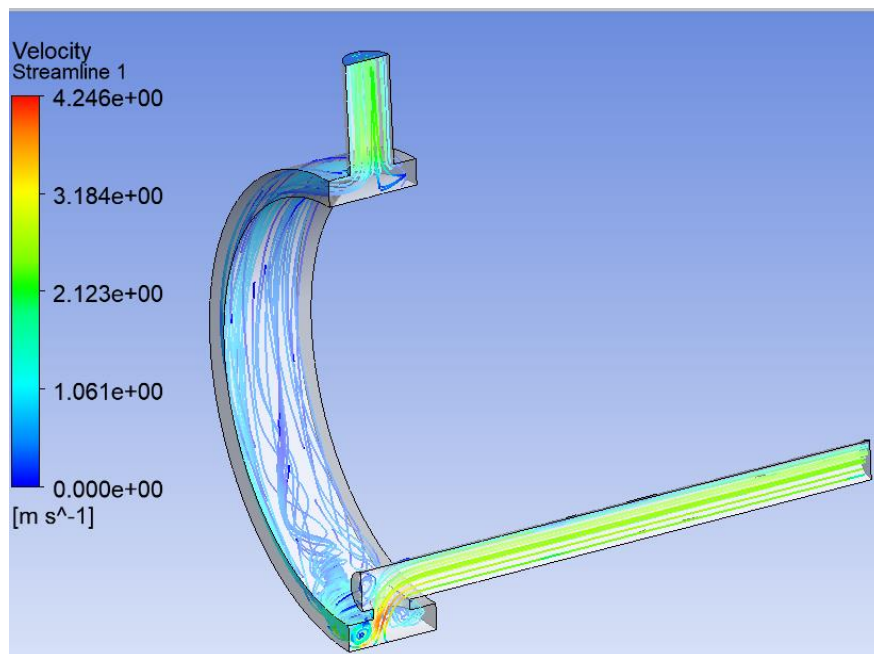
Figure 3-12 Streamlines in return line
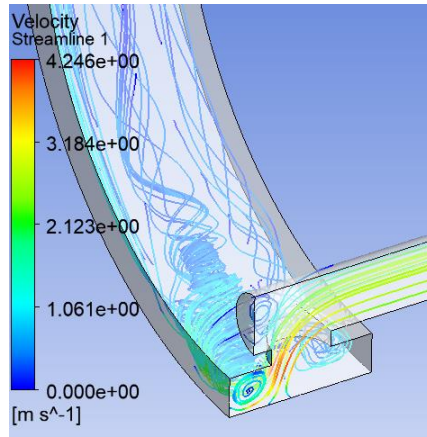
Figure 3-13 Vortex region at separation in return line
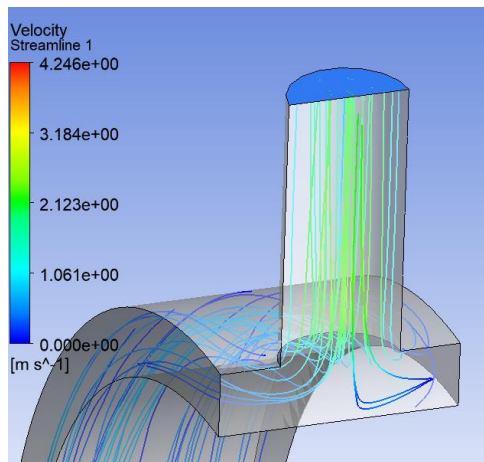
Figure 3-14 Joining region in return line
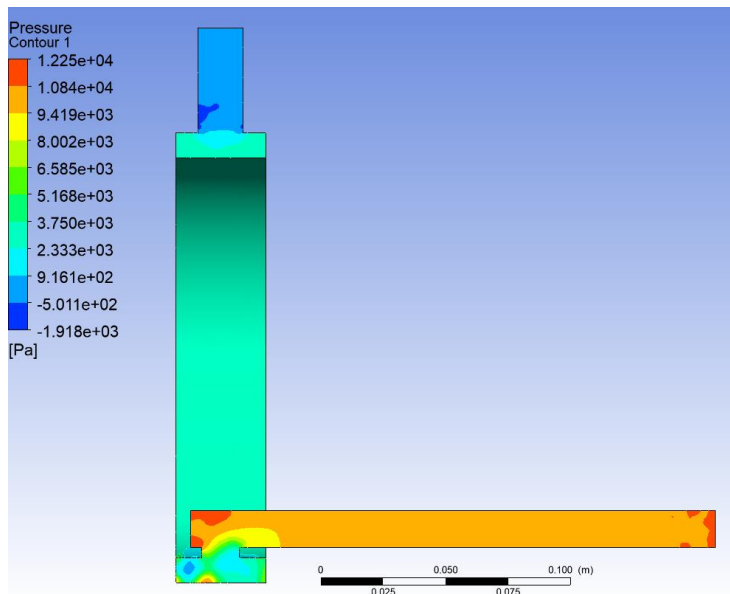
Figure 3-15 Pressure contour in return line

40
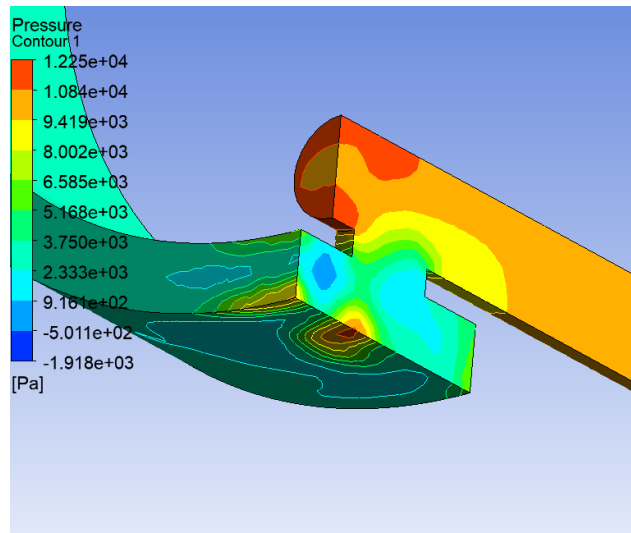
Figure 3-16 Pressure contour at separation region in return line

When the analytical calculations in the preliminary design phase are compared with the CFD analysis results, it is seen that the pressure loss values obtained are close to each other.

Table 3-1 Analytical calculation and CFD pressure loss results comparison

Pressure Loss [bar]	
Analytical	CFD
0.25	0.24

3.2 Material and Surface Engineering

3.2.1 Requirement

Dynamic sealing requires continuous contact between moving parts which causes wear. Dynamic seal movement is basically investigated in three categories: rotary, reciprocal and mixed. In reciprocal and mixed movements, the mating region is a cylinder area. Unlike them, the mating region is a circle in rotary motion, a much smaller area. Since the mating area is smaller in rotary seals, wear increases due to continuously applying almost the same amount of force to a relatively much smaller area. This situation increases the wear rate of the seal and mating material. Compared with the harder materials, the wear rate of the softer materials is much higher. Hence, lip material of dynamic seals must be made of a relatively hard elastomer. As mentioned before, two mating materials apply wear to each other and amount of wear of softer material will be

higher as a rule of thumb. Eventually either seal or rotor will become too worn that impermeability cannot be provided anymore. At this point, worn material should be replaced or repaired. The easiest method is to replace the seal with a new one. Thus, rotary seal is desired to be worn before the rotor. To ensure that, rotor surface must be harder from the seal material. Besides, rotor surface must procure a roughness value to provide impermeability which is also stated in 2.4.1. Seal manufacturer gives an ICD which describes the surface specifications and groove dimensions of mating material (Figure 3-17). With respect to the ICD; hardness value of rotor must greater than 30 HRC, roughness of rotor surface must be lower than 0.4 µm Ra, roughness of seal groove at stator must be lower than 0.7 µm Ra.

Ref.	Description	Dimension
A	Gland Diameter	170.0 +0.1 / -0.0
B	Shaft Diameter	160.0 +0.0 / -0.1
G	Gland Length (min.)	7.0
M	Gland Chamfer Length	0.4 / 0.6
J	Shaft Chamfer Length	3.0 / 3.4
E	Radial Clearance @21°C	0.15
L	Seal Length (installed)	6.35 / 6.71

| Suggested dynamic sealing surface finish is 0.1-0.4 (µm Ra) |
| Suggested static sealing surface finish is 0.4-0.7 (µm Ra) |
| Suggested minimum shaft hardness is 30Rc |
| All non-dimensioned Gland and Shaft Chamfers are 25° |

Figure 3-17 Balseal X625753 ICD [Balseal technical support, personal communication, June 20, 2021]

3.2.2   Basics of Hardness Theory

Hardness is the measure of a material's resistance to localized plastic deformation [33]. It can also be described as the resistance over scratching or carved. If two materials are rubbed together, one of them will be scratched. Likewise, if a hard material with a pointy tip is pressed against a relatively softer material, the softer material will be dented. This phenomenon leads to a testing method of hardness of different materials. If a hard, conical, and pointy object, called as indenter is pressed against different test specimens, it leaves different marks on each specimen. The more the indenter penetrates, the larger the diameter of the dent. Since penetrating depth is directly relevant with the hardness of the test specimen, dent diameters on the test specimens

give information about the hardness of the materials. This phenomenon forms the basis of hardness tests. The most common hardness tests are Rockwell, Brinell and Vickers hardness tests. Steel or tungsten carbide sphere; diamond pyramid; and diamond cone or steel sphere are used as indenter in Brinell, Vickers and Rockwell hardness tests, relatively [34]. Tests are also divided into scales within themselves in order to have a precise measurement for different ranges of hardness values. Rockwell hardness scales are listed from letter "A" to "K" which are using combinations of different intender sizes and different major loads. A diamond cone with a major load of around 150 kg is used in Rockwell C hardness scale tests. Rockwell C scale hardness is used in applications like testing the safety of airplane landing gear, the strength of fasteners, the safety of gas cylinders under accidental impact, and the performance of rotary lawn mower blades.

3.2.3   Material Comparison

Two main metals used in defense industry are compared as rotor material which are aluminum and steel (Table 3-2).

Table 3-2 Rotor material comparison

Rotor Material	Weight	Hardness	Life	Ease of Manufacturing
Aluminum	•			•
Steel		•	•	

The density of aluminum is one-third that of steel. Reducing the weight of each part is important to reduce the total weight of the unit, but reducing the weight of the rotor is of greater importance as it is directly related to reducing the weight of the dynamic part. So, using aluminum is preferable if hardness requirements are met.

The hardness range of aluminum without any surface treatment can also vary depending on the specific alloy and temper of the aluminum. Generally, pure aluminum (aluminum 1100) has a hardness of about 15-30 HB or 16-23 HRB which are lower than 1 HRC. Aluminum alloys, which are the most used form of aluminum, have varying hardness depending on their alloy composition and temper. For example, the widely used aluminum alloy AA 6061-T6 has a hardness of about 95 HB, while AA 2024-T351 has a hardness of about 120 HB, which are also lower than 1 HRC. Thus, if aluminum is

intended to be used, a proper surface treatment method must be used to increase the surface hardness.

Steels, on the other hand, have higher hardness values compared to aluminum. For example, AISI 4140 QT has a hardness value of 316-375 HB (34-41 HRC), 1.2379 cold work tool steel has a hardness value of 50 HRC, 17-4 PH has a hardness value of 46 HRC. High Speed Steels also have hardness values over 60 HRC. Most of the hard steels have high carbon density since carbon content increases hardness and brittleness in steels. But high carbon steels have also lower corrosion resistance than stainless steels which is not demanded for a hydraulic unit [35]. If steel is selected as the rotor material, it will either be stainless steel, or a suitable coating will be applied to provide corrosion resistance.

Considering that wear is the bottleneck in terms of life, it is directly related to the hardness and roughness of the rotor surface. Fatigue may be another consideration in terms of life. Steel has an infinite life assumption under cyclic load which aluminum has not when considering fatigue as a life parameter, but wear would be the main problem since internal stress values caused by fatigue can be decreased by adjusting the wall thickness of material.

Although high surface hardness leads to long life, hard materials are more difficult to be machined. As mentioned above, harder material scratches or cut softer materials. HSS and tungsten carbide are some of the commonly used materials as CNC milling cutter. But if rotor is desired to be made of hard materials like HSS or 1.2379, milling cutter should be much harder. Also, the cutter would be blunted in a short period of time and changing it would cause extra manufacturing cost.

Hence, using aluminum would be advantageous in terms of weight and ease of manufacturing if a proper surface hardening method is applied.

3.2.4 Surface Treatment Methods

Various methods are applied to increase the surface hardness. The surface treatment method to be selected must provide a decent surface roughness or must be suitable for a

second surface treatment method like grinding or polishing. The final product must also satisfy corrosion resistance. The most common methods which may be suitable for that purpose are listed below.

- Anodizing: Anodizing is an electrochemical process that creates a layer of aluminum oxide (Al_2O_3) on the surface of aluminum which increases the surface hardness up to 60-65 HRC [36]. Since this layer is harder than the underlying aluminum, it provides improved wear resistance.

- Hard anodizing: Hard anodizing is a variation of anodizing that produces a thicker and harder oxide layer. This process is typically used when greater wear resistance is required.

- Electroplating: Electroplating is a process that involves coating the aluminum with a layer of another metal, such as nickel or chromium. These metals are harder than aluminum and provide increased wear resistance.

- Thermal spraying: Thermal spraying involves spraying a coating material, such as ceramic or metal, onto the surface of the aluminum. This process can produce a very hard and wear-resistant coating.

- Nitriding: Nitriding is a process that involves diffusing nitrogen into the surface of the aluminum. This creates a hard nitride layer on the surface that provides improved wear resistance.

- Shot peening: Shot peening involves bombarding the surface of the aluminum with small metal particles. This process creates compressive stresses in the surface of the aluminum, which can increase its hardness and resistance to fatigue.

- Hard chrome plating: Hard chrome plating is a surface treatment process that involves depositing a layer of chromium onto a metal substrate to improve its wear and corrosion resistance, and surface hardness. The process typically involves cleaning and pretreating the substrate surface, applying an electrolytic solution containing chromium ions, and passing an electrical current through the solution to deposit the chromium onto the substrate. Hard chrome plating is highly wear-resistant, with a hardness of up to 70 HRC, and provides excellent resistance to corrosion, abrasion, and erosion, making it commonly used in industrial applications. However, due to its toxicity and environmental concerns,

alternative surface treatment methods are increasingly being used as a replacement.

- Electroless nickel plating: Electroless nickel plating, also known as autocatalytic nickel plating, is a process of depositing a layer of nickel onto a substrate without the use of an external electrical current. This is achieved through a chemical reaction between a reducing agent and a nickel salt solution, which produces a layer of nickel-phosphorus or nickel-boron on the substrate surface. Electroless nickel plating is commonly used in industrial applications for its excellent wear resistance, corrosion protection, and uniformity of deposition, making it ideal for coating complex and irregularly shaped surfaces.

- Plasma spray coating: Plasma spray coating is a process used to deposit a coating material onto a substrate using a plasma torch. The process involves heating the coating material to a molten or semi-molten state, then spraying it onto the substrate using a high-velocity gas stream. The resulting coating is typically very dense and can have a variety of properties, depending on the coating material and the process parameters used. In plasma spray coating process, metallic materials like nickel, cobalt, tungsten can be used as well as ceramics materials. Thus, high hardness values can be achieved with this method.

- High Velocity Oxygen Fuel: High Velocity Oxygen Fuel is a thermal spray process that uses a high-velocity flame to propel small particles of coating material onto a metal substrate, creating a strong and tightly bonded coating. Although it appears quite similar to plasma spray coating, the main difference between HVOF and PSC is the heat source used to melt and propel the coating material. In HVOF, the heat is generated by a combustion process, while in plasma spray coating, an electric arc is used to create a high-temperature plasma that melts and accelerates the coating material.

- PVD/CVD Coatings: PVD (Physical Vapor Deposition) and CVD (Chemical Vapor Deposition) are two common types of thin film coating technologies used to deposit a wide range of coatings onto a variety of substrates. PVD coatings are formed by vaporizing a solid metal or alloy using a high-energy source, while CVD coatings are formed by introducing a gas or vapor containing the desired coating material into a heated reaction chamber. Both PVD and CVD

46

coatings offer many advantages over traditional coating technologies, including precise control over coating thickness and composition, high coating quality, and the ability to deposit coatings onto complex geometries and small parts. These coatings are widely used in various industries, such as automotive, aerospace, medical devices, and electronics, to enhance the properties and performance of materials and components [37].

- Composite additive coatings: Composite coatings are made of two or more materials which are reinforcement and matrix material. This type of coating can be applied using a variety of techniques such as thermal spray, electroplating, and electrodeposition. The outcome of composite additive coatings is to increase hardness, wear resistance, corrosion resistance, and thermal stability. Examples of composite additive coatings include metal-matrix composites (MMCs), ceramic-metal composites (CMCs), and polymer-matrix composites (PMCs).

- Carburizing/carbonizing: Carburizing, a widely used surface-hardening process in various industries, is carried out by introducing carbon into the surface of a low-carbon steel component using different methods such as vacuum, gas, liquid, and pack carburizing. This method increases hardness and fatigue resistance of steel. One of the advantages of this method is increasing surface hardness without decreasing the ductility of the core [38].

Despite most of methods stated above seems suitable, in "Treatments of Metal Surfaces to Improve Bal Seal Spring-Energized Seal Performance in Dynamic Applications" technical report [35], manufacturer highlights four of them, which are "Hard Anodizing", "Chrome Plating", "Electroless Nickel Plating" and "Plasma Spray Coatings or High Velocity Oxygen Fuel".

While these four methods are compared, another aspect came up, which is plating thickness. For most Trelleborg dynamic seals, it is stated that hardness depth of shaft material has to be greater than 0.3 mm. This requirement may not be taken into account, but it may be used as a selection factor among these four methods.

3.2.4.1 Hard Anodizing

Aluminum and its alloys have become widely used in various engineering applications due to their desirable properties, such as high strength-to-weight ratio, corrosion resistance, and low density. However, aluminum and its alloys are susceptible to wear and corrosion, which can limit their service life. One effective surface treatment to improve the wear and corrosion resistance of aluminum is hard anodizing. Hard anodizing is an electrochemical process that creates a hard and wear-resistant oxide layer on the surface of aluminum, increasing its hardness and improving its corrosion resistance. The thickness of the anodized layer can be controlled by adjusting the process parameters, such as voltage, current density, and anodizing time. Furthermore, the surface roughness of anodized aluminum can also be controlled to achieve the desired surface finish. Roughness value of AA6061 alloy after hard anodizing can be decreased to 0.074 µm Ra. Several studies have investigated the effect of hard anodizing on the hardness, roughness, and thickness of the anodized layer on aluminum alloys. These studies have shown that hard anodizing significantly increases the hardness and thickness of the anodized layer while reducing the surface roughness of aluminum alloys. Hardness value of AA6061 can be increased to 45 to 68 HRC.

Military standard for hard anodizing is specified as MIL-A-8625F, Type III, Hard Anodic Coatings, which is widely used in Turkey. Nominal thickness of coating is specified as 0.002 inch (0.051 mm) in chapter 3.7.2.1. Average coating thickness required is stated as 0.0003 to 0.0008 inch (0.0076 to 0.0203 mm) for hard anodizing for Bal Seal, which is applicable. Also, it states that Type III coatings cannot be applied to aluminum alloys with a copper content higher than 5% and silicon content higher than 8% in chapter 3.4.3, Type III coatings. AA6061-T6 is a widely used aluminum alloy in military products having 0.4% copper and 0.8% silicon which suits the requirement of the standard.

After processing, a relatively coarse surface is resulted, and it has to be grinded after the coating. Upon discussions with coating companies, it was decided not to apply hard anodized coating, even though it is theoretically possible, since there is no company capable of performing this process.

3.2.4.2 Chrome Plating

Chrome plating is a popular surface treatment technique used to improve the hardness, wear resistance, and corrosion resistance of metallic substrates. In particular, hard chrome plating on aluminum has gained significant attention in the automotive and aerospace industries due to the lightweight nature of aluminum and the need for high-strength components. The hard chrome plating process involves the electroplating of a thin layer of chromium onto a metallic substrate. The thickness of the chrome layer can vary depending on the specific application and ranges typically from 0.020 to 0.127 mm. The hardness of the chrome layer is typically measured in HRC, which ranges from 65 to 70 HRC [39].

In Turkey, hard chrome plating is mostly applied on steel surfaces. This process involves electroplating which requires a conductive surface. Aluminum has a non-conductive oxide layer on its surface, and it forms rapidly after machining. To overcome this, the aluminum substrate to be plated undergoes a pre-process including cleaning and chemically etching to remove that oxide layer. A chrome plating company capable of performing this pre-treatment could not be found. Therefore, the direct chrome plating process was carried out on an AA7075-T6 cylindrical specimen without pre-treatment. Although sufficient hardness (53 HRC) is achieved at the end of the process, the coating lack of penetration into the metal (Figure 3-18). Hence, like hard anodizing, even though it is theoretically possible, since there is no company capable of performing this process, this option is eliminated.
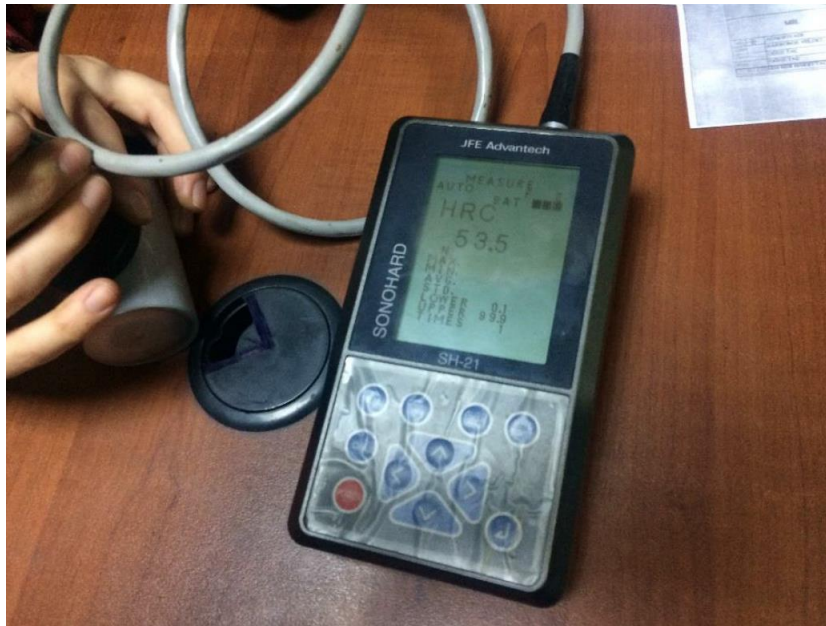
Figure 3-18 Hard chrome plating hardness measurement on AA7075-T6

3.2.4.3 Electroless Nickel Plating

Electroless nickel plating (ENP) is a widely used surface treatment technique in the industry due to its excellent wear resistance, corrosion resistance, and uniformity of deposit. ENP on aluminum has become increasingly popular in recent years due to the lightweight nature of aluminum and the need for high-strength components. The ENP process involves the deposition of a nickel-phosphorus (Ni-P) alloy onto a metallic substrate through a chemical reaction, without the need for an external power source. The thickness of the ENP layer can vary depending on the specific application and ranges typically from 0.001 to 0.015 inches (0.0254 to 0.381 mm). The hardness of the ENP layer is typically measured in HRC, which ranges from 58 to 62 HRC for a 10% phosphorus (P) deposit and 62 to 65 HRC for a 5% P deposit. Additionally, the surface roughness of the ENP layer is also an important consideration, with roughness values typically in the range of 0.2 to 0.5 μm Ra [40]. ENP has the advantage of not requiring a conductive surface since the process does not involve electroplating. Hence, a pre-process is not needed like chrome plating. Another advantage of electroless plating technique is uniformity [41] (Figure 3-19). Achieving uniform thickness in electrodeposited nickel is a challenging issue due to uniform current distribution. But in electroless plating, current is not involved in the process. By this means, all surfaces of even complex parts have almost the same thickness because they have been exposed to the chemical bath for the same time.
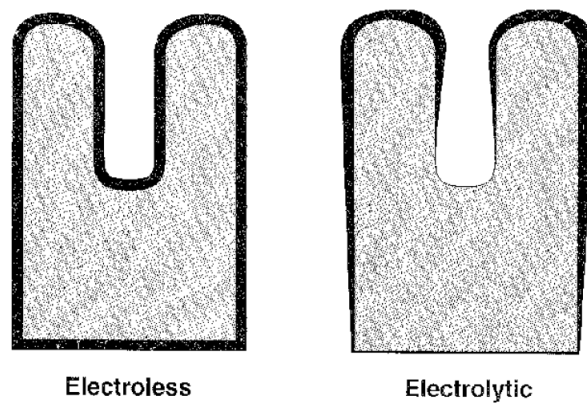
Figure 3-19 Comparison of deposit uniformity [41]

In military applications, ENP is applied according to MIL-C-26074. Class 2 defines "Heat treated to obtain required hardness: May be used on all metals not affected by heating to 500 F and above", which is applied for high surface hardness. On the other hand, grades, which are listed as A, B and C define the coating thickness from 0.0005 inch (0.00125 mm) to 0.0015 inch (0.05 mm) minimum thickness.

Corrosion resistance is another important factor since the material will be constantly exposed to water. In electroless plating, porosity has an obvious effect on the corrosion resistance [42]. In order to reduce porosity, it is necessary to increase the bath time, and accordingly the coating thickness. Porosity of the plating applied on AA6061 decreases to zero at a coating thickness at 0.025 mm. Thus, Grade A (0.0010-inch, 0.025 mm) in MIL-C-26074F is sufficient in terms of corrosion resistance. On the other hand, as the coating thickness increases, the surface roughness first decreases to Ra 0.2 μm and then increases to Ra 0.8 μm after 0.02 mm coating thickness.

High coating thickness decreases porosity, but surface roughness increases over some point. So, one of the solutions below can be applied to meet both requirements.

- Finding an optimum coating thickness that provides sufficient porosity and roughness.

  Optimum coating surface roughness is achieved around 0.020 mm coating thickness which is reached in 60 min plating time. At that point, the porosity is

not zero, but it is quite low. In MIL-C-26074 chapter 3.3.2, 0.0010-inch (0.026 mm) plating thickness is recommended for aluminum-based alloys.

- Machining the surface after plating

  In order to apply some machining operation like grinding, diamond turning or polishing, binding force between the coating and the substrate must good enough. More or less, this operation would weaken the bond between the coating and the substrate. So, this application should be considered as the last option.

- Grinding the surface before plating

  Research of Peter Xia [43] et al showed that initial roughness of the substrate affects the final surface quality of the coated product. If initial roughness of the AA6061 aluminum alloy is above 0.3 µm Ra, roughness of the final product decreases. On the other hand, if the substrate roughness is below 0.3 µm Ra, it increases (Figure 3-20). As a result, it seems that the best roughness of ENP coated on AA6061 aluminum alloy is 0.3 µm Ra which meets the requirement, 0.4 µm Ra.
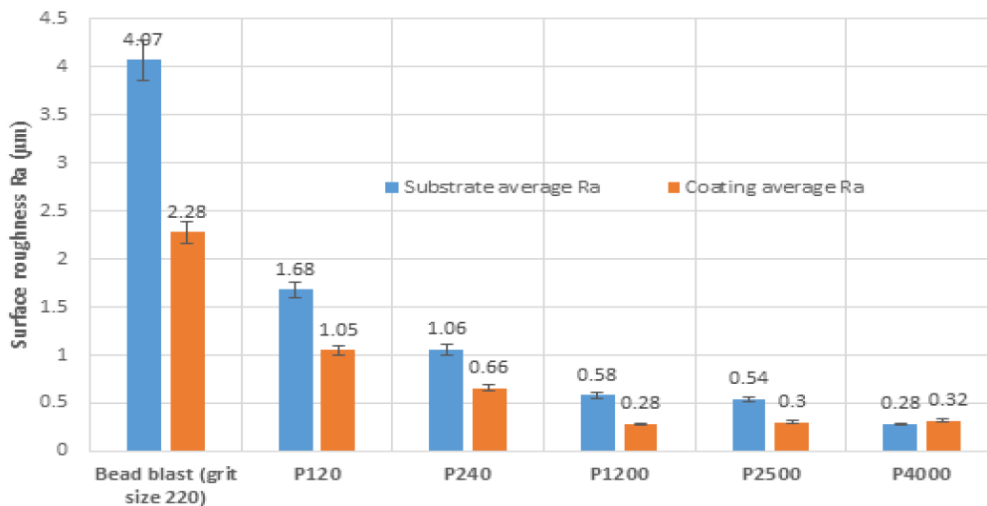
Figure 3-20 Initial and Final Roughness Results of ENP on AA6061 Specimens [43]

As a result, ENP appears to be a suitable coating to be applied on aluminum alloy. In MIL-C-26074, Class 2 is stated as the hardness coatings thanks to the heat treatment in chapter 3.4.2.1. On the other hand, Grade A supplies a suitable thickness value (0.0010-inch, 0.025 mm) which is optimum for surface roughness and sufficient for corrosion resistance regarding low porosity. Machining the base surface below 0.3 µm Ra would eliminate the post machining processes. Moreover, the whole material would be coated to provide corrosion resistance on all surfaces of the rotor.

3.2.4.4 Plasma Spray Coating or High Velocity Oxygen Fuel

Plasma spray coating (PSC) is a widely used surface treatment technique in the industry due to its ability to produce dense, high-quality coatings with excellent wear resistance, corrosion resistance, and thermal insulation properties. PSC on aluminum has become increasingly popular in recent years due to the lightweight nature of aluminum and the need for high-performance components. The PSC process involves the deposition of a molten material onto a metallic substrate through the use of a plasma arc. The thickness of the PSC layer can vary depending on the specific application and ranges typically from 0.003 to 0.015 inches (100 to 300 µm) [44]. The hardness of the PSC layer is typically measured in HRC and can vary depending on the specific material used, ranging from 20 to 70 HRC [45].

High Velocity Oxygen Fuel (HVOF) is a surface coating technique that is known for its ability to produce high-quality coatings with exceptional wear and corrosion resistance properties. HVOF coatings on aluminum have become increasingly popular in recent years due to the lightweight nature of aluminum and the need for high-performance components. The HVOF process involves the combustion of a mixture of oxygen and fuel gases in a high-pressure chamber, which accelerates and heats the coating material to high velocities. The coating material is then deposited onto the substrate at high speed, resulting in a dense, high-quality coating. The thickness of the HVOF coating can vary depending on the specific application and ranges typically from 0.002 to 0.015 inches (50 to 500 µm) [46]. The hardness of the HVOF coating is typically measured in HRC and can vary depending on the specific material used, ranging from 50 to 70 HRC [47]. A very rough surface is achieved at the end of the process, but roughness value can be decreased down to 0.1 µm Ra by grounding.

Both methods involve the use of high temperatures to melt the coating material before deposition. In HVOF, the coating material is heated through the combustion of a mixture of oxygen and fuel gases, while in PSC, the coating material is melted through the use of a plasma arc. Also, both techniques result in coatings with high density and excellent adhesion to the substrate. The high velocities and temperatures involved in both processes create a strong bond between the coating material and substrate, resulting in a high-quality coating. Moreover, in both techniques, various substrate materials like steel, aluminum, titanium, nickel-based alloys and various coating materials like chromium oxide, aluminum oxide, tungsten carbide, cobalt-chromium, and nickel-chromium.

The coating hardness varies depending on the material used but it can be higher than 70 HRC. If ceramic coating is applied, 90 HRC can be achieved. Besides, coating thickness can reach up to 0.3 mm. That property may be needed if a Trelleborg seal is wanted to be used.

The surface is extremely rough after coating. Therefore, as a general practice, grinding is done, and the surface is ground until the desired surface roughness is achieved.

HVOF coatings have been shown to provide excellent corrosion protection to a range of substrates, including aluminum alloys, steels, and titanium alloys. On the other hand, PSC coating is a low-pressure spray process that produces a highly porous and rough coating with low adhesion and moderate hardness. PSC coatings are typically ceramic or metal-ceramic composites, such as alumina, zirconia, or titania. PSC coatings have been shown to provide moderate to good corrosion protection to substrates, including aluminum alloys, steels, and titanium alloys. Considering this information, the HVOF method was considered more appropriate from a corrosion point of view. Since HVOF is a type of coating which is applied with a gun, it cannot be applied to all the surfaces. Even if it is possible to be applied, it is not necessary to be applied to the surfaces which is not exposed to friction. But all the surfaces must be coated in order to have corrosion resistance. Hence, pre-coating like alodine, electroless nickel, anodizing, etc. can be applied before the HVOF coating process.

Bal Seal recommends chromium oxide, aluminum oxide and tungsten carbide as coating material. All of them meet the requirements stated above but tungsten carbide offers greater ductility and flexibility. A structure exposed to shock and impact needs to be flexible and tough to avoid damage. Shock is one of the technical requirements, so, tungsten carbide would be an appropriate choice for coating material.

3.2.5   Selection

Although all these four methods are theoretically suitable applications, hard anodizing and chrome plating are not feasible within the means of implementer facilities. Among the remaining two options, which are ENP and HVOF, the most suitable options is appeared to be ENP for the following reasons. ENP is applied chemically at all the surfaces in one operation. On the other hand, pre-coating is required in HVOF to ensure corrosion resistance. Besides, the surface to which HVOF is applied needs to be ground after the coating process. On the other hand, the operational cost of HVOF is much higher than that of ENP in terms of money and time.

As a result, these steps are decided to be followed during surface treatment process:
- The rotor will be manufactured from AA6061-T6 aluminum alloy regarding structural concerns.
- Outer surface of rotor will be grounded or machined to 0.3 µm Ra.
- MIL-C-26074 Class 2, Grade A will be applied to the rotor.

3.3   Final Geometrical Design

As shown in "2.2 Initial Geometrical Design", conceptual geometry of RU consists of rotor, stator, dynamic seals, and bearings (Figure 3-21). Although geometry seems simple, a lot of detail is hidden in design such as material selection, surface engineering, seal selection, flow geometry, structural considerations. Most of them are determined above which constitutes input for detailed geometrical design. Geometrical design is one of the design methods as mentioned in Table 2-1. This design method is used in meeting the requirements of the number of channels, mechanical dimensions, operating pressure, leakage rate, frictional torque and structural considerations. The main design method is not geometrical design for some of them like pressure loss and leakage rate

since they are directly dependent on the seals used but the way seals are used in geometry is in the content in design method. Apart from that, pressure loss is calculated using CFD analysis, but the flow geometry is an input for detailed geometrical design. On the other hand, some of the design inputs are directly related to the geometrical design like number of channels and mechanical dimensions. The final geometrical design is made regarding the outputs of other design methods, requirements of RU, requirements of the standard parts and COTS products, ease of manufacturability and assembly, material cost and robustness.
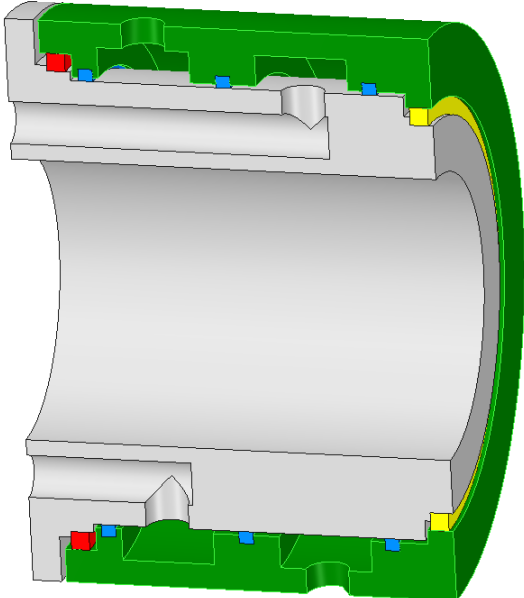
Figure 3-21 Initial geometry of RU

First, the stator is divided into parts unlike the initial design. Dynamic seal (Balseal X625753) consists of PTFE ring, stainless steel spring and aluminum alloy locking ring. Aluminum locking ring and PTFE ring are too rigid structures to be bent and inserted into the housing. Since Balseal provides one-sided sealing, at least four seals are used. Two seals facing each other are used for each channel as seen in Figure 3-22. Outer seals prevent external leakage and internal seals prevent internal leakage. External leakage of 0.1 ml/h is one of the technical requirements and it certainly must be met. On the other hand, internal leakage will not be measured but it must be avoided not to reduce the performance of the unit. If internal leakage occurs, incoming and outcoming liquids are mixed and the temperature of incoming (to the unit to be cooled) liquid rises. At that point, the cooling capacity of the liquid decreases and therefore performance of

the unit decreases also. So, although it is not a must and it will not be measured, internal leakage must be avoided as well.
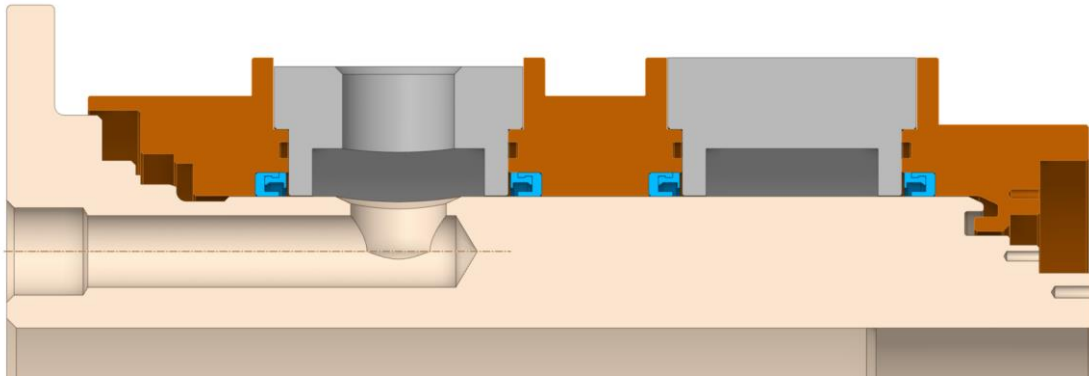
Figure 3-22 Seal configuration

Drainage channels are added to measure the leakage rate and drain the accumulated liquid. Drainage configuration is shown in Figure 3-23. In general, secondary seals are used which can withstand less pressure and cause less friction, but this drainage design utilized gravity. Since RU is meant to be used in radar, its rotation axis should lie on vertical axis. It is assumed that the flow rate will be so small such that drainage channels with small diameters and small basins would be sufficient. In the upper drainage region, liquid leaks upwards and passes through the drainage channel. Also, a V-ring is used for two reasons: to restrain contamination from outside and to prevent external leakage in shock or negative g conditions. The middle drainage is the most appropriate use since drainage channel is trapped between two seals. In lower drainage, a pool-like geometry is designed where the liquid can accumulate with the help of gravity. Also, a V-ring is used to prevent contaminant and excess liquid passing through. In the final product, these three drain channels united to be connected to the drainage line which should be monitored in order to control the MTBR. But in performance tests, they need to be separated to be monitored one by one. So that root cause of the problem can be found.
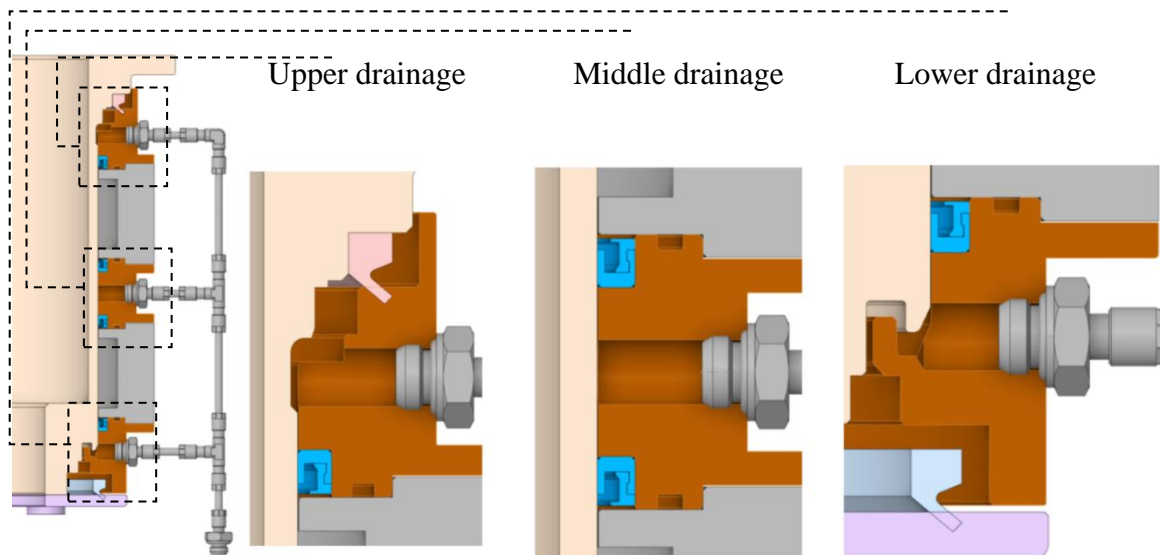
Figure 3-23 Drainage configuration

Static sealing between stators is provided with 70 shore 177.47x2.62 (inner diameter x cross-sectional diameter) NBR o-rings (Figure 3-24).
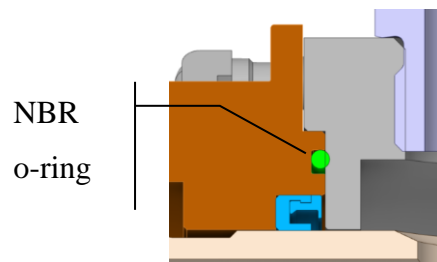
Figure 3-24 Static sealing

The flow geometry was designed by adhering to the dimensions obtained from the CFD analysis results (Figure 3-25). Additional pressure drops due to manufacturing requirements, imperfections caused by manufacturing or assembly, surface quality and the structure of the hydraulic elements used were included in the safety factor when evaluating the CFD analysis results. ½ inch BSPP male nipples are used for hydraulic interface since inner diameters are almost same with the flow inlet and outlet diameter.

Inlet

Outlet
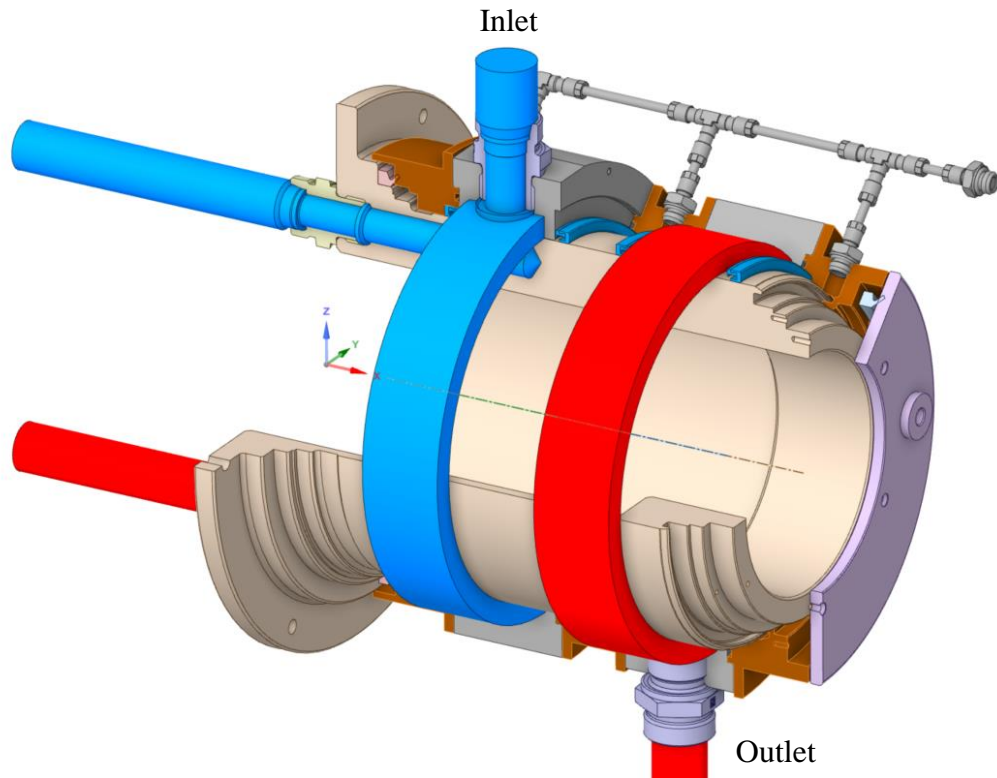
Figure 3-25 Final flow geometry in detailed design

After the geometric design reached sufficient maturity, the mass of the structure was calculated as 11.6 kg. During this calculation, the rotor and stator were defined as aluminum alloy; seals as a combination of PTFE, aluminum alloy and stainless steel; fasteners as steel; o-rings and v-rings as NBR, drainage hoses as polyurethane and finally the drive pin as steel in the CAD program and the mass and center of gravity information was obtained. The whole structure is fixed from stators and bearings hold the rotating parts. Approximately 88% of the weight of these rotating parts, calculated as 4.36 kg in total, is made up of the rotor, while the rest consists of hydraulic fittings (3%), aluminum cover (7%), fluid (2%) and fasteners. As mentioned above, the bearings will carry the rotor in the vertical position. After determining the placement of the bearings in the structure, the position of the center of gravity relative to the bearings was shown on the free body diagram (Figure 3-26) and the load distribution was calculated.

There are three load configurations in service life: normal operation, shock, and vibration. Gyroscopic effect, centrifugal force, water hammer effect, possible orientation changes are neglected. Bearings have three different load capacities in two cases. Load capacities are radial, thrust, and moment where load cases are dynamic and

static. Static case indicates the highest load that bearing can withstand instantaneously and these loads capacities are non-brinell limits based on rigid support from the shaft and housing. That means plastic deformation does not occur between balls and internal surfaces of the raceways up to these limits. On the other hand, dynamic capacities are based upon one million revolutions in L10 life [48]. Normal operation and vibration load conditions must be evaluated regarding the dynamic capacities since they are continuous loads. On the other hand, shock load condition is the maximum load simulating mine explosion which occurs rarely. Thus, shock load can be compared to the static capacity of bearings.
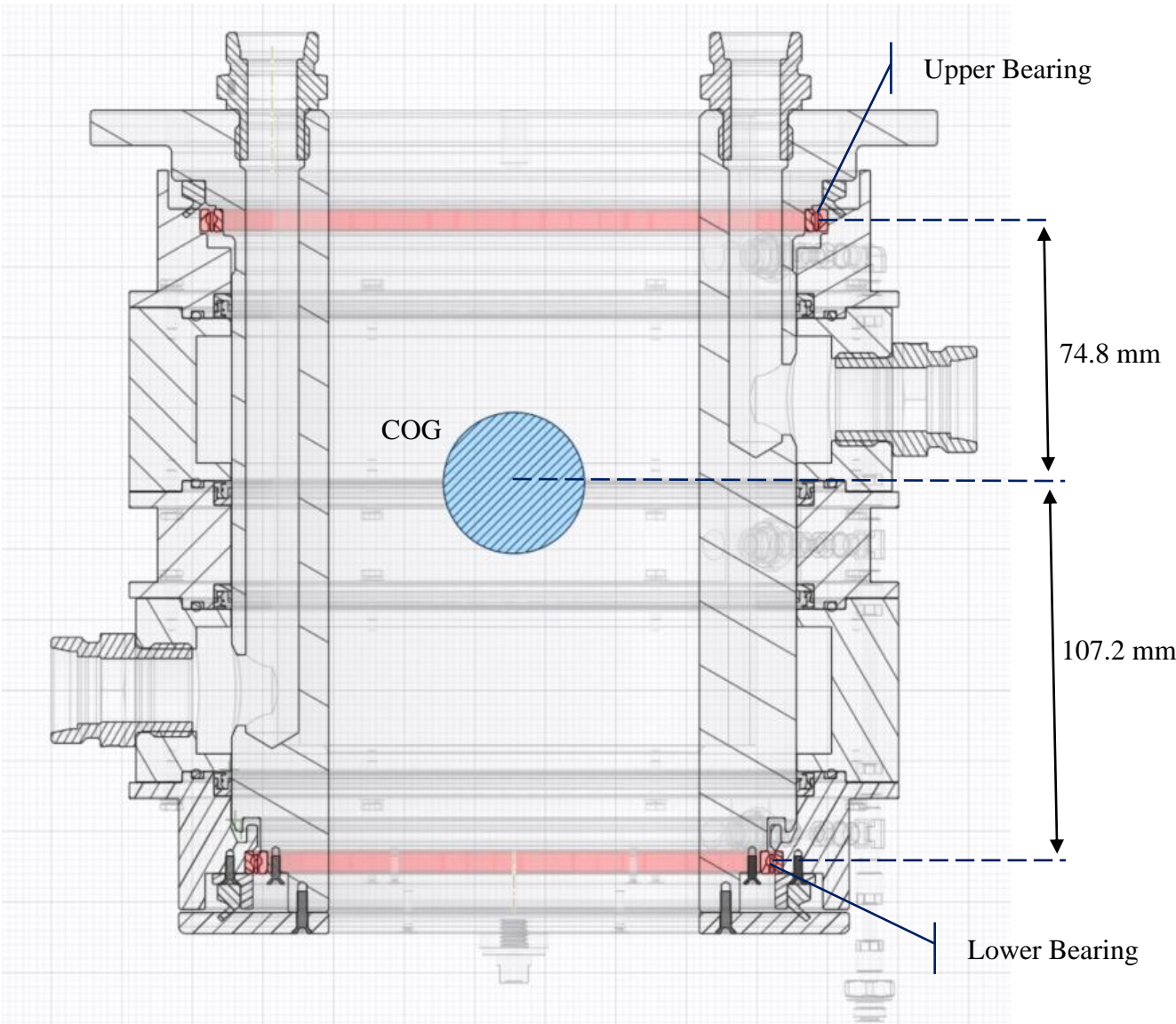
Figure 3-26 Free body diagram of RU

As seen in Figure 3-26, COG is closer to the upper bearing which means higher bearing is subjected to the higher radial loads. Since the stator is divided into multiple parts, there will be an accumulation of tolerances in the axial direction during assembly. Therefore, setting the axial distance between two bearings perfectly will be very difficult in terms of production, so giving one of the bearings freedoms in the axis of rotation will facilitate production and assembly. In this case, only one bearing will carry the thrust load. Since there is not a big difference between the dimensions of the bearings, it is assumed that their load capacities are very close to each other. Since the COG is close to the upper bearing, the upper bearing will carry most of the radial load. To avoid combined radial and thrust loads on a single bearing, the thrust load is carried by the lower bearing. In this case, only the thrust load is analyzed when evaluating the dynamic load condition and the radial and thrust loads are analyzed when evaluating the static load condition. The loads calculated in normal and shock conditions are shown below (Table 3-3). Also, since there is a possibility of changing the rotor material from aluminum to steel according to the results of the tests, care has been taken to select bearings that can withstand this load as well. Although the loads were calculated with reference to the aluminum rotor, the safety factor was kept above 4.5 because steel has three times the aluminum density. In this way, when steel is chosen as the rotor material, the safety factor will be reduced to 1.5. This safety factor is considered to cover the assumptions mentioned above (gyroscopic effect, centrifugal, etc.).

Table 3-3 Bearing loads

| | Loads applied on bearings (N) | | | |
| | Normal | | Shock | |
	Radial Force	Thrust Force	Radial Force	Thrust Force
Upper Bearing	0	0	1007,717697	0
Lower Bearing	0	42,7716	703,1463033	1710,864

Due to mounting constraints, the bore diameter of the upper bearing must be larger than the seal diameter of 160 mm (6.3 in) and the lower bearing must be smaller. Also, the inner diameter of the lower bearing must be larger than 100 mm (3.9 in) and the outer diameter of the larger bearing must be smaller than 280 mm (11 in) in order for the unit to fit in the envelope. For the upper bearing, a bearing with a bore diameter of 6.5 in. was selected because the load capacities of the closest bearing with a diameter larger than 6.3 in. In the Kaydon bearing catalog exceeded the calculated loads. It is important

that the inner diameter of the lower bearing is as large as possible in order to ensure that the inner diameter of the rotor is large. Although 6 inches is the closest value to 6.3 inches, after taking into account the distance required for the bottom drainage basin, the 5.5-inch bearing was selected based on the load capacities.

Table 3-4 Safety factors of bearings for aluminum rotor

	Dynamic capacity (N)		Static capacity (N)		SF, Normal		SF, Shock	
	Radial Force	Thrust Force	Radial Force	Thrust Force	Radial Force	Thrust Force	Radial Force	Thrust Force
Upper Bearing	4452,67	7339,56	9118,85	22774,88	N/A	N/A	9,05	N/A
Lower Bearing	4038,98	6583,36	7784,38	19394,23	N/A	153,92	11,07	11,34

A gap is left between the rotor and the stator in the axial direction to provide axial freedom for the upper bearing. On the other hand, after the lower bearing has been installed, it is tightened in place with a steel ring to ensure that the system is axially in the correct position.
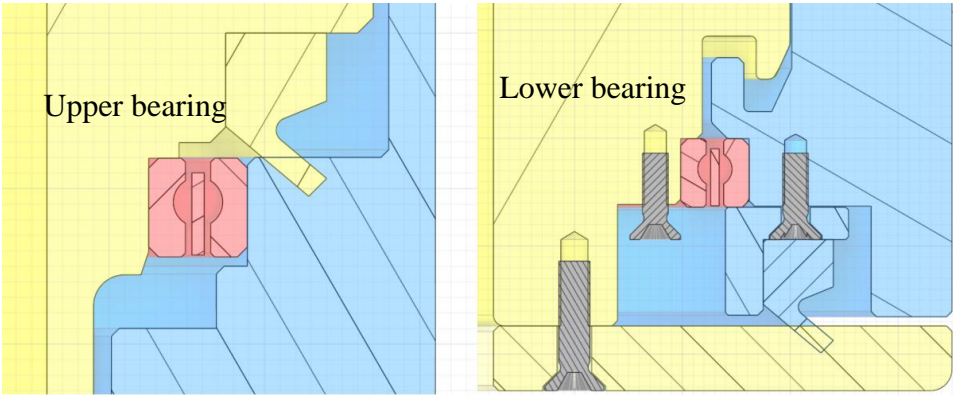
Figure 3-27 Bearing housing design

The RU is planned to be fixed to the ground from its stator and connected to the rotating system with M6 bolts through six holes in the rotor flange (Figure 3-28). Shear stresses applied on these bolts are calculated below (Table 3-5). Looking at the shear stress values, it can be considered that over-engineering has been done, but the reason for the high quantity of bolts is to ensure that the o-rings are uniformly compressed.

Table 3-5 Loads and shear stress values on bolts

Description	Rotor	Stator	Unit
Bolt diameter	6	3	mm
CS Area	28,27	7,07	mm^2
Distance from the center	0,11	0,105	m
Maximum Torque	50	50	Nm
Applied Force	454,55	476,19	N
Bolt count	6	8	Quantity
τ	2,68	8,42	MPa
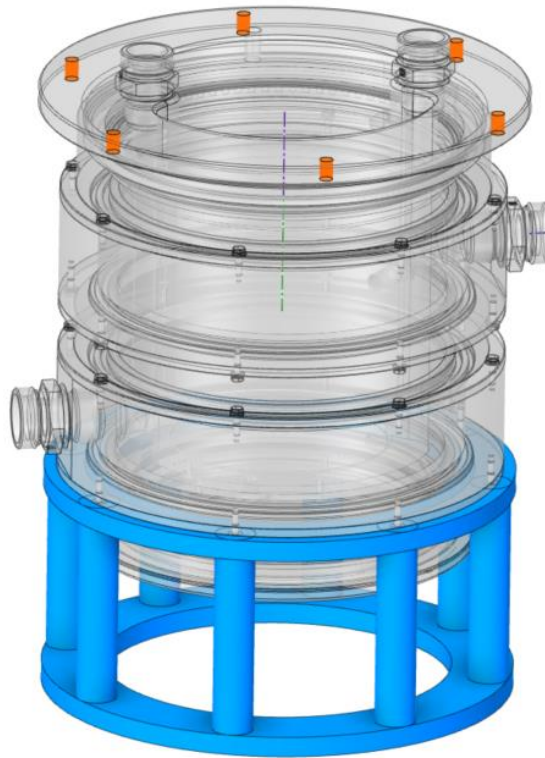
Figure 3-28 RU is fixed to the ground by its stator

As a result, in final geometrical design phase, stator is divided into multiple parts considering seal configuration, drainage regions are designed, static sealing is ensured with o-rings, flow geometry which is obtained from CFD analyses is transferred through the final design, bearings loads are calculated and proper bearings are selected, bearing housings are designed, hydraulic and power transmission interfaces are designed. Besides, dimensions are determined based on the mechanical dimensions requirement (Table 1-1). During this process, the wall thicknesses of the parts were adjusted as uniformly as possible in order to make a pre-optimization before FEM analyses. The final geometry is made and get ready for structural analyses (Figure 3-29).
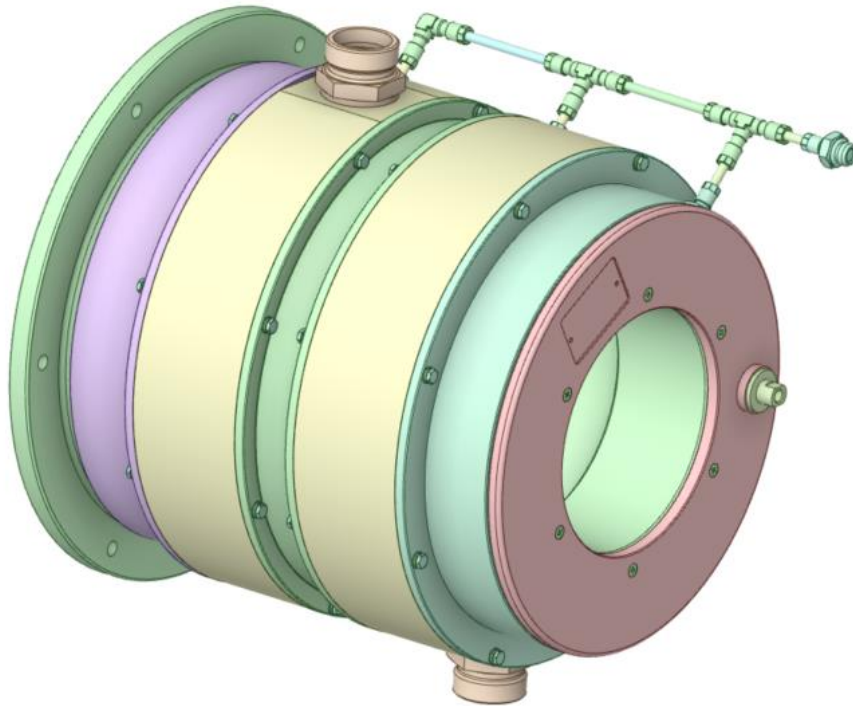
Figure 3-29 Detailed design output

3.4 Structural Analyses

3.4.1 Theory

The finite element method (FEM) was used to mechanically analyze the structure of the RU. Structural finite element analysis (FEA) is a widely used numerical method which analyses complex engineering problems using FEM in various fields. In FEM, the complex geometry is divided into a finite number of elements that are interconnected at discrete points called nodes. Each element is modeled as spring and stiffness matrix is produced using the interconnections between these elements [49]. Hooke's law between the elements is produced the stiffness matrix, displacements matrix and force matrix and solved simultaneously to analyze the behavior of the structure [50].

The reliability of the FEA results depends on various factors like mesh quality, trueness of the boundary conditions, material properties, etc. In large structures, the part to be analyzed can be isolated in order to reduce the analysis cost, but in such cases, it is necessary to define the boundary conditions as close to reality in order to obtain accurate results. It is also necessary to correctly select the type of analysis according to

the requirements of the analysis to be performed. Analysis types may include steady-state, transient, rigid mechanics, eigenvalue, modal, random vibration contents. The appropriate analysis model should be used according to conditions such as whether inertia values are desired to be examined in the analysis content, whether time-dependent values are important.

In this study, the mechanical properties of the structure under vibration, shock, pressure, and temperature were investigated. ANSYS Workbench 2022 R2 was used as the FEM software. Since the main feature that determines the behavior of the structure under vibration and shock is the modal behavior of the structure, modal analysis was performed first, and the natural frequencies of the structure were calculated. The vibration analyses in which these values were input were examined in the "random vibration" module. 11 ms sawtooth shock analyses were performed in the "transient" module since they are time dependent, non-rigid elements are used and inertial effects are important. Steady-state static analysis was performed for pressure and temperature analyses since only the behavior of the structure under final pressure and temperature values was to be examined.

3.4.2   FEM Analyses

3.4.2.1   Pre-processing

The structure is simplified to increase the mesh quality in SpaceClaim CAD software. hydraulic fittings and connecting elements like bolts and nuts are omitted to reduce element size. Part is simplified regarding structural considerations. Seals are also omitted since they do not have a great mechanical effect. Although bearings are omitted in CAD, they are modeled as proper joints in analysis model. Parts other than bearing cover rings, which are defined as structural steel, are defined as aluminum alloy. Ansys library database is used for material properties.

Half of the structure was used in the analysis model to reduce the element number. Symmetry region is defined as all the surface in symmetry plane (Figure 3-30).
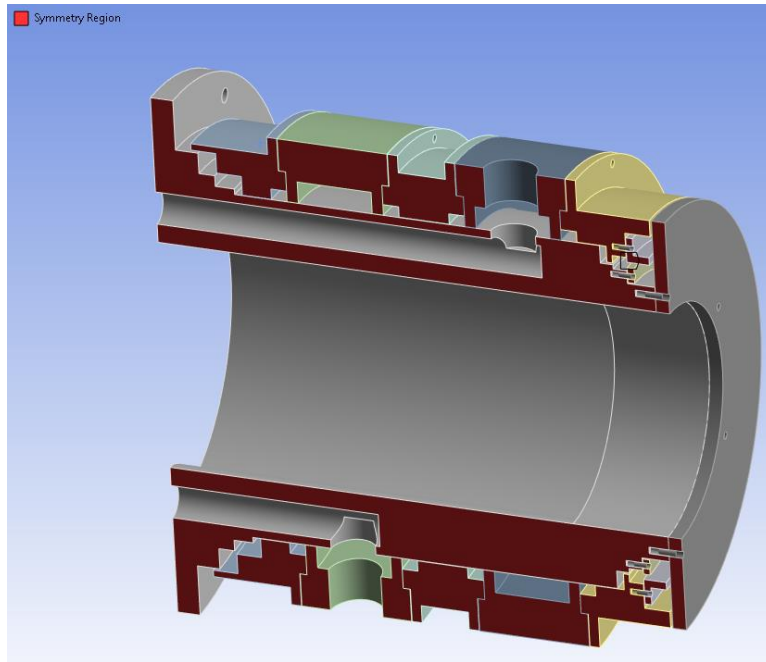
Figure 3-30 Symmetry region

Steel beam elements are used to simulate the bolts used in the structure. On the other hand, bearings are modeled as joints. A cylindrical joint is used to simulate the upper bearing since it allows translation in axial translation other than rotation (Figure 3-31).
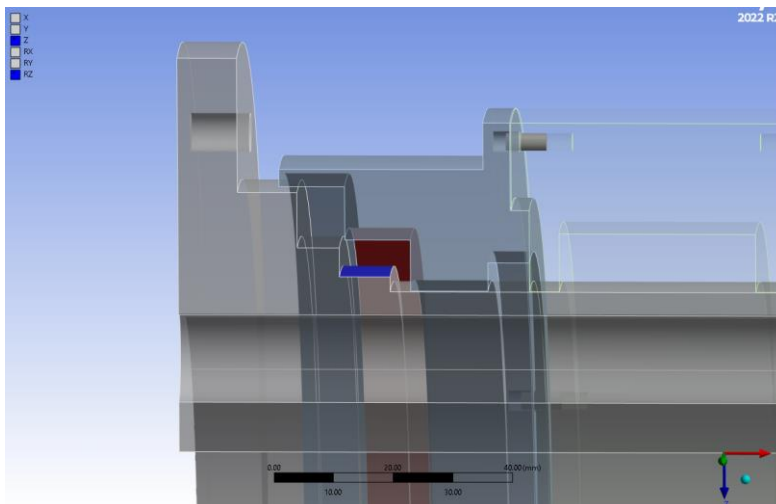
Figure 3-31 Cylindrical joint is used for modeling the upper bearing

Lower bearing is also modeled as cylindrical joint instead of revolute joint, but axial displacement is restricted using planar joints between the rotor and stator.
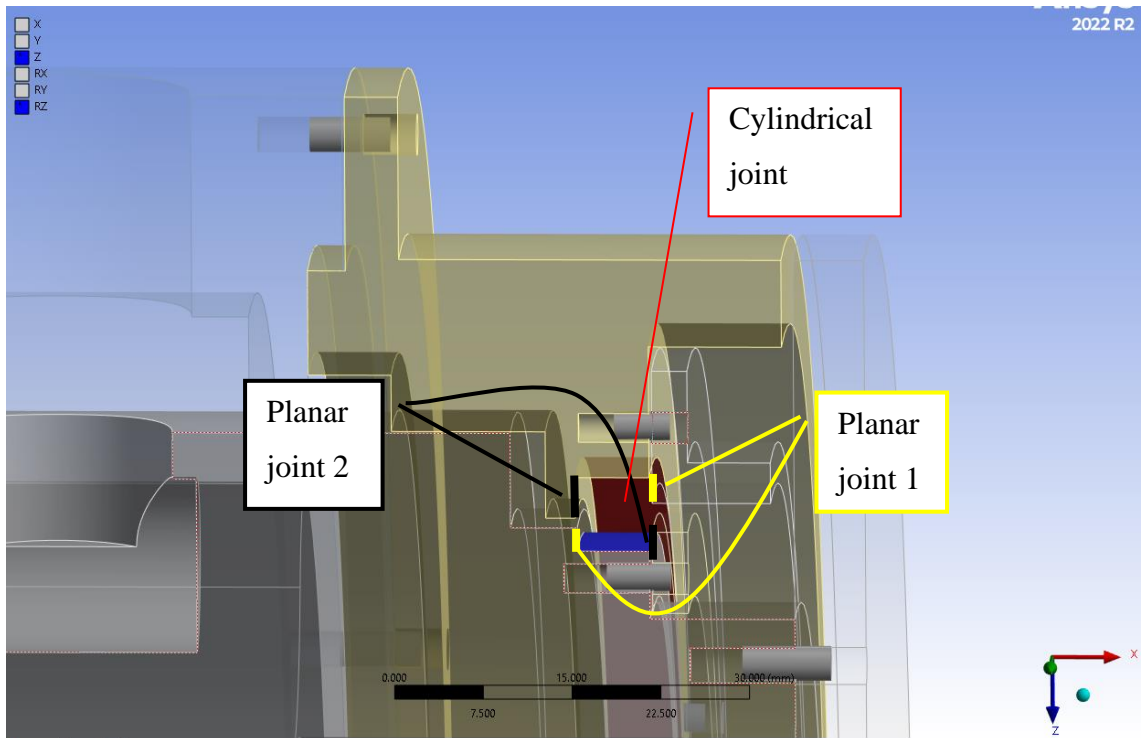
Figure 3-32 Lower bearing modeled as cylindrical and planar joints

Multiple parts of the stator are connected with bolts axially. In order to eliminate shear stress in bolts, H6/j7 cylindrical fit is used between stator parts. These fits are modeled as cylindrical joints to prevent unrealistic high stress values around steel beam elements.
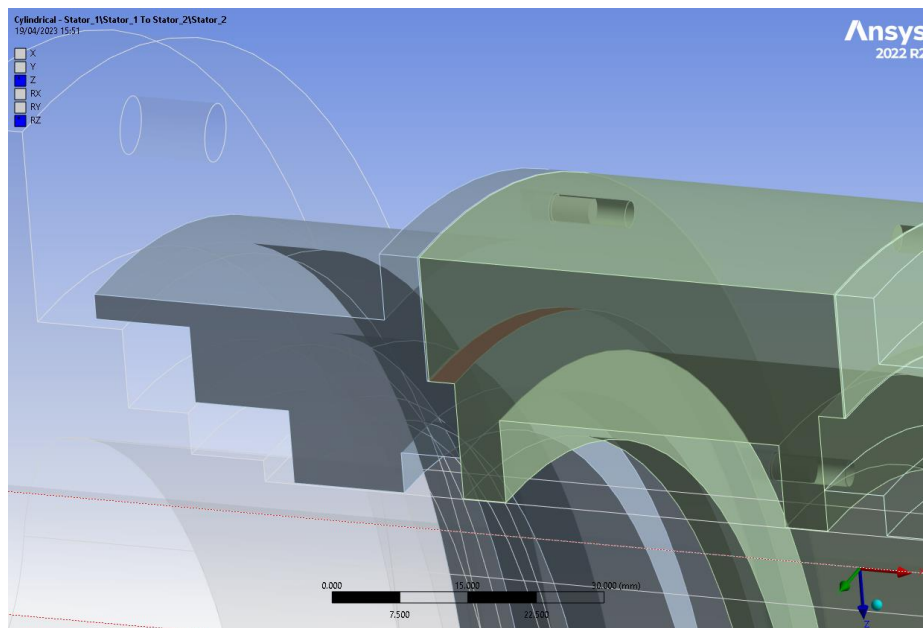
Figure 3-33 Cylindrical joint between stator elements

Sweepable bodies are meshed using sweep method and all the other bodies are meshed with tetrahedron elements. 361850 elements with an average element size of 2.5 mm were used (Figure 3-34).
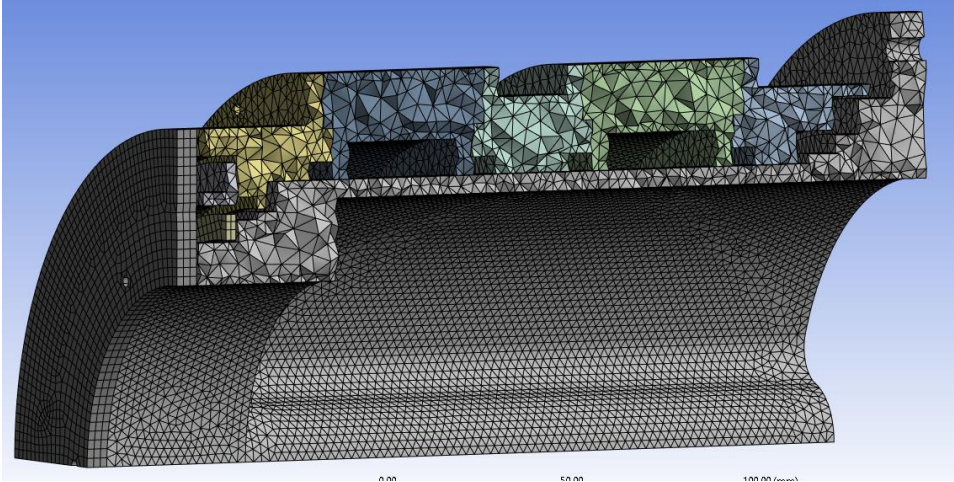
Figure 3-34 Meshed bodies

Since RU is planned to be fixed to the ground from its stator shown in Figure 3-28, corresponding holes are described as named selection.

Body weight is the only load in modal, vibration and shock analyses. Vibration and shock boundary conditions are defined as PSD G acceleration and linear acceleration. Modal analysis results are used as initial condition. In temperature and pressure analyses, steady-state assumption is made. Pressure is defined to the surfaces which are subjected to the fluid. Ambient temperature is given as boundary condition in temperature extremum analysis.

3.4.2.2 Post-processing

Modal analysis mode shape results are shown in Figure 3-35. Although the RU has one degree of freedom, the first mode is non-zero because the model is plane symmetric. As seen in Table 3-6, most of the mode shapes are in rotation y and rotation z axes, which are radial rotation axes of RU. The reason behind this is that the RU is fixed to the stator flange from the x-axis all the way around.

Table 3-6 Participation factors of first 12 modes

Mode	Frequency	Participation Factor					
		x	y	z	Rot x	Rot y	Rot z
1	1055.1	-0.0018	-0.0001	0.052313	-2.9274	-1.7348	-0.10212
2	1138.5	-0.02591	1.54E-05	-0.00141	0.082429	-0.07926	-1.3938
3	1273.4	0.05107	1.47E-05	0.000977	-0.04842	-0.194	3.0295
4	1334.5	0.005141	-1.1E-05	-0.0114	0.60569	1.8366	0.25912
5	1684	-0.0385	0.000628	0.001549	-0.06362	-0.68009	-1.6228
6	1758.3	-0.00375	-0.0003	0.000214	-0.00956	-0.07754	-0.49765
7	2566	-0.00411	0.00018	-0.03876	1.9814	8.5755	-0.18805
8	2995.9	-0.00035	3.68E-05	-0.00855	0.45459	1.9022	-0.0141
9	3158.7	0.000223	4.6E-05	-0.0254	1.3805	5.6757	0.023738
10	3525.1	4.62E-05	0.000417	-4.3E-05	0.003773	0.009594	0.17807
11	3767.5	-0.00501	0.001876	-0.00576	0.50827	1.2675	-0.12501
12	3848.4	0.014967	0.001202	-0.00289	0.30238	0.54114	1.0741
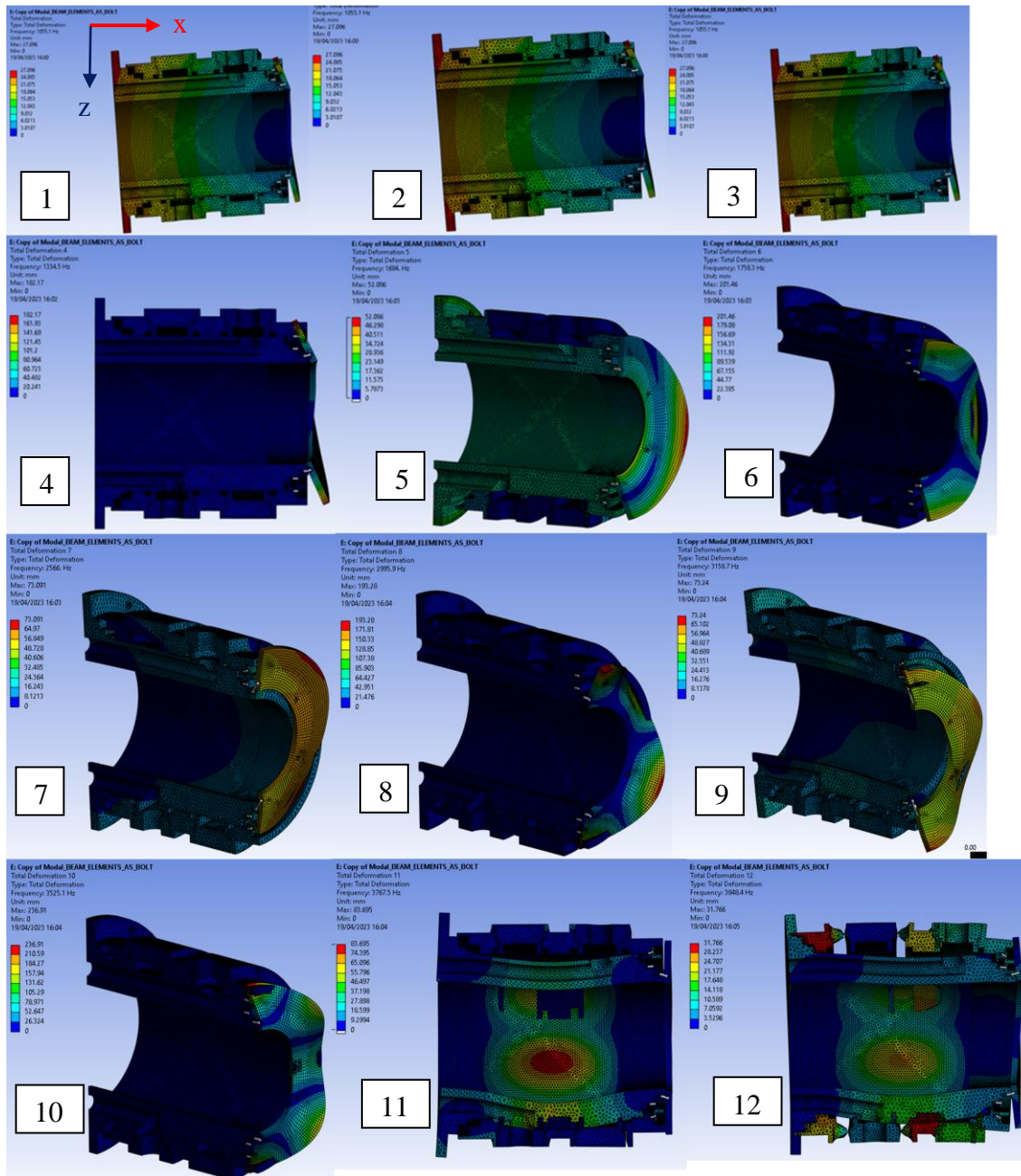
Figure 3-35 Mode shapes of first 12 natural frequencies

Vibration and shock analyses are based on modal analysis results. In vibration analysis, PSD G Acceleration curve is defined as the boundary condition that is a vibration input from the fixed support. Maximum stress values under predefined PSD G acceleration inputs are calculated. In shock analysis, acceleration input is given according to the equation of $g = 40 \cdot \left(9.81 \, \frac{m}{s^2}\right) \cdot \frac{t[sec]}{0.011}$. Transient shock analysis is divided into two steps. The acceleration defined in equation above is applied in the first step and disabled in the second step. In the second step, the oscillation behavior of the body is observed.

In both vibration and shock analyses, maximum stresses are produced around the screw holes.
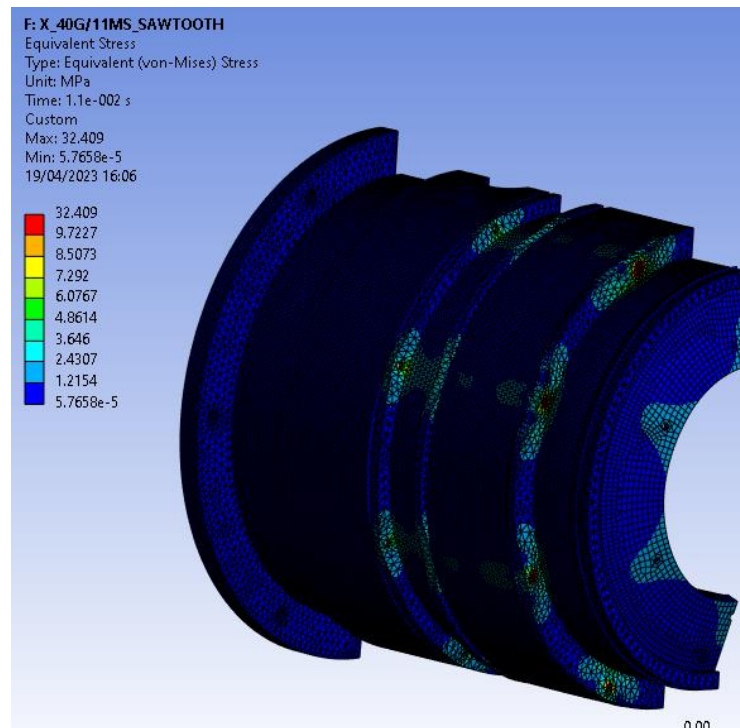
Figure 3-36 Von-mises stress distribution under shock in x direction

In both vibration and shock analyses, stress values are quite low since a high number of screws are used to ensure static sealing.

Table 3-7 Maximum stress values under shock and vibration analyses

σ_{max} [MPa]	Shock	Vibration
x	32.409	11.699
y	0.4085	0.12269
z	35.429	7.4139

Pressure analysis is made in three steps:

- Step 1, nominal pressure, 6 bar
- Step 2, maximum pressure, 10 bar
- Step 3, burst pressure, 15 bar

All the surfaces which are exposed to the pressure are selected as pressure boundary condition.

71
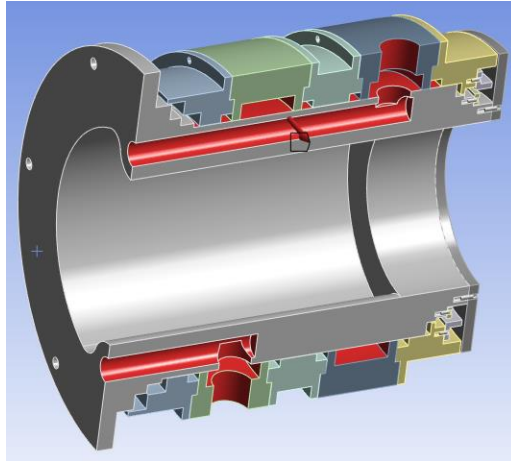
Figure 3-37 Pressure boundary condition surfaces marked with red

Maximum stress values under certain hydraulic values are shown in Table 3-8 and deformation shape result under burst pressure is shown in Figure 3-38.

Table 3-8 Maximum stress values under certain hydraulic pressure values

Inlet pressure	σ_{max} [MPa]
6 bar	34.092
10 bar	56.82
15 bar	85.23
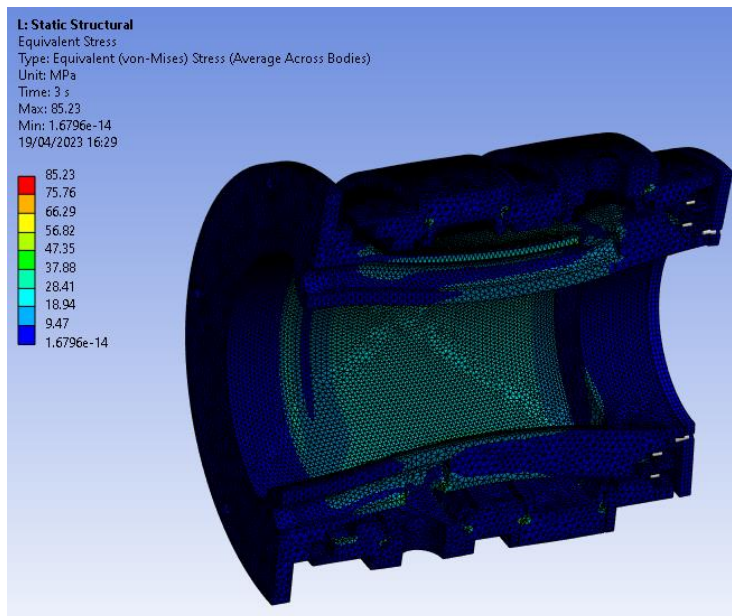
Figure 3-38 Stress distribution under 15 bar hydraulic pressure

RU is exposed to hot (63°C) and cold (-35°C) temperature extremums in two steps. As mentioned above, cylindrical joints are defined between stator parts. In hot and cold temperatures, parts tend to separate from each other. Cylindrical joint restricts that behavior, which is an unrealistic situation. For that reason, cylindrical joints between stator parts are suppressed for thermal analyses. On the other hand, cylindrical joints which are simulating bearings share the same problem but if they are removed, rotor remains free. Thus, these joints are saved in anticipation of high stress values at corresponding surfaces.
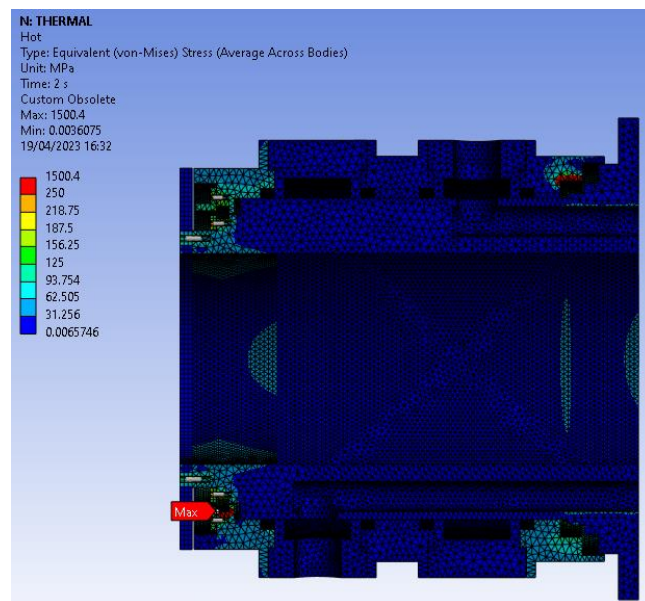
Figure 3-39 Stress distribution under 63°C

High stress values are seen in bearing surfaces as expected. In addition, although the cylindrical joint is defined on the entire diameter surface, the fact that very high stress is observed pointwise close to the symmetry plane indicates singularity in this region.
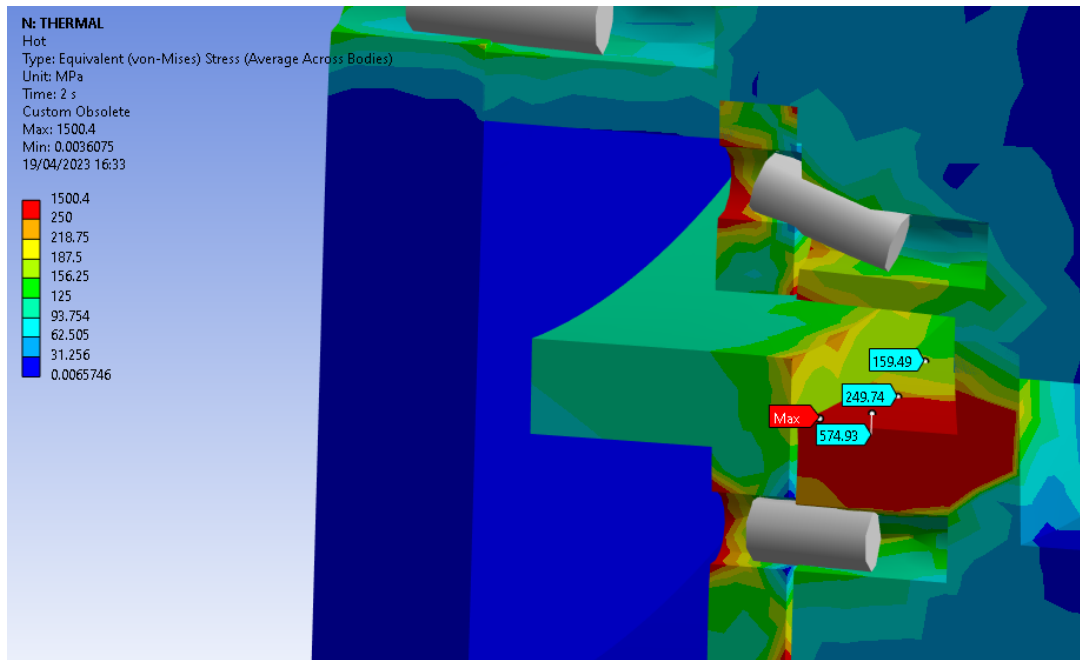
Figure 3-40 High stress values in lower bearing region under 63°C

A similar stress distribution is seen in -35°C since these two steps share a common constraint configuration. Directions of deformation of the beam elements are reversed in this step.
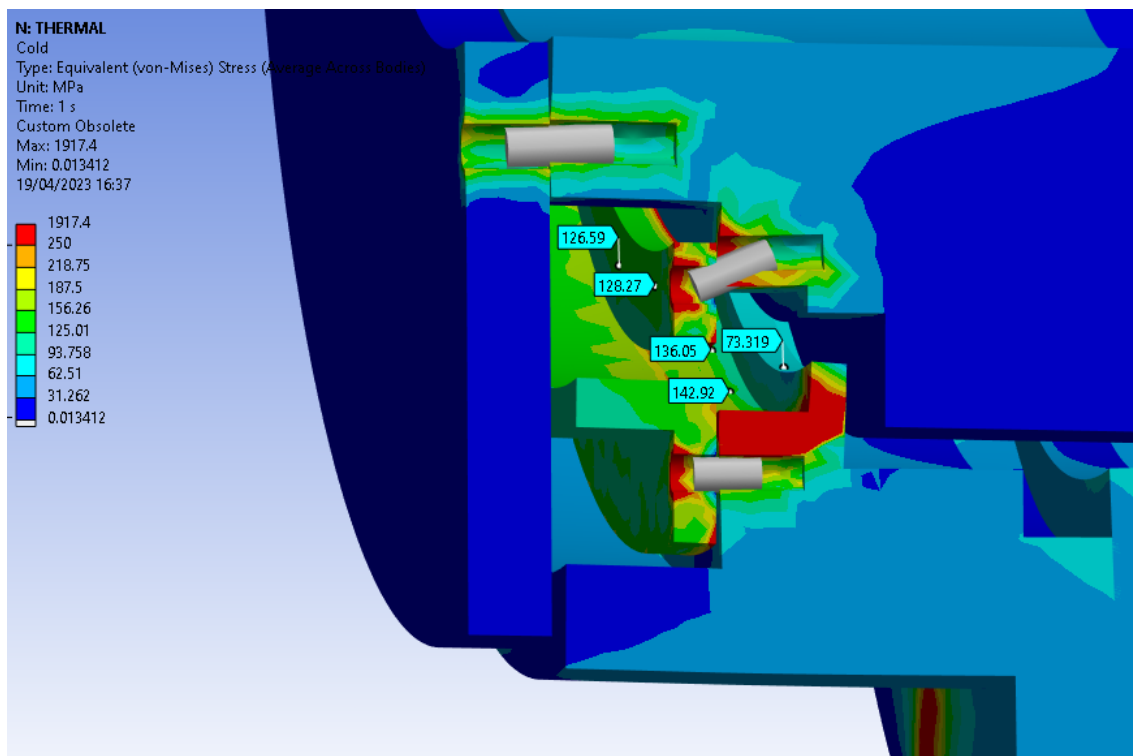
Figure 3-41 High stress values in lower bearing region under -35°C

3.4.2.3 Discussion

When the results of the modal analysis results are evaluated, it can be said that the natural frequency value in the lowest mode is 1055.1 Hz, considering the size and mass of the structure, it has a very rigid character. Although the unit has one degree of freedom under the defined connections and joints, the first mode, whose natural frequency should be zero, was not seen in the analysis results due to the fact that the symmetry axis is the y axis, and the unit is free on the rotation x axis.

In the unit, the requirements arising from the production and surface treatment processes and the dimensions of the fittings determined the wall thickness values rather than the structural requirements. In addition, the number of bolts used in the connection of the stators remained at a degree with a high safety factor from a structural point of view, since the o-rings require a certain distance between screws to ensure static sealing. Taking all these into account, the stress values under vibration and shock remained well below the yield stresses of the materials used in the structure.

The maximum value of 500 Hz was given in the PSD G acceleration values determined as the boundary condition in the vibration analysis. It is a design requirement from the vibration perspective that the natural frequencies of the structure do not coincide with the frequencies to which the structure will be exposed in order to avoid high stresses due to vibration. Since the natural frequency value of the first mode of the structure is 1055.1 Hz, which is higher than 500 Hz, it can be concluded that no natural frequency of the structure will coincide with the vibration values to be exposed. Apart from the PSD G acceleration values, a frequency of 1 Hz should also be avoided since the structure will rotate with an angular velocity of 60 rpm, but this value is not considered as a design parameter since it is very small compared to the natural frequencies of the structure.

As a result of the hydraulic pressure analysis performed in three steps, nominal, maximum and burst, it was seen that the maximum Von-mises stress values that the structure would be exposed to were below the yield stress of the materials.

While examining the stresses that high and low temperatures will create in the structure, cylindrical support was removed on these surfaces in order to prevent the joints between

the stator parts from behaving as bonded and high stresses from occurring. In this case, the parts were allowed to be separated from each other in hot temperatures. On the other hand, in order to prevent the parts from interfering with each other in cold temperatures and unrealistically low stresses, frictionless support connection type was defined at these joints. In this way, realistic stress and deformation were observed between the stator parts. However, not using bearing cad models and instead defining the bearings as cylindrical support led to high stress values in the bearing housings. In order to minimize this problem, these joints were defined as deformable instead of rigid, but still unrealistically high stresses were observed, especially in the symmetry plane. In all regions except these regions, the stresses in the structure remained below the yield stress of the materials.

As a result of the structural analysis, it was seen that the yield strength of the unit would not be exceeded under vibration, shock, pressure and temperature conditions. This was verified by examining the unit after the tests.

Upon finalization of the detail design, manufacturing, coating and assembly processes were completed and the unit was ready for testing.
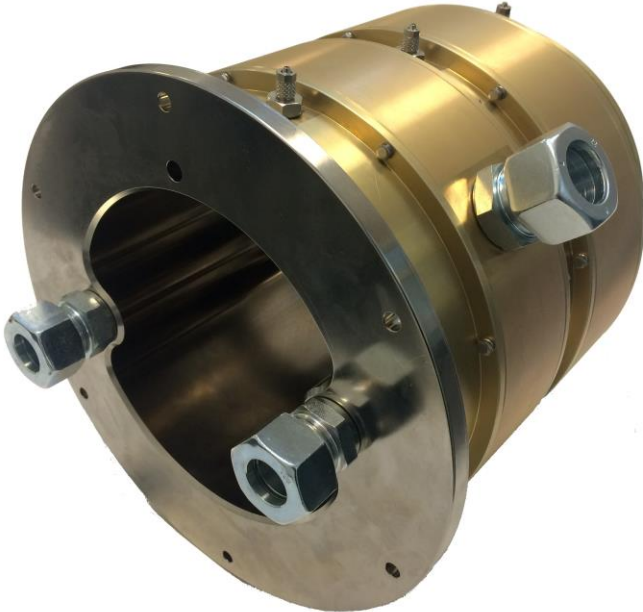
Figure 3-42 First RU prototype

4. FIRST PROTOTYPE TESTS

4.1 Test Content

Test procedure is planned considering Table 1-1. According to the procedure, following tests are made:

- Environmental condition tests
    - Minimum and maximum temperatures
        - Pressure loss
        - Leakage rates
        - Frictional torque
    - Vibration (non-operational)
    - Shock (non-operational)
- Life
    - Leakage rate after 1 million cycles

4.2 Test Setup
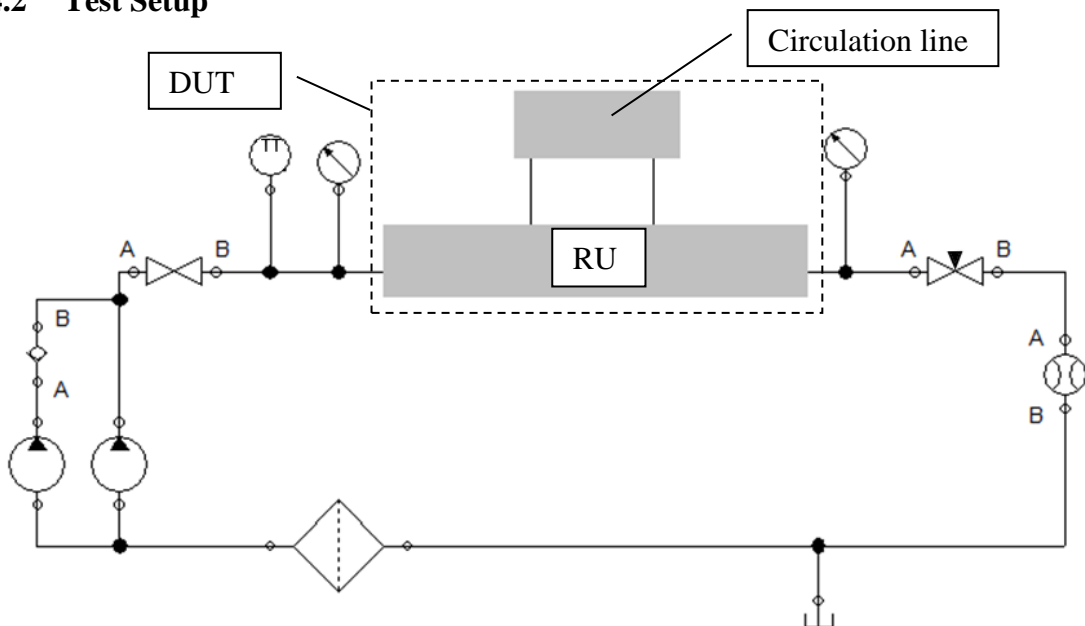
Figure 4-1 P&ID scheme of performance test setup

P&ID scheme shown in Figure 4-1 represents the test setup which is used in both room temperature and temperature extremums. This setup allows us to adjust and measure

inlet and outlet static pressure, volumetric flow rate and inlet temperature. Hydraulic elements used in test setup are stated below.

Figure 4-2 Tank representation

Polyethylene water tank is used as an atmospheric tank. A water tank with a volume that can hold three times the amount of liquid used in the system was used.
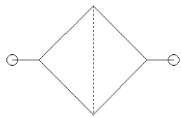
Figure 4-3 Filter representation

A suction filter is used to protect the pumps from foreign objects like metal chips, polymer particles which may be caused by hoses, or any other contamination.
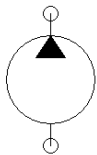
Figure 4-4 Pump representation

Although centrifugal pumps are generally more suitable with water, required inlet pressure is high for most of the centrifugal pumps having a flow rate of 25 lpm. A multistage centrifugal pump can be used but most of the multistage centrifugal pumps are so large and heavy. Since the test setup must be put in a thermal test chamber, compact units are preferred. Also, positive displacement pumps are easier to use than centrifugal pumps since their pressure does not vary much with respect to the change in flow rate. On the other hand, positive displacement pumps generally work with lubricating media not to worn. In order to eliminate lubricating problems, vane pumps are used since it has graphite vanes which eliminate the lubricating problem. Vane pumps are generally used for low flow rates. The flow rate value of the vane pump that could provide the largest flow rate among the pumps investigated was 18 lpm.

Therefore, two pumps were connected in parallel, so that it could transfer a flow rate above 25 lpm. Burst pressure tests could also be performed since the maximum pressure value that the vane pumps used could create was 17 bar.
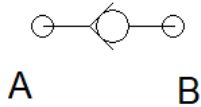
Figure 4-5 Check valve representation

Check valves are hydraulic elements that allow one-way flow in the broadest sense. In case of low flow testing, only one of the two pumps may need to operate. In this case, a check valve is used to prevent reverse flow through the other pump.

Figure 4-6 Shutoff valve representation

In order to prevent leakages during assembly and disassembly processes, globe valves are used.
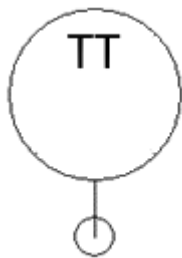
Figure 4-7 Temperature transmitter representation

Tetcis K type in-line thermocouple is used at RU inlet to measure the inlet temperature of media. Outlet temperature is assumed to be same as inlet since frictional pressure loss is low.
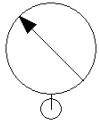
Figure 4-8 Pressure sensor representation

Keller 0-25 bar 4-20 mA 24 VDC gauge in-line pressure transmitters are used at inlet and outlet of RU. Pressure sensors are installed closest to the RU to avoid pressure losses in the pipes. The value at inlet sensor represents the maximum internal pressure and the difference of the sensor values represents the pressure loss in RU and circulation line.

Figure 4-9 Needle valve representation

Needle valve is used to increase the internal pressure of RU precisely. The proper flow rate and pressure combination is procured adjusting needle valve and pump speed together.
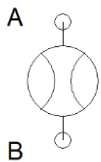
Figure 4-10 Flow meter representation

VFA stainless steel turbine flow meter is used to measure the volumetric flow rate. Since inlet and outlet flow rates are the same because of the conservation of mass, one flow meter is sufficient for the test setup.

Pumps are driven by asynchronous three phase AC motors. The liquid sucked by pumps goes through the suction filter and transferred to the DUT by pumps. Flow rate is adjusted by changing frequency of motor driver and measured by flow meter. Since motors and pumps do not work efficiently under specific frequencies, that situation

brings a limitation for minimum flow rate. In this case, the pump which has check valve is stopped and system is fed by single pump. Temperature and pressure of the liquid are measured at the inlet of DUT. Since there is no unit to be cooled, a virtual circulation line is created by connecting the axial channels of the RU. Liquid passes through the RU and circulation line, and exits the DUT. Pressure and volumetric flow rate of the liquid are measured at the outlet of the DUT. Besides, inlet pressure is adjusted precisely using a needle valve at DUT outlet. This valve is selected with respect to its Cv (flow coefficient) regarding flow and pressure range it is subjected to. After the needle valve, liquid passes through the turbine flow meter and turns back to the tank.

While DUT is fed with liquid, rotor must be rotated, and torque must be measured simultaneously. For this application, rotor is driven using a DC servo motor with a reducer and torque is measured with a torque sensor. 750 W DC servo motor is connected to the 1:50 reducer with an elastomer coupling. Likewise, power is transmitted to the Magtrol 100 Nm in-line torque transducer with elastomer coupling. A lever, which drives the drive pin connected to the rotor, is clamped to the output shaft of the torque transducer.
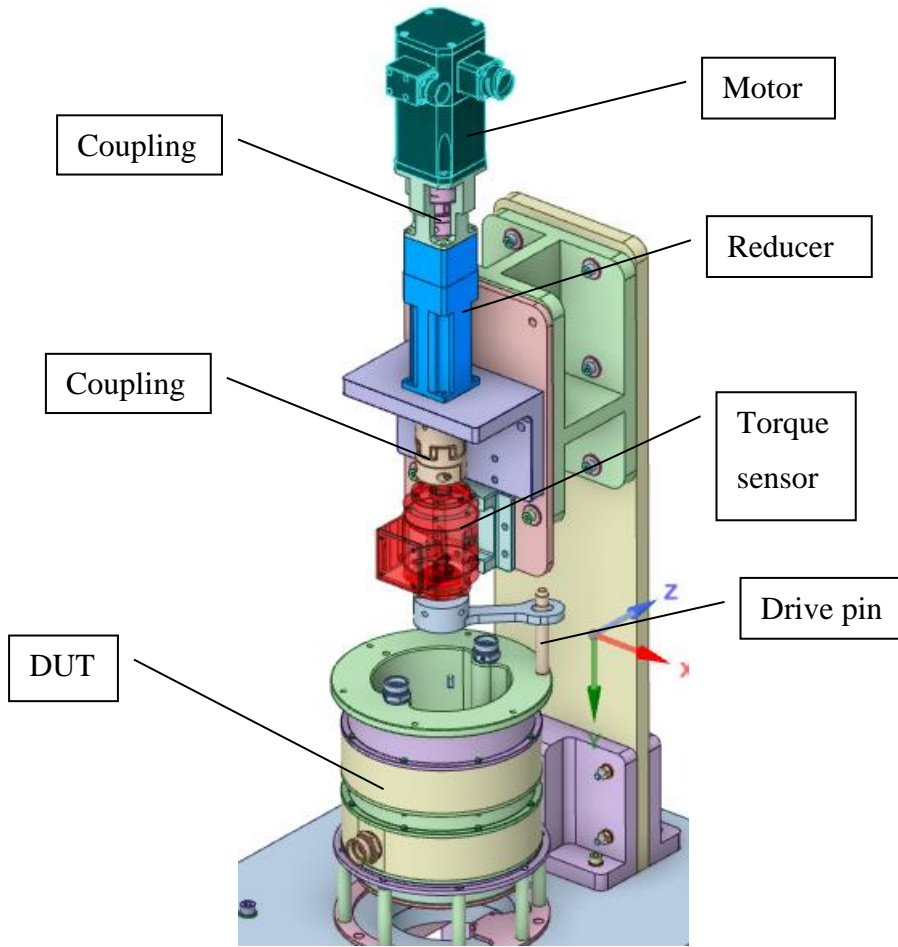
Figure 4-11 Power transmission in test setup

The rotational speed and friction torque values required in the test were 60 rpm and 50 Nm respectively. However, in case of higher friction in the seals, a value of 75 Nm, which is 1.5 times this value, was taken as the basis for motor selection. Taking into account the losses due to motor, motor drive and reduction efficiencies, the required motor power was calculated as follows.

$$P_{shaft} = T \cdot \omega$$

where T=75 Nm and ω=60 rpm
Hence, P_{shaft}=0.47 kW

Since total efficiency caused by motor, motor driver and reducer is approximately 70%, required motor power is 0.67 kW. Thus, a 0.75 kW motor is selected.

Since the optimum operating speed of the selected motor is 3000 rpm, a 50:1 planetary reducer was selected to reduce this speed to 60 rpm.

Most of the hydraulic, mechanical, and electronic elements in the test rig have been selected to operate simultaneously at extreme temperature points. But pumps and motor of the pumps are not suitable for low temperature extremum. In this case, the DUT is in the thermal test chamber while the pumps and the motors driving the pumps supply the DUT from outside the cabinet. At room temperature and at extreme temperature points, the DUT can be fed with liquid at the same time as the rotor rotates and all necessary data logs can be stored.

In addition, since the measured pressure loss will also include the loss in the circulation line, it is necessary to measure the loss there as well, since comparing it with the analysis will not give a reliable result. For this purpose, pressure sensors were installed at the inlet and outlet of the circulation line and the system was pressurized while the rotor was stationary and the pressure data at these points were read. In this test, the rotor was positioned in the orientation in the analysis geometry in order to obtain data consistent with the analysis. This test was performed in a stationary state as the cables of the pressure sensors would get tangled when the rotor rotates.

4.3   Environmental Conditions Tests

4.3.1   Vibration and Shock

Figure 4-12 Vibration and shock test

In order to connect the RU to the vibration and shock shaker table rigidly, a proper interface must be done. This interface must be sufficiently rigid in order not to isolate or

amplify the shock and vibration inputs. To ensure that vibration text fixture is designed regarding the first resonance mode of the DUT to be connected to the shaker table is over 2000 Hz. Non-operational vibration and shock tests are made one after the other in three axes.

Before and after the vibration and shock tests, the system was pressurized to the maximum and burst pressure and no leakage was observed. No deterioration in the integrity of the DUT was observed during the non-operational vibration and shock tests.

4.3.2 Low Temperature

Both low and high temperature tests are done in a walk-in temperature and humidity test chamber. Firstly, DUT, sensors and valves are placed in the test chamber. Then, temperature is decreased in a rate of 3°C per minute with respect to the standard. DUT is fed by the pumps from the outside of the chamber without active cooling and sensor data was logged.

Operational low temperature and high temperature tests and non-operational vibration and shock tests were performed. Before and after all tests, a performance test was performed to monitor sensor data and leakage status. Sensor data before and after low temperature test is shown below.

Table 4-1 Data collected before and after the low temperature test

	Before	After	Unit
Inlet pressure	9.96	9.91	bar
Outlet pressure	9.14	9.05	bar
Pressure loss	0.82	0.86	bar
Flow rate	24.54	21.76	lpm
Angular velocity	60	59.1	rpm
Torque	13	13.17	Nm
Fluid temperature	21	14.2	°C

Although the ambient temperature was -30°C, the liquid temperature could not be reduced to sub-zero temperatures because the pumps were outside the thermal test chamber. Low temperature test sensor data is shown in the table.

Table 4-2 Data collected during the low temperature test

	t₀	t₀+15 min.	t₀+30 min.	t₀+45 min.	t₀+60 min.	Unit
Inlet pressure	10.91	10.79	10.78	10.74	10.72	bar
Outlet pressure	9.96	9.84	9.83	9.8	9.79	bar
Pressure loss	0.95	0.95	0.95	0.94	0.93	bar
Flow rate	24.53	24.62	24.71	24.83	24.91	lpm
Angular velocity	57	57.9	58.6	58.6	58.9	rpm
Torque	16.8	14	13.34	13.66	13.65	Nm
Fluid temperature	0.2	5.9	7.5	8.6	9.5	°C

4.3.3 High Temperature

Sensor data before and after low temperature test is shown below.

Table 4-3 Data collected before and after the high temperature test

	Before	After	Unit
Inlet pressure	9,91	9,9	bar
Outlet pressure	9,05	9,2	bar
Pressure loss	0,86	0,7	bar
Flow rate	21,76	24,37	lpm
Angular velocity	59,1	60,6	rpm
Torque	13,17	13,8	Nm
Fluid temperature	14,2	30	°C

As in the low temperature test, the pumps were located outside the thermal test chamber in the high temperature test. Although the test started at 65°C, the liquid temperature decreased during the test and converged to room temperature. The ambient temperature remained 63°C during this period.

Table 4-4 Data collected during the high temperature test

	t₀	t₀+15 min.	t₀+30 min.	t₀+45 min.	t₀+60 min.	Unit
Inlet pressure	9,94	9,69	9,8	9,9	9,75	bar
Outlet pressure	9,14	8,9	9,1	9,22	9,15	bar
Pressure loss	0,8	0,79	0,7	0,68	0,6	bar
Flow rate	24,73	23,75	23,68	24,5	23,7	lpm
Angular velocity	59,8	60	61,1	62,1	61,8	rpm
Torque	22,6	16,35	15,28	12,7	13,37	Nm
Fluid temperature	65,5	31,5	36,5	39,8	42,7	°C

4.4 Life Test

The test rig was subjected to a life test under nominal operating conditions of 6 bar, 25 lpm, 60 rpm. After 385,000 cycles of continuous operation, the total leakage from the drainage channels was observed to be approximately 1 ml/hour, the test was stopped, and the DUT was disassembled to investigate the cause of the leakage.

Figure 4-13 Black particles on the cover

When the bottom cover was opened, black particles were observed on the surface. The cause of these particles was thought to be one of the following.

- Particles breaking off the seals
- Steel dust caused by wear of the drive pin
- Nitrile rubber fragments from hoses
- Contamination caused by frictional wear of the graphite pallets of the pumps and their inclusion in the line

When the lips of the seals were examined, no obvious wear was observed, but the grooves were found to be filled with grease.

Figure 4-14 Rotary seals after life test of first prototype

When the lips of the seals were examined, no obvious wear was observed, but the grooves were found to be filled with grease. When the seals were removed, it was observed that there were traces on the rotor at a level that could be felt by hand in the areas where the seals worked. When these marks were examined closely, it was seen that there were also abrasions in the form of scratches in two concentric circles with palpable depth. Considering the form of the surface of the felt in contact with the rotor, it was understood that the two-channel felt abraded the rotor surface in its own shape.
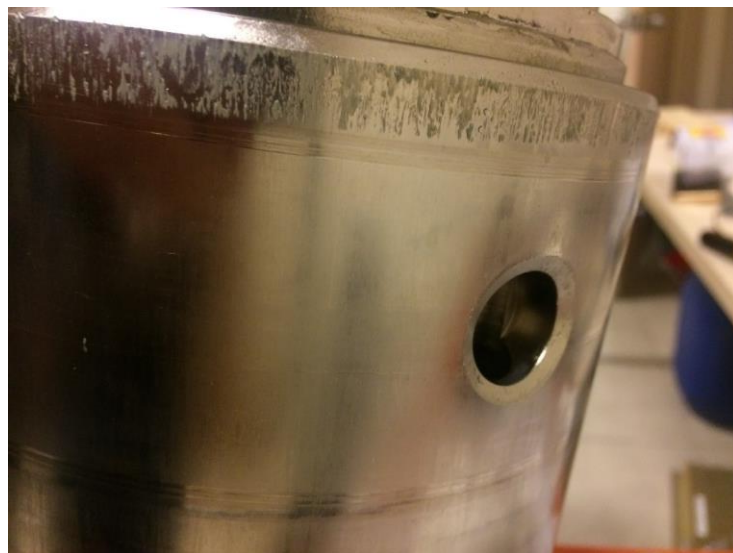
Figure 4-15 Scratches on the rotor caused by the seals

In this case, in order to verify the design and manufacturing, the consistency of the dimensions and tolerances given in the design with each other, the consistency of the

seal with the ICD, the accuracy of the interfaces prepared for ready-made products such as bearings, seals, dust seals, hydraulic elements, etc., material and coating certificates, CMM reports were checked again, and no error was found. The seal manufacturer was then contacted; rotor material, surface treatments and measurement reports, seal seat dimensions were shared, and no error was found by them either.

In this case, considering the possibility that the particles seen on the cover may have somehow entered the system, entered between the seals and the rotor and acted as abrasive dust, a test setup was prepared to slide the seals on the axis and perform a quick and simple test. As can be seen, the axial glands are under the radial grooves in the rotor. In this way, the middle two seals are integrated to work 10 mm below, and the outer seals are not included in the assembly. Since the possibility of contamination coming from the liquid line was considered, no design was made to ensure the integrity of the liquid line, and the seals were turned dry. Since cooling could not be provided in this case, the system was stopped at certain intervals and passive cooling was provided.
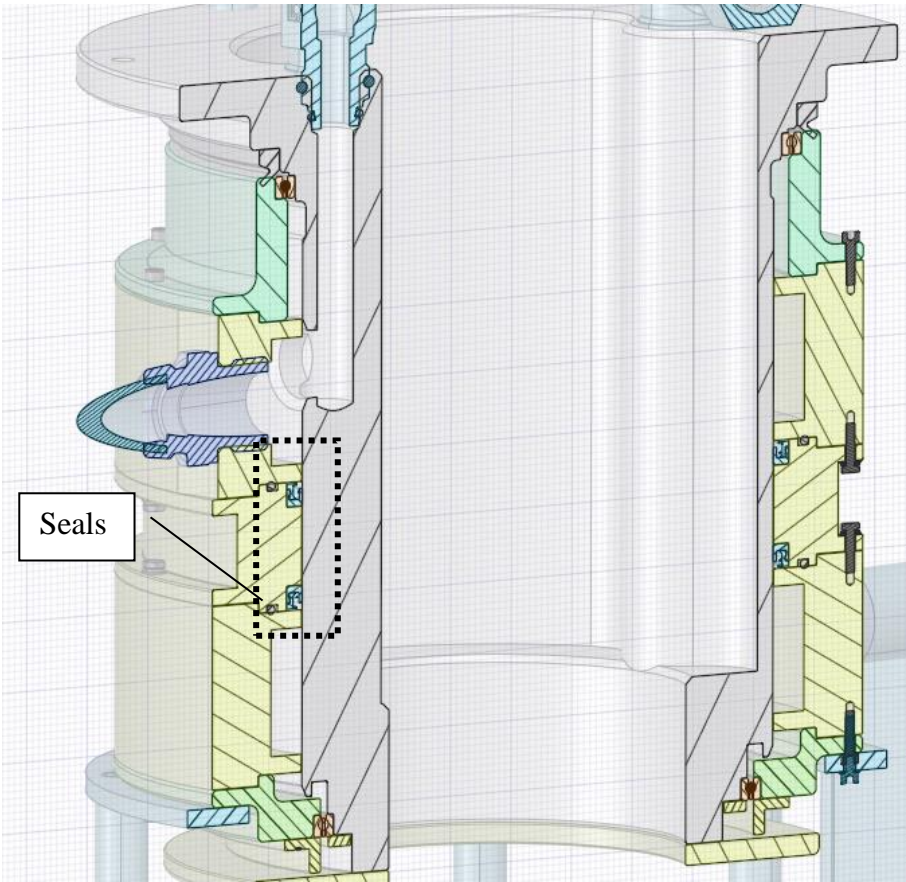
Figure 4-16 Seals offset in rotation axis

After 400,000 cycles of intermittent operation at 60 rpm, the system was disassembled and the rotor was examined, and the same abrasion was observed in the new working area of the seals as before. As a result of this situation, it was concluded that the scratching on the rotor was not caused by the abrasive effect of contaminants such as dust from the system. Although electroless nickel plating on AA6061-T6 base material was recommended by the seal supplier company, this application failed in the life test.
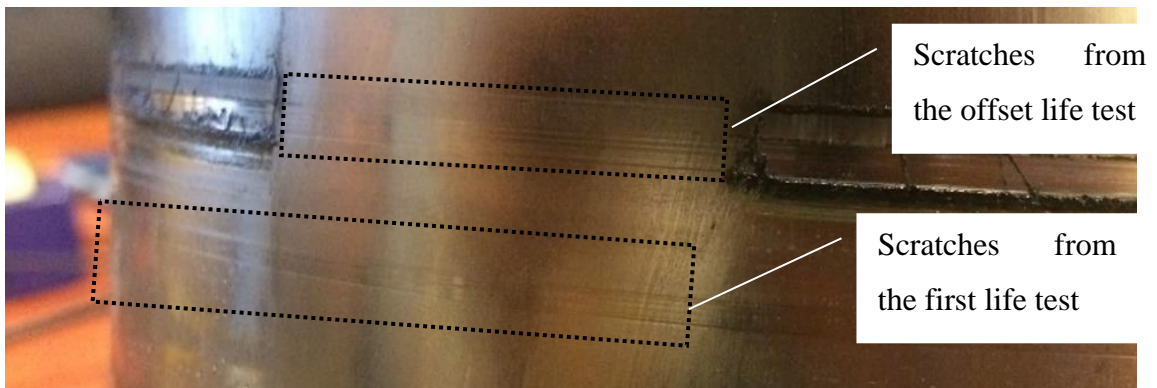
Figure 4-17 Rotor body after the offset life test

4.5   Results & Discussion About the First Prototype Tests

4.5.1   Requirements to Be Fulfilled Under Certain Working Conditions

Testing is one of the verification methods such as analysis, demonstration, and inspection. Testing is used to fulfil the following technical requirements as indicated in Table 1-1.

Working conditions:

- Ambient temperature range of -30°C to 63°C
- Fluid temperature range of -30°C to 63°C
- Operating under of 6 bar nominals, 10 bar maximum and 15 bar burst pressure
- 60 rpm angular velocity
- 25 lpm maximum flow rate
- Vibration and shock according to the data given in Table 1-1

Requirements to be fulfilled under the working conditions as stated above:

- Pressure loss must be below 0.5 bar.

- The leakage rate must be below 0.1 ml/h.

- Frictional torque must be below 50 Nm.

- Corrosion must not have occurred in any part of the structure.

- The unit must not be damaged in such a way as to impair its performance after being subjected to vibration and shock.

- When the unit is pressurized from static to burst pressure, the leakage should be below 0.1 ml/h.

4.5.2 Pressure loss

Pressure loss is above 0.5 bar in every test as seen in test result tables. But in fact, the pressure loss requirement indicates the drop in the pressure within the unit which means the circulation line must be excluded from the pressure loss calculation. For that reason, pressure transducers are positioned on axial ports of the unit and sensor data was collected in room temperature (Figure 4-18).
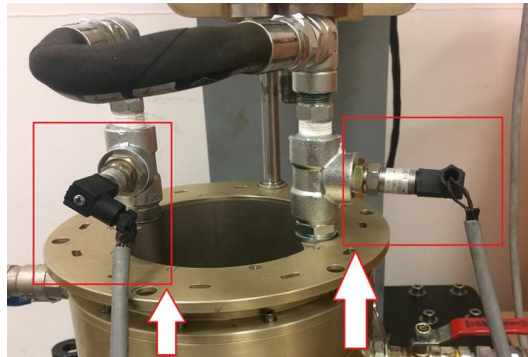
Figure 4-18 Pressure transducers positioned on axial ports

The data collected in this configuration is shown below.

Table 4-5 Pressure loss data in circulation line

Inlet pressure	10.03	bar
Outlet pressure	9.56	bar
Pressure loss	0.47	bar
Flow rate	25.33	lpm
Fluid temperature	25.6	°C

A performance test was made in room temperature before the low temperature test. This test can be compared with the pressure loss data in the circulation line since both tests are performed in room temperature. Pressure loss of DUT in room temperature is 0.82 bar (Table 4-1) and 0.47 bar of this value is the pressure loss in the circulation line. So, the circulation line accounts for 57% of the pressure loss in the DUT. In other words, roughly 43% of the measured pressure losses represent the pressure loss inside the RU. Considering that there is also pressure loss in the pipes, valves and fittings between the pressure transducer and the DUT as seen in, 43% of the pressure loss data obtained contains a safety factor in itself.
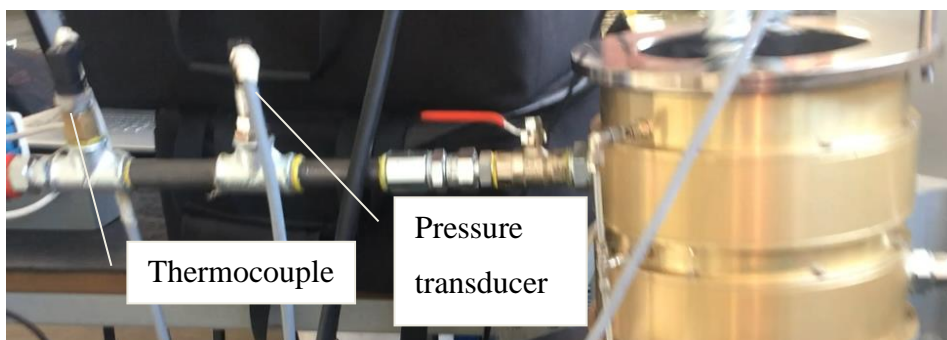
Figure 4-19 Sensor locations at inlet line

The actual pressure loss values are calculated by taking 43% of all pressure loss data.

Table 4-6 Pressure loss in RU before and after the thermal tests

	Before	After	Unit
$\Delta P_{Low\ Temp}$	0.3526	0.3698	bar
$\Delta P_{High\ Temp}$	0.3698	0.301	bar

Table 4-7 Pressure loss in RU during the thermal tests

	t_0	t_0+15 min.	t_0+30 min.	t_0+45 min.	t_0+60 min.	Unit
$\Delta P_{Low\ Temp}$	0.4085	0.4085	0.4085	0.4042	0.3999	bar
$\Delta P_{High\ Temp}$	0.344	0.3397	0.301	0.2924	0.258	bar

In the CFD analysis, only the maximum pressure loss in the RU was calculated to be 0.24 bar. Since many factors such as losses between the pressure sensors and the RU inlet and outlet, the margin of error in the liquid mixture, manufacturing variations,

sensor measurement error, etc. will increase the actual pressure loss, it is concluded that the test results are consistent with the analysis.

4.5.3 Leakage Rate

No leakage was observed under nominal, maximum and burst pressures in both environmental conditions tests and performance tests under room conditions. Upon success in these tests, DUT was subjected to a life test under nominal pressure under room conditions. The small amount of leakage is observed after approximately 350,000 cycles but it increased in a short time to 1 ml/h, ten times the acceptance criterion of 0.1 ml/h, at 385,000 cycles. The test was then stopped, and the unit was disassembled to be inspected.

4.5.4 Frictional Torque

The friction torque was well below the acceptance criterion of 50 Nm in all tests. The highest friction torque data was 22.6 Nm in the high temperature test at 63°C ambient temperature and 65.5°C liquid temperature. Although the reason for this situation seems to be that the RU structure and the seals are made of different materials, it is understood that this is not the case when the thermal expansion coefficients of these two structures are compared. The RU rotor and stator are made of aluminum alloy. On the other hand, the seal contains a PTFE sealing element, stainless steel spring and aluminum alloy locking. In general, the coefficient of thermal expansion of seal assembly is higher than that of aluminum alloy. But there is a preloaded compression spring in seal assembly which continuously applies radial compression in all temperature range. So, the compression applied by spring would increase in high temperature since rotor expands. On the other hand, when the ambient temperature decreases, both rotor and seal would shrink and the preload of the spring would decrease.

Contrary to what was thought, there was no significant correlation between friction torque and hydraulic pressure. Friction torque increased when the pressure increased, but this effect was not very pronounced since the maximum working pressure was 80 MPa, a small lower part of the operating range of the seal.

4.5.5 Other requirements

In addition to the performance tests, the behavior of the structure under burst pressure was also examined. The DUT was pressurized up to burst pressure of 15 bar and no external leakage was observed under this condition.

No deterioration in the integrity of the structure was observed during the vibration and shock tests. No loosening of bolts and fittings was detected in the inspection after the tests. The performance tests carried out before and after the vibration and shock tests showed that the unit was not damaged in the vibration and shock tests.

The RU was disassembled, and all parts were examined, and no evidence of corrosion was found. Grease residues on the seals and metal dust from scratching the rotor were observed.

4.5.6 Discussion

As a result of all the tests performed, it was determined that the unit was successful in the environmental tests but failed in the life test. As the same result was observed in the additional test performed to examine whether the failure in the life test was due to an error in the test setup, it was concluded that the surface treatment of the rotor was inadequate, and a change was required in this regard.

In 3.2.4.3, it was mentioned that electroless nickel plating is suitable in terms of hardness and surface roughness, and although this coating is one of the coatings recommended by the felt manufacturer, the expected performance was not achieved in the life test. Although there is no clear prediction about working life, it is expected that the felt will be damaged because of wear, not the rotor, since the part to be replaced at the end of MTBR will be the felt. Therefore, it can be clearly said that the coating is insufficient for this application.

It was also observed that a coupon part produced by applying the same coating on the same base material for another purpose, the coating deteriorated under -30°C conditions. Although it seems theoretically appropriate, it was decided to change the

electroless nickel plating application since the adequacy of the application and the repeatability of the process failed.

As mentioned in 3.2.4.4, HVOF is also a coating that provides adequate hardness and roughness properties, but it is not preferred as the first option due to the difficulty and higher cost of the process. Since ENP failed the life test, it was decided to use HVOF as a surface treatment and repeat the life test.

5. DESIGN REVISION

5.1 Surface Treatment Method

As mentioned before, HVOF is a suitable application to meet the requirements of seal, but it is not chosen as the first option due to its cost and complexity of the process. Since ENP failed the life test, HVOF application is selected to be used as the surface treatment method of rotor.

Various types of powders are used in HVOF for various applications. Powders can be categorized into three main types: metal-based materials, metal-ceramic composites, and ceramics. Metal-based powders are mostly used to repair parts consisting of the same base material as aluminum, iron, copper, nickel, etc. Metal-ceramic composites mostly consists of a base metal and carbide reinforcement to increase hardness and wear resistance. Finally, oxide ceramics also offer high hardness, but they have poor impact resistance and resistance to fatigue load. The advantage of oxide ceramics is having the highest hardness values, thermal and electrical insulation. Among all these three options, MCMs are the most suitable powders because of offering high wear resistance in fatigue loads, good corrosion resistance, and high impact resistance [51].

Although they all offer excellent wear resistance, there are differences between the metal-ceramic composites that influence the choice. Among them, tungsten-carbide based powders exhibit properties similar to hard chrome plating, but superior in most properties. WC/Co/Cr 86/10/4 was chosen because it offers excellent wear resistance, improved corrosion resistance and high coating hardness. This powder contains 80.6% W, 5.4% C, 10% Co, 4% Cr and offers a coating hardness above 64 HRC.

Unlike coatings such as alodine, ENP, anodizing, etc., a much thicker coating can be made with the HVOF method. However, since a very coarse surface will be obtained after coating, the surface will be brought to the desired size and roughness value by grinding. Although aluminum is a suitable base material for ENP, its suitability for HVOF was investigated and aluminum and steel base materials were compared in terms of bonding strength. When comparing the bonding resistance of aluminum and steel with HVOF tungsten carbide coating, there are several factors that can influence the bonding quality and strength. The thermal properties of the substrate material can affect

95

the bonding resistance of the coating. For example, aluminum has a lower melting point and higher thermal conductivity compared to steel, which can make it more challenging to achieve proper bonding of the tungsten carbide coating. Having higher thermal conductivity, aluminum dissipates heat more quickly. Steel, on the other hand, has a higher melting point and lower thermal conductivity, which can help to create a stronger bond between the coating and substrate. On the other hand, any surface contaminants or oxidation on the substrate material can also negatively impact the bonding of the coating. Aluminum alloys have naturally aluminum oxide on their surface which negatively affects the bonding stress. Because of the reasons stated above, steel is decided to be used as the base material for the rotor. A carbon steel like AISI 4140 QT has sufficient mechanical properties regarding structural considerations like vibration, shock, and fatigue load. On the other hand, a proper stainless steel like AISI 304 also would be a good choice to eliminate the ENP process.

5.2   Seal Comparison

In 2.4, three different seal options are stated which are Balseal X625753, Trelleborg TG3201600-M15N, and Kastaş K702-160. Trelleborg and Kastaş are eliminated for two reasons:

- High frictional torque
- High mating surface hardness

Performance tests showed that the actual frictional torque of Balseal is way above the estimated value. Trelleborg and Kastaş provides us to design the stator as a single piece in terms of ease of assembly. On the other hand, hardness requirement of all three seals is met since HVOF offers more than 65 HRC. Thus, all three seals are decided to be compared in performance tests. Furthermore, since the Trelleborg catalog states that the hardness depth of the mating material should be 0.3 mm, a process was applied to achieve this final thickness of the coating.

Three seal configurations are made to measure the frictional torques of all three seals. Seal 1 to 4 refer to the seal from top to bottom of the RU.

Table 5-1 Seal configurations (K: Kastaş, B: Balseal, T: Trelleborg)

	Configurations		
Seal No	First	Second	Third
1	K	K	T
2	K	K	K
3	K	K	K
4	K	B	B

Firstly, four Kastaş seals are planned to be used in the performance test. The frictional torque of the Kastaş seal is planned to be calculated as follows.

$$T_K = \frac{T_1}{4}$$ where T_1 and T_K refer to the torque sensor data of the first performance test and frictional torque of the Kastaş rotary seal, respectively.

In the second configuration, the fourth seal is planned to be changed with Balseal and frictional torque of Balseal can be calculated as follows.

$$T_B = T_2 - 3 * T_K$$ where T_2 and T_B refer to the torque sensor data of the second performance test and frictional torque of Balseal rotary seal, respectively.

In the third configuration, the first seal is planned to be changed with the Trelleborg and frictional torque of the Trelleborg can be calculated as follows.

$$T_T = T_3 - 2 * T_K - T_B$$ where T_3 and T_T refer to the torque sensor data of the second performance test and frictional torque of Trelleborg rotary seal, respectively.

After calculating the frictional torque values of all three seals separately, the life test is planned to be conducted in third configuration. As can be seen in the Figure 3-23, there are three separate drainage channels: the upper drainage channel drains only the leakage from seal 1, the middle drainage channel drains the leakage from any of seals 2 and 3, and the lower drainage channel drains only the leakage from seal 4. If a life test is performed on the third configuration, Trelleborg fails if the upper drainage channel leaks, Kastaş fails if the middle drainage channel leaks, and Balseal fails if the lower drainage channel leaks. Therefore, it was decided to perform the life test in this configuration where three different seals can be life tested at once.

5.3 Geometrical Changes

Minor geometric modifications were made to the structure so as not to necessitate the repetition of the environmental tests.
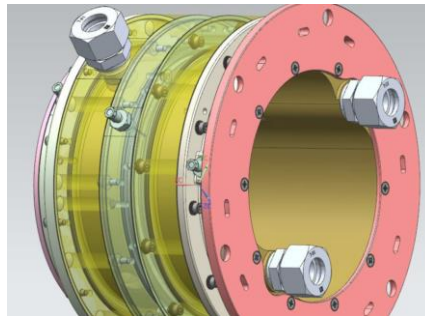
Figure 5-1 Second prototype design

- As different felts were to be tried, the housing design of the felts had to be changed. Provided that form-fit-function features are maintained, the stator parts containing the seal housings are designed in a variant way and these structures are also changed together with the seals.
- Due to the difficulties in the assembly process and to make the structure more compact, the bolts were installed from the inside of the stators.
- In order to reduce the rotor raw material, the rotor flange is designed as a separate part and integrated into the rotor with bolts.
- Rotor material is changed from AA6061-T6 to AISI 4140 QT. FEM analysis is not repeated since stress is independent from the material and steel has higher yield strength than aluminum. On the other hand, weight of the rotor is increased, and load applied on bearings should be investigated. The safety factor for bearings was kept above 4.5 in anticipation of such a change. Since the density of steel is approximately three times that of aluminum, the safety factors shown in Table 3-3 were divided by three to approximate the new safety factors.

Table 5-2 Safety factors of bearings for steel rotor

Normal		Shock	
Radial Force	Thrust Force	Radial Force	Thrust Force
N/A	N/A	3,43	N/A
N/A	58,36	4,20	4,30

6. TEST RESULTS OF THE SECOND PROTOTYPE

6.1 Performance Tests

The RU is assembled according to the first configuration specified in Table 5-1 for performance testing. 80 Nm was measured on the motor shaft, but this torque was not enough to move the rotor. The 4th seal was removed, and the test was repeated, but the rotor still could not be rotated at a torque of 80 Nm. In this case, it was calculated that the friction torque of one Kastaş seal was above 26.7 Nm, and it was decided not to use Kastaş seals since the friction torque of the unit would be over 107 Nm if four seals were used. Since the second and third configurations in Table 5-1 also contain Kastaş seals, these configurations were canceled, and two new seal configurations were defined instead (Table 6-1). Separate frictional torque values are calculated similarly to the first three configurations.

Table 6-1 Seal configurations (B: Balseal, T: Trelleborg)

Seal No	Configurations	
	Fourth	Fifth
1	B	B
2	B	T
3	B	T
4	B	B

The friction torque values measured in the tests performed at certain pressures in the fourth configuration are shown below (Table 6-2).

Table 6-2 Fourth configuration performance test sensor data

Inlet pressure	Outlet pressure	Dynamic frictional torque	Static frictional torque	Flow rate
[bar]	[bar]	[Nm]	[Nm]	[lpm]
1	0.76	8	12	13.07
1.5	1.17	12	16.5	16
2	1.51	16	19	18.5
2.5	1.88	16	20.5	20.8
3	2.29	17	21	23
3.6	2.68	20	23.5	25
4	3.12	20	20.5	28.09
5	4.1	21	26	24.41
6	5.1	21	27.5	24.17
7	6.22	21	27.5	23.9
8	7.17	17	25	23.65
9	8.2	17	25	23.41
10	9.16	20	24.5	23.14

The system was assembled according to the fifth configuration and data was collected in a similar way. The test results are shown below.

Table 6-3 Fifth configuration performance test sensor data

Inlet pressure	Outlet pressure	Dynamic frictional torque	Static frictional torque	Flow rate
[bar]	[bar]	[Nm]	[Nm]	[lpm]
1	0.8	12		11.3
2	1.5	14.3	15.5	16
3	2.3	15	16.6	19.7
4	3	15.2	16.4	22.8
5	3.8	16.3	17.8	25.3
6	4.9	17.8	18.2	25
7	5.9	18.8	19.4	24.7
8	6.9	19.5	21	24.6
9	7.9	18.5	20	24.3
10	9	20	21	24

Using the results of fourth and fifth configurations, frictional torque of Balseal and Trelleborg are calculated and compared in table.

Table 6-4 Comparison of Balseal and Trelleborg frictional torque values

Inlet pressure	4th configuration frictional torque	5th configuration frictional torque	Frictional torque of one Balseal rotary seal	Frictional torque of one Trelleborg rotary seal
bar	Nm	Nm	Nm	Nm
1	8	12	2	4
2	16	14.3	4	3.1
3	17	15	4.3	3.3
4	20	15.2	5	2.6
5	21	16.3	5.3	2.9
6	21	17.8	5.3	3.7
7	21	18.8	5.3	4.2
8	17	19.5	4.3	5.5
9	17	18.5	4.3	5
10	20	20	5	5

Frictional torque values of Balseal and Trelleborg seals are quite similar as seen in Table 6-4. RU is operated in fifth condition for 200 cycles and torque log is collected in room temperature. Polynomial and linear trendlines are shown in Figure 6-1. The mean frictional torque value is 12.9 Nm.
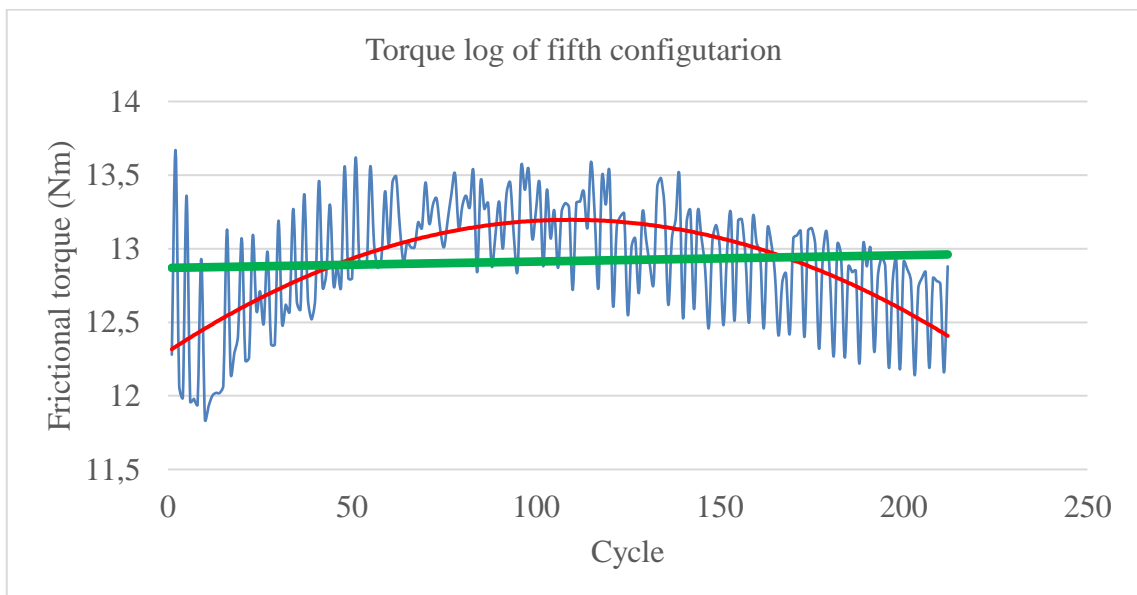
Figure 6-1 Torque log of RU in fifth configuration

6.2   Life Test

In order to perform the life test of both seals that may be used at the same time, the life test was started in the fifth configuration. Although the Trelleborg seals used in this test are brand new, the Balseal seals have been used for 400,000 cycles before. This will be taken into consideration in the comparison and seal selection to be made after the life test.

In the performance test in the fifth configuration and at the beginning of the life test, the drains leaked within the acceptance criteria, but this leakage stopped a few hours after the start of the test. In the life test, which was measured daily, after 600,000 cycles, the Trelleborg drain leaked 0.11 ml/h and the Balseal drain leaked 0.067 ml/h. Since there were two of each seal, the amount of leakage was calculated by taking twice the measured liquid. Since the Trelleborg seals exceeded the acceptance criteria after 600,000 cycles and the Balseal seals were below the acceptance criteria after a total of 1,000,000 cycles, it was determined that the Balseal seals passed the life test.

6.3   Thermal Tests of Final Configuration

Although frictional torque data with respect to temperature change is measured in the first prototype, change in base material of the rotor constitutes a major effect in the aspect of thermal expansion. For that reason, RU is assembled in fourth configuration, which is the final configuration and frictional torque is measured in thermal extremum points. Tests are conducted in thermal test chamber, which means that tests are performed in ambient temperatures extremums. Sensor values at certain inlet pressure values and frictional torque log in room temperature, -35°C, and 63°C are shown below.

Table 6-5 Second prototype frictional torque at room temperature

Room temperature		
Pressure (bar)	Flow rate (lpm)	Torque (Nm)
1	10.1	3.5
2	14.7	4.5
3.04	18.5	5
4.02	21.6	7
5.04	24.2	8
6	24.6	9
7	24.4	10.5
8	24	11
9	23.9	12.5
10.03	25.5	14

Table 6-6 Second prototype frictional torque at -35°C ambient temperature

-35°C Ambient temperature			
Pressure (bar)	Flow rate (lpm)	Torque (Nm)	Media temperature (°C)
1	10.4	3.5	9
2	15.5	4	11
3	19.3	5	9
4.06	22.5	6	9
5.04	24.7	7	9
6.07	24.5	8	9.4
7	24.2	9.5	10
8.08	24	11.3	10.8
9.04	23.7	11.8	11.5
10.06	23.4	13.2	12

Table 6-7 Second prototype frictional torque at 63°C ambient temperature

63°C Ambient temperature			
Pressure (bar)	Flow rate (lpm)	Torque (Nm)	Media temperature (°C)
1.03	11.5	4	29.2
2.01	16.7	5.3	30.7
3.02	20.5	5.5	32
4.01	23.6	6	35.5
5.1	12.6	9	36
6.01	12.5	10	37
7.05	12.3	11	38.1
8.04	12.1	13	38.8
9.05	11.9	15	39.3
10.04	11.7	16	39
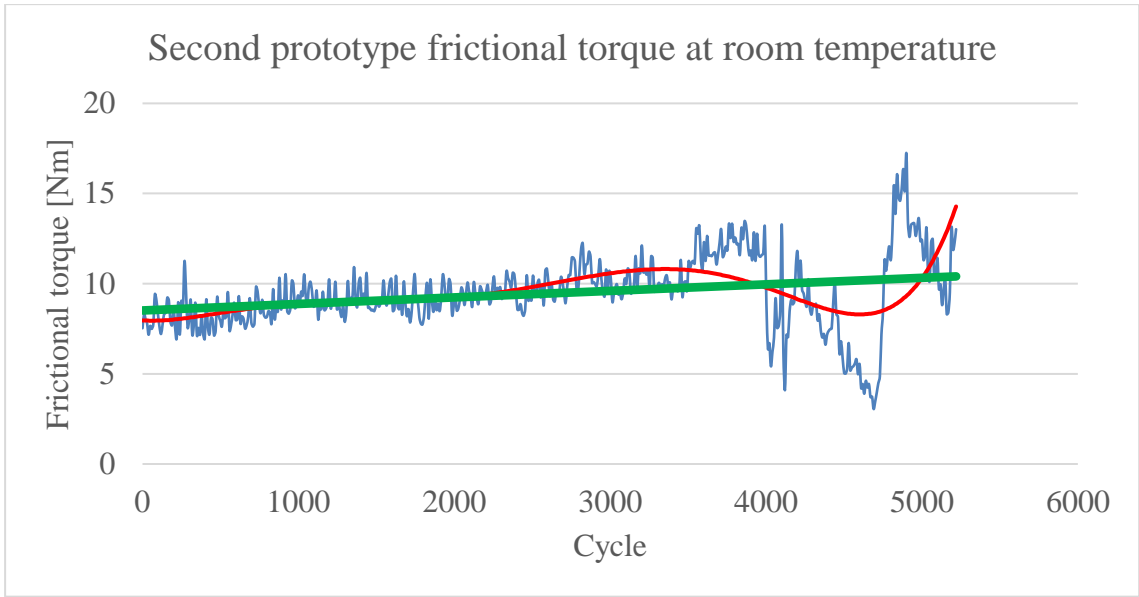
Figure 6-2 Torque log of RU in fifth configuration
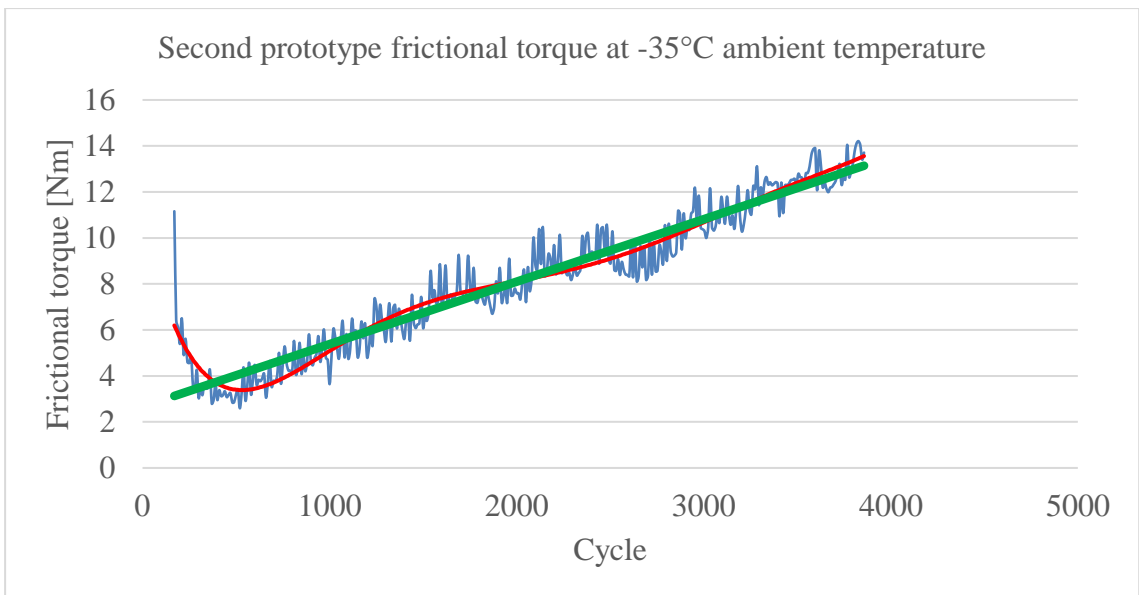
Figure 6-3 Torque log of RU in fifth configuration
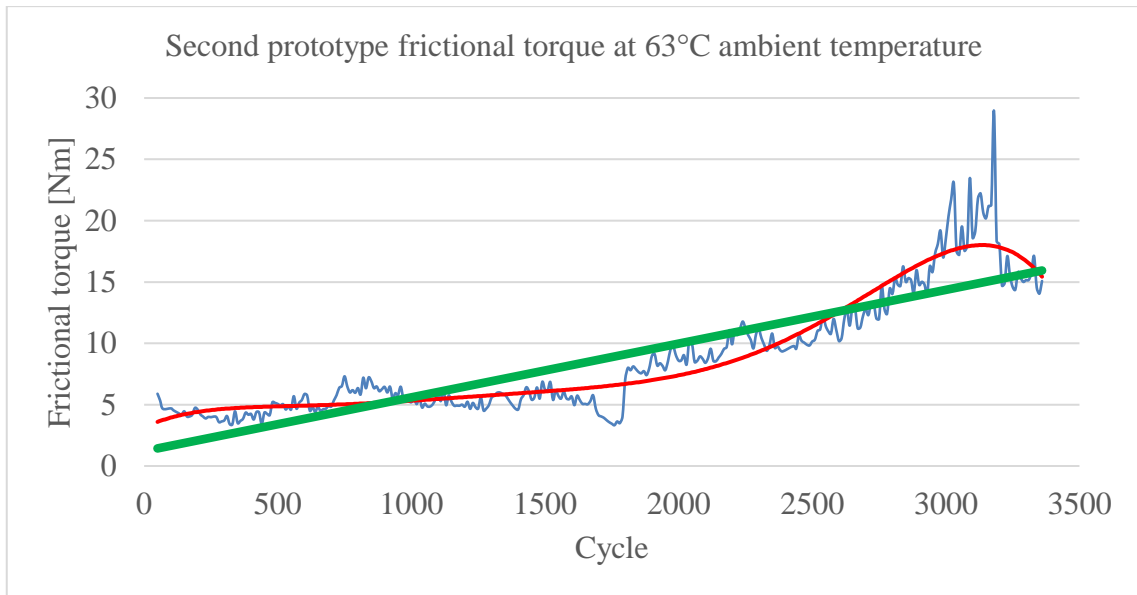
Figure 6-4 Torque log of RU in fifth configuration

In the test where the rotational speed was the control group, friction torque was read at three different temperatures and ten different pressure values, and it was observed that the friction torque increased as the temperature increased (Table 6-8). Since the hydraulic elements such as pump, heat exchanger and tank are outside the cabin, the line temperature is between the cabin temperature and ambient temperature. However, to condition the system temperature before the tests were performed, at least three hours were waited after the cabin reached the desired temperature at 3°C/min.

Table 6-8 Frictional torque comparison of second prototype with respect to the ambient temperature (Blue: -35°C, White: 24°C, Red: 63°C)

Pressure [bar]	Media temperature [°C]	Torque [Nm]
1	9	3.5
1	24	3.5
1	29.2	4
2	11	4
2	24	4.5
2	30.7	5.3
3	9	5
3	24	5
3	32	5.5
4	9	6
4	24	7
4	35.5	6
5	9	7
5	24	8
5	36	9
6	9.4	8
6	24	9
6	37	10
7	10	9.5
7	24	10.5
7	38.1	11
8	10.8	11.3
8	24	11
8	38.8	13
9	11.5	11.8
9	24	12.5
9	39.3	15
10	12	13.2
10	24	14
10	39	16

6.4 Results & Discussion About the Second Prototype Tests

The main purpose of the second prototype tests is to ensure that HVOF coating meets the life requirement. Trelleborg and Balseal rotary seals are subjected to life test under nominal inlet pressure and room temperature. The leakage rate of Trelleborg seals was 0.11 ml/h after 600,000 cycles and increased afterwards. On the other hand, the leakage

rate of the Balseal was under 0.1 ml/h after 1,000,000 cycles. Thus, Balseal X625753 is decided to be used.

Friction torque values of two seals are compared in various inlet pressure values (Figure 6-5). It can be seen from the curves below that frictional torque values of both seals are close to each other. Hence, friction torque is not a selection criterion between these two seals. Also, the increasing trendlines of the curves show that the friction torque increases with pressure. But this correlation is not fully observed because there is a pressure in the lower parts of the working pressure of the seals.
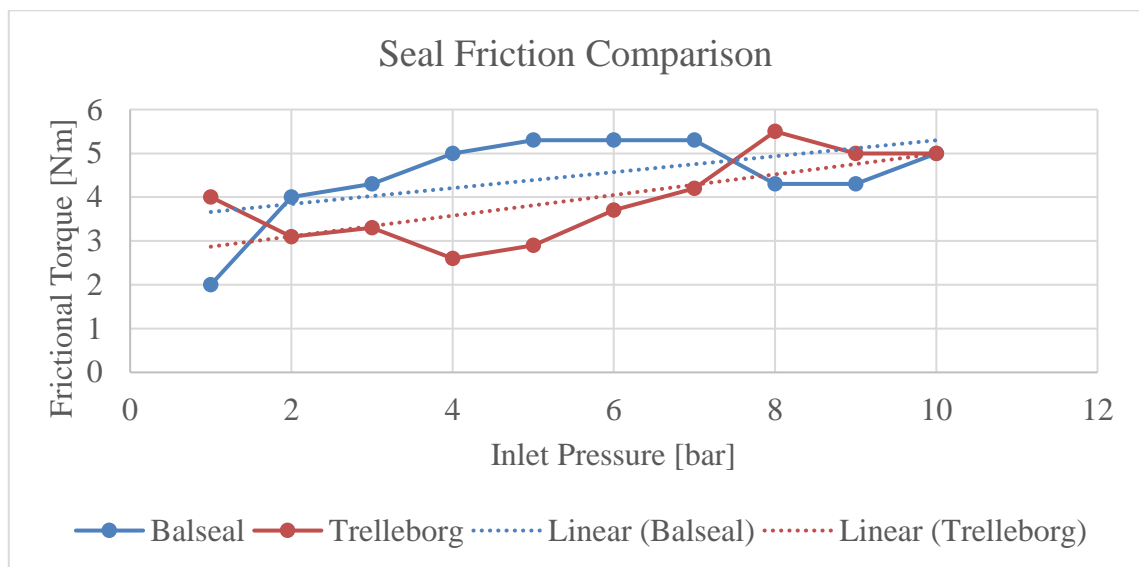
Figure 6-5 Seal friction comparison with respect to inlet pressure

When the curve of the data in the Table 6-8 is plotted, it is seen that the friction torque increases at high temperature (Figure 6-6). The main reason for this is the difference in the coefficient of thermal expansion between the rotor and the felt. Friction torque with increasing temperature can only be realized if the expansion coefficient of the felt is smaller than that of the rotor. Although PTFE has a higher coefficient of thermal expansion than steel [52], such a phenomenon can be explained by the carbon content in the alloy of the elastomer structure of the felt, which has a very low coefficient of thermal expansion, and more importantly by the fact that the felt lip is continuously pressed radially against the rotor with a stainless-steel spring (Figure 2-7). In addition, in these tests, the pressure-dependent variation of the friction torque could be observed more clearly.
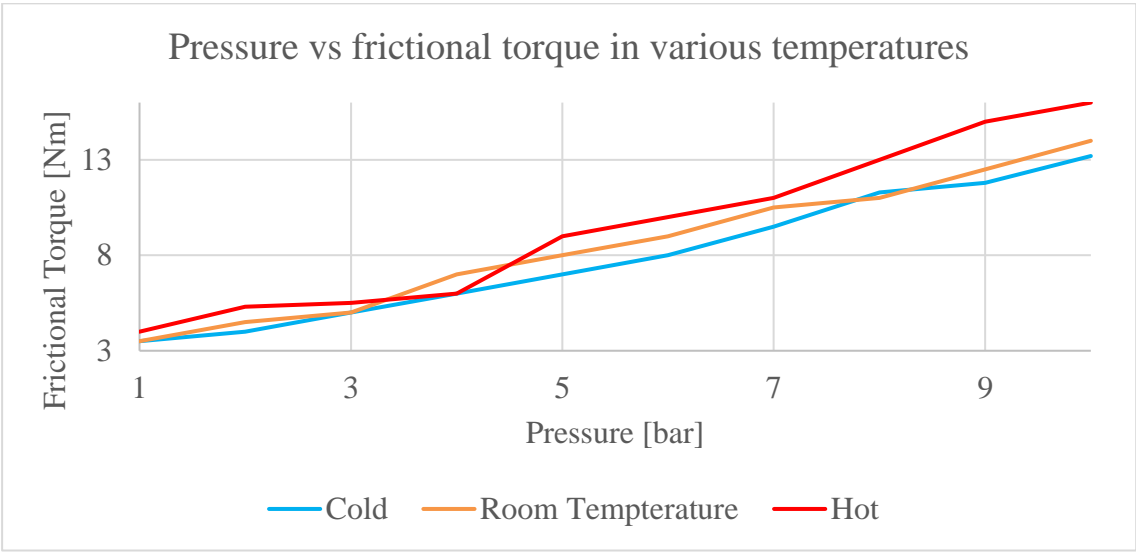
Figure 6-6 Pressure vs frictional torque of Balseal in various temperatures

7. CONCLUSION

In this thesis, an RU has been designed for use in radar. In the process, literature review, geometric design, structural analysis and CFD analysis methods were utilized. Appropriate design methods were determined according to the technical requirements and conceptual design and detail design processes were carried out with these methods. Afterwards, operational and non-operational environmental conditions tests and life tests were conducted to verify the technical requirements. The unit successfully passed all environmental conditions tests, but it failed the life test. Subsequently, in order to pass the life test, a corrective action was taken, the life test was repeated, and the life test has been succeeded. In addition, controlled tests were carried out at different temperatures, different hydraulic pressures and different seals and the results were compared.

Since the unit is designed to be used in a wheeled military land vehicle, the relevant sections of the military standard were taken as reference when determining the technical requirements for environmental conditions such as vibration, shock and temperature. Market research was conducted on issues such as pressure, friction, and permeability, which are related to the performance of the unit, and products with similar features were taken as reference.

After the rough geometry was created in the preliminary design, the flow diameters were determined in order of magnitude for the selection of COTS elements such as seals and bearings. Seals and bearings of the appropriate size were also selected considering their dimensions and the detailed selection was left to the detailed design phase.

In the detailed design phase, CFD analysis was performed to determine the pressure drop more precisely. Material selection and surface treatment issues were examined in detail in order to provide the desired surface properties according to the selected seal, and the most reasonable four options were selected. The geometric design was elaborated by considering issues such as assembly, manufacturability, static sealing, bearing selection and the final geometric model was subjected to structural analysis.

In the vibration and shock tests of the first prototype manufactured, it was observed that the structure did not undergo plastic deformation, the fasteners on it did not loosen and its structural integrity was not impaired. In this way, the structural analyses were verified. Pressure loss, leakage rate and frictional torque values remained under limit in performance tests. Pressure loss value meets the CFD results and frictional torque results meet the manufacturer's data. In the life test, the unit failed this test as 1 ml/h leakage was measured after 385,000 cycles.

The problem experienced in the life test was that the rotor surface did not meet the seal requirements. Although the electroless nickel plating hardness was measured as 35 HRC and was above the seal's technical requirement of 30 HRC, the failure of the life test was interpreted as a failure of the coating to adhere properly to the surface. Therefore, it was decided to use the second surface treatment method choice, tungsten-carbide coating with HVOF. Since the surface hardness of the HVOF coating is above 60 HRC, it was decided to test the seals that were previously eliminated due to high hardness requirements within the scope of these prototype tests. Of the Kastaş, Trelleborg and Balseal seals tested, the friction torque of the unit was over 107 Nm when Kastaş was used, so this seal was eliminated from the options. The friction torques of Balseal and Trelleborg seals were measured close to each other, but in the simultaneous life test, it was decided to use the Balseal seal since Trelleborg exceeded the leakage limit after 600,000 cycles while Balseal remained below the leakage limit even after completing 1,000,000 cycles. After 1,000,000 cycles, since the leakage of the Balseal seal was below 0.1 ml/h and there were no scratches on the rotor surface, the design was validated, and the final configuration was frozen.

8. REFERENCES

[1] Dynamic Sealing Technologies Inc. (2023). *What is a rotary union?* DSTI. https://www.dsti.com/learn/what-is-a-rotary-union

[2] Bily, P. J. (1951, March 30). Swivel Joint Construction for Handling Fluids.

[3] *Quick Release Couplings*. (n.d.). RFS Hydraulics. Retrieved June 4, 2023, from https://www.rfshydraulics.com/quick-couplings.html

[4] Kim, N.-Y., Wu, Y.-T., Qin, Z., Cho, Y.-M., & Lyu, S.-K. (2021). A Study on the Optimal Design According to the Piston Shape of the 3/8″Hydraulic Quick Coupler. *The Korean Society of Manufacturing Process Engineers*, *20*(2), 66–71. https://doi.org/10.14775/ksmpe.2021.20.02.066

[5] *Motion Technology Catalog* (p. 183). (n.d.). Moog Inc. Retrieved June 4, 2023, from https://www.moog.com/content/dam/moog/literature/MCG/srcatalog.pdf

[6] Dynamic Sealing Technologies Inc. (n.d.). *Lightweight, Compact Rotary Unions LT Series* (p. 10). Retrieved May 2, 2023, from https://www.dsti.com/pdfs/catalogs/DSTI-LT-Series-Catalog.pdf

[7] *LT Series Rotary Unions & Joints*. (n.d.). Retrieved June 4, 2023, from https://www.dsti.com/rotary-unions/standard/lt/

[8] *MIL-STD-810G Department of Defense Test Method Standard: Environmental Engineering Considerations and Laboratory Tests*. (2008). Department of Defense, United States of America.

[9] Conrad, F.H., Hill, E.F., & Ballman, E.A. (1940). Freezing Points of the System Ethylene Glycol–Methanol–Water. Industrial & Engineering Chemistry, 32(4), 542–543. https://doi.org/10.1021/ie50364a023

[10] Çengel Y.A., & Cimbala, J.M. (2006). *Fluid Mechanics: Fundamentals and Applications* (p. 324). Mcgraw-Hillhigher Education.

[11] Crane Co. (1982). *Flow of Fluids Through Valves, Fittings, and Pipe: Vol. Technical Paper No.410M* (Metric Edition - SI Units, p. 15).

[12] Moody, L. F., & Princeton, N. J. (1944). Friction Factors for Pipe Flow. *Transactions of the American Society of Mechanical Engineers*, *66*, 671–678.

[13] Crane Co. (1982). *Flow of Fluids Through Valves, Fittings, and Pipe: Vol. Technical Paper No.410M* (Metric Edition - SI Units, p. 22).

[14] Ethylene Glycol Product Guide. (2019). *ME Global*. https://www.meglobal.biz/wp-content/uploads/2019/01/Monoethylene-Glycol-MEG-Technical-Product-Brochure-PDF.pdf

[15] Plath, S., Mayer, S., & Wollesen, V. M. (2005). Friction Torque of a Rotary Shaft Lip Type Seal - A Comparison between Test Results and Finite Element Simulation. *Mechanika*, *54*(4), 55–59. https://doi.org/10.5755/j01.mech.54.4.14499

[16] Parker. (2018). *Rotary Seal Design Guide: Vol. Catalog EPS 5350/USA*.

[17] Stachowiak, G. W. (Ed.). (2005). Third-Body Reality –Consequences and Use of theThird-Body Concept to Solve Friction and Wear Problems. In *Wear: Materials, Mechanisms and Practice* (p. 294). John Wiley & Sons, Ltd.

[18] Lingerkar, K., & Khonsari, M. M. (2010a). On the effects of sliding velocity and operating pressure differential in Rotary O-Ring Seals. Proceedings of the Institution of Mechanical Engineers, Part J: Journal of Engineering Tribology, 224(7), 649–657. https://doi.org/10.1243/13506501jet755

[19] Bal Seal Engineering. (2023). Rotary Shaft Seals. Bal Seal Engineering. Retrieved April 5, 2023, from https://www.balseal.com/seal/rotary/

[20] Trelleborg. (2009). *Rotary Seals* (p. 243).

[21] Trelleborg. (2009). *Rotary Seals* (p. 246).

[22] Trelleborg. (2009). *Rotary Seals* (p. 244).

[23] KASTAŞ. (n.d.). *K702 – Rod Seal*. Www.kastas.com.tr. Retrieved August 2, 2022, from https://www.kastas.com.tr/it/tenute-rotanti/k702-rod-seal-1

[24] Budynas, R. G., & Nisbett, J. K. (2011). *Shigley's Mechanical Engineering Design* (Ninth Edition, p. 570). Mcgraw-Hill.

[25] SKF. (2018). *Rolling bearings* (p. 20). https://www.skf.com/binaries/pub12/Images/0901d196802809de-Rolling-bearings---17000_1-EN_tcm_12-121486.pdf

[26] SAIBO. (n.d.). *Thin Section Bearing*. Www.saibo-Motion.com. Retrieved March 15, 2023, from https://www.saibo-motion.com/product-item-26.html

[27] UNASIS. (n.d.). *Thin Section Bearings.* Www.unasisbearings.com. Retrieved February 15, 2023, from https://www.unasisbearings.com/bearings/thin-section-bearings-

[28] Hu, H. H. (2012). Chapter 10 - Computational Fluid Dynamics. In P. K. Kundu, I. M. Cohen, & D. R. Dowling (Eds.), *Fluid Mechanics (*5th ed., pp. 421–472). Academic Press.

[29] Rennels, D. C., & Hudson, H. M. (2012). *Pipe Flow: A Practical and Comprehensive Guide*. Wiley.

[30]   Thompson, S. M., Paudel, B. J., Jamal, T., & Walters, D. K. (2014). Numerical Investigation of Multistaged Tesla Valves. *Journal of Fluids Engineering*, *136*(8). https://doi.org/10.1115/1.4026620

[31]   Çengel Y.A., & Cimbala, J.M. (2006). *Fluid Mechanics: Fundamentals and Applications* (p. 364). Mcgraw-Hillhigher Education.

[32]   Versteeg, H. K., & Malalasekera, W. (2011). *An Introduction to Computational Fluid Dynamics: The Finite Volume Method* (2nd ed., p. 48). Pearson Education.

[33]   Callister, W. D., & Rethwisch, D. G. (2018). *Materials Science and Engineering: An Introduction* (10th ed., p. 165). Wiley.

[34]   Callister, W. D., & Rethwisch, D. G. (2018). *Materials Science and Engineering: An Introduction* (10th ed., p. 167). Wiley.

[35]   Schutze, M., Bender, R., & Roche, M. (2003). *Corrosion Resistance of Steels, Nickel, Alloys and Zinc in Aqueous Media: Waste Water, Seawater, Drinking Water, High-Purity Water*. Wiley-VCH.

[36]   Bal Seal Engineering Inc. (2010). *Solutions for Rotary Applications*.

[37]   Carlsson, J.-O., & Martin, P. M. (2010). Chapter 7 - Chemical Vapor Deposition. In *Handbook of Deposition Technologies for Films and Coatings* (pp. 314–363). Elsevier.

[38]   Hiremath, P., Sharma, S., Gowrishankar, M. C., Shettar, M., Kowshik, C. S. Suhas., & Naik, N. (2019). Effect of carburization on microstructure of low carbon steel and the influence of process parameters on its tribological behavior. *International Journal of Mechanical and Production Engineering Research and Development*, *9*(Special Issue 2), 718–725. https://researcher.manipal.edu/en/publications/effect-of-carburization-on-microstructure-of-low-carbon-steel-and

[39]   Bal Seal Engineering. (2016). *Chrome Plating: A Guide for Selectinf the Type of Chrome Plating for Use in Contact with Bal Seal Spring-energized Seals in Rotary and Reciprocating Service, Technical Report TR-14*.

[40]   *MIL-C-26074D, Military Specification: Coatings, Electroless Nickel Requirements*. (1989).

[41]   Parkinson, R. (2001). *Properties and Applications of Electroless Nickel*. https://www.semanticscholar.org/paper/Properties-and-applications-of-electroless-nickel-Parkinson/39368bf8785af539d62ae2ae67167cbcd3cea247

[42]   Sheng, G. (2016). Study on Growth Mode and Properties of Electroless Nickel Plating on Aluminum Alloy. *Chemical Engineering Transactions*, *55*. https://doi.org/10.3303/CET1655054

[43] Xia, P., Almond, H., & Impey, S. A. (2016, June 30). Investigation of Pre and Post Plating Surface Roughness of Electroless Nickel Phosphorus Coated Substrate for Diamond Turning Application. *Staff Publications (SATM)*. 16th International Conference of the European Society for Precision Engineering and Nanotechnology, Nottingham, UK.

[44] Pourbafrani, M., Razavi, R. S., Bakhshi, S. R., Loghman-Estarki, M. R., & Jamali, H. (2014). Effect of Microstructure and Phase of Nanostructured YSZ Thermal Barrier Coatings on Its Thermal Shock Behaviour. *Surface Engineering*, *31*(1), 64–73. https://doi.org/10.1179/1743294414y.0000000397

[45] Sathish, S., & Geetha, M. (2016). Comparative Study on Corrosion Behavior of Plasma Sprayed Al2O3, ZrO2, Al2O3/ZrO2 and ZrO2/Al2O3 Coatings. *Transactions of Nonferrous Metals Society of China*, *26*(5), 1336–1344. https://doi.org/10.1016/s1003-6326(16)64236-x

[46] *HVOF Coating Services*. (n.d.). Www.praxairsurfacetechnologies.com. Retrieved May 16, 2022, from https://www.praxairsurfacetechnologies.com/en/coating-services/application-processes/thermal-spray/hvof-coating-services#:~:text=Typical%20thickness%20of%20HVOF%20thermal

[47] Murugan, K., Ragupathy, A., Balasubramanian, V., & Sridhar, K. (2014). Optimizing HVOF spray process parameters to attain minimum porosity and maximum hardness in WC–10Co–4Cr coatings. *Surface and Coatings Technology*, *247*, 90–102. https://doi.org/10.1016/j.surfcoat.2014.03.022

[48] Kaydon. (2014). *Catalog 300 - Engineering and Selection Guide* (Kaydon Thinfinite Bearing Solutions: Precision Reali-Slim Thin Section Bearings).

[49] Cook, R. D., Malkus, D. S., Plesha, M. E., & Witt, R. J. (2001). *Concepts and Applications of Finite Element Analysis: A Treatment of the Finite Element Method as Used for the Analysis of Displacement, Strain, and Stress* (4th ed.). Wiley.

[50] Dean, J. (n.d.). *Introduction to the Finite Element Method (FEM) Lecture 1 The Direct Stiffness Method and the Global StiffnessMatrix*. Retrieved January 6, 2023, from https://www.ccg.msm.cam.ac.uk/system/files/documents/FEMOR_Lecture_1.pdf

[51] GTV. (n.d.). *GTV Spray Powder Catalogue*. Retrieved April 2, 2023, from https://www.gtv-mbh.de/_Resources/Persistent/6/e/5/f/6e5f4797ae63a4997fab31e9f3499962cf20a980/GTV%20Spray%20Powder%20Catalogue%20v1.10.pdf

[52] Kirby, R. K. (1956). Thermal Expansion of Polytetrafluoroethylene (Teflon) From -190° to +300°C. *Journal of Research of the National Bureau of Standards*, *57*.

9. APPENDIX
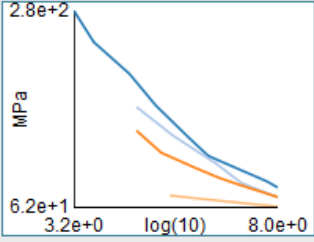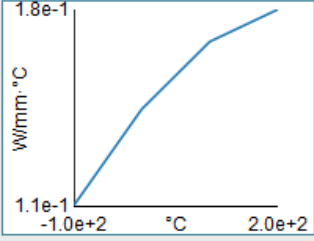
Aluminum Alloy

General aluminum alloy. Fatigue properties come from MIL-HDBK-5H, page 3-277.

Density	2.77e-06 kg/mm³

Structural

Isotropic Elasticity	
Derive from	Young's Modulus and Poisson's Ratio
Young's Modulus	71000 MPa
Poisson's Ratio	0.33
Bulk Modulus	69608 MPa
Shear Modulus	26692 MPa
Isotropic Secant Coefficient of Thermal Expansion	2.3e-05 1/°C
Compressive Ultimate Strength	0 MPa
Compressive Yield Strength	280 MPa
S-N Curve	
Tensile Ultimate Strength	310 MPa
Tensile Yield Strength	280 MPa

Thermal

Isotropic Thermal Conductivity	
Specific Heat Constant Pressure	8.75e+05 mJ/kg·°C

Figure 9-1 Aluminum alloy material properties used in FEA

Structural Steel

Fatigue Data at zero mean stress comes from 1998 ASME BPV Code, Section 8, Div 2, Table 5-110.1

Density	7.85e-06 kg/mm³

Structural

Isotropic Elasticity	
Derive from	Young's Modulus and Poisson's Ratio
Young's Modulus	2e+05 MPa
Poisson's Ratio	0.3
Bulk Modulus	1.6667e+05 MPa
Shear Modulus	76923 MPa
Isotropic Secant Coefficient of Thermal Expansion	1.2e-05 1/°C
Compressive Ultimate Strength	0 MPa
Compressive Yield Strength	250 MPa
Strain-Life Parameters	
S-N Curve	
Tensile Ultimate Strength	460 MPa
Tensile Yield Strength	250 MPa

Thermal

Isotropic Thermal Conductivity	0.0605 W/mm·°C
Specific Heat Constant Pressure	4.34e+05 mJ/kg·°C

Figure 9-2 Structural steel material properties used in FEA

Table 514.6C-IV. Category 4 – Composite two-wheeled trailer vibration exposure. (Break points for curves of Figure 514.6C-2.)

Vertical		Transverse		Longitudinal	
Frequency, Hz	PSD, g²/Hz	Frequency, Hz	PSD, g²/Hz	Frequency, Hz	PSD, g²/Hz
5	0.2252	5	0.0736	5	0.0521
8	0.5508	6	0.0438	7	0.1046
10	0.0509	7	0.0761	8	0.1495
13	0.0253	13	0.0130	13	0.0140
15	0.0735	15	0.0335	16	0.0303
17	0.0301	16	0.0137	18	0.0200
18	0.0319	21	0.0102	19	0.0342
19	0.0402	23	0.0268	20	0.0160
20	0.0366	25	0.0090	23	0.0378
43	0.1004	28	0.0090	27	0.0079
50	0.0308	30	0.0137	30	0.0208
102	0.0740	34	0.0055	32	0.0100
109	0.1924	37	0.0081	33	0.0267
117	0.0319	46	0.0039	35	0.0065
138	0.0869	51	0.0068	51	0.0040
150	0.0286	55	0.0042	53	0.0081
190	0.0605	106	0.0033	56	0.0035
263	0.0613	108	0.0045	59	0.0066
332	0.0097	111	0.0033	63	0.0037
360	0.0253	148	0.0030	65	0.0127
452	0.0053	163	0.0054	73	0.0026
500	0.0045	175	0.0023	93	0.0117
		235	0.0013	109	0.1635
rms = 4.43 g		262	0.0028	120	0.0180
		265	0.0025	132	0.0320
		317	0.0016	138	0.0738
		326	0.0057	153	0.0236
		343	0.0009	158	0.0549
		384	0.0018	164	0.0261
		410	0.0008	185	0.0577
		462	0.0020	257	0.0062
		500	0.0007	280	0.0032
				304	0.0068
		rms = 1.30 g		323	0.0045
				343	0.0193
				386	0.0014
				444	0.0054
				476	0.0018
				490	0.0046
				500	0.0014
				rms = 2.86 g	

Figure 9-3 Vibration profile